T.R.

GEBZE TECHNICAL UNIVERSITY

GRADUATE SCHOOL OF NATURAL AND APPLIED SCIENCES

APPROXIMATION OF EIGENVALUE PROBLEMS USING FINITE ELEMENT METHODS

EYLEM BAHADIR

A THESIS SUBMITTED FOR THE DEGREE OF

MASTER OF SCIENCE

DEPARTMENT OF MATHEMATICS

GEBZE

2021

T.R.

GEBZE TECHNICAL UNIVERSITY

GRADUATE SCHOOL OF NATURAL AND APPLIED SCIENCES

APPROXIMATION OF EIGENVALUE PROBLEMS USING FINITE ELEMENT METHODS

EYLEM BAHADIR

A THESIS SUBMITTED FOR THE DEGREE OF

MASTER OF SCIENCE

DEPARTMENT OF MATHEMATICS

THESIS SUPERVISOR

ASSIST. PROF. DR. ÖNDER TÜRK

GEBZE

2021

T.C.
GEBZE TEKNİK ÜNİVERSİTESİ
FEN BİLİMLERİ ENSTİTÜSÜ

ÖZDEĞER PROBLEMLERİNİN SONLU ELEMANLAR YÖNTEMLERİ İLE YAKLAŞIMI

EYLEM BAHADIR
YÜKSEK LİSANS TEZİ
MATEMATİK ANABİLİM DALI

DANIŞMANI
DR. ÖĞR. ÜYESİ ÖNDER TÜRK

GEBZE
2021

GEBZE TEKNİK ÜNİVERSİTESİ	**YÜKSEK LİSANS JÜRİ ONAY FORMU**

GTÜ Fen Bilimleri Enstitüsü Yönetim Kurulu'nun 21/05/2021 tarih ve 2021/22 sayılı kararıyla oluşturulan jüri tarafından 14/06/2021 tarihinde tez savunma sınavı yapılan Eylem BAHADIR'ın tez çalışması Matematik Anabilim Dalında YÜKSEK LİSANS tezi olarak kabul edilmiştir.

JÜRİ

ÜYE
(TEZ DANIŞMANI) :Dr. Öğr. Üyesi Önder TÜRK

ÜYE :Prof. Dr. Mansur İSGENDEROĞLU

ÜYE :Prof. Dr. Canan BOZKAYA

ONAY

Gebze Teknik Üniversitesi Fen Bilimleri Enstitüsü Yönetim Kurulu'nun
...…/…..../……… tarih ve ….…/…..... sayılı kararı.

SUMMARY

In this thesis, the numerical analysis of the Laplace and Steklov eigenvalue problems (EVPs) using the finite element method (FEM) is considered. The EVPs are posed on a number of both one- and two-dimensional domains which are discretized using linear and quadratic triangular elements. Then, the Galerkin approximations of the variational formulations that consist in constructing finite dimensional subspaces and in solving the discrete problems are presented. The convergence analysis is mainly based on the well known Babuška-Osborn theory in which the orders of convergence of the eigenvalues and the eigenvectors are estimated. Apart from the abstract spectral approximation theory, a proof of convergence of the eigensolutions that is based on the standard aspects of the Rayleigh quotient is presented for elliptic EVPs.

A formalism is considered to estimate the changes in the eigenvalues of the Laplace and Steklov EVPs due to a perturbation in the boundary of the problem domain. The influence of these boundary perturbations on the eigensolutions is investigated both analytically and numerically for several one- and two-dimensional perturbed domains that are assumed to be inscribed in the original domains. The convergence behavior of the perturbed solution to the original solution in terms of a characteristic perturbation parameter is obtained by a Taylor series expansion of the errors between the two solutions. The analogous convergence behavior of the FEM solution of the perturbed problem is obtained numerically. Besides, the Laplace and Steklov EVPs are considered on regular polygons inscribed in the unit disc. It is numerically shown that both simple and multiple eigenvalues of the Laplace EVP on the polygon domain obey a representation in inverse powers of the number of sides of the polygon. Analogous results are numerically shown to hold for the Steklov EVP in terms of several characteristic properties which are not available in the open literature to the best of the author’s knowledge.

Keywords: Laplace EVP, Steklov EVP, FEM, Boundary Perturbations.

ÖZET

Bu tezde, Laplace ve Steklov özdeğer problemlerinin (ÖDP) sonlu elemanlar yöntemi (SEY) kullanılarak sayısal analizi ele alınmaktadır. ÖDPler, doğrusal ve kuadratik üçgensel elemanlar kullanılarak ayrıklaştırılan hem bir hem de iki boyutlu bir dizi tanım bölgesi üzerine yerleştirilmektedir. Daha sonra, sonlu boyutlu alt uzayların oluşturulmasına ve ayrık problemlerin çözümüne dayanan varyasyonel formülasyonların Galerkin yaklaşımları sunulmaktadır. Yakınsama analizi esas olarak, özdeğerlerin ve özvektörlerin yakınsama mertebelerinin tahmin edildiği, iyi bilinen Babuška-Osborn teorisine dayanmaktadır. Soyut spektral yaklaşım teorisinin yanı sıra, Rayleigh oranının temel özelliklerine dayanan, özçözümlerin yakınsamasının bir kanıtı eliptik ÖDPler için sunulmaktadır.

Problem tanım bölgesinin sınırındaki bir pertürbasyona bağlı olarak, Laplace ve Steklov ÖDPlerinin özdeğerlerinde meydana gelen değişiklikleri tahmin etmek için bir formalizm ele alınmaktadır. Bu sınır pertürbasyonlarının özçözümler üzerindeki etkisi, orijinal tanım bölgelerinin içine kaydedildiği varsayılan çeşitli tek ve iki boyutlu pertürbe tanım bölgesi için hem analitik hem de sayısal olarak araştırılmaktadır. Pertürbe çözümün orijinal çözüme yakınsama davranışı, iki çözüm arasındaki hataların karakteristik bir pertürbasyon parametresi cinsinden Taylor seri açılımı ile elde edilmektedir. Pertürbe problemin SEY çözümünün benzer yakınsama davranışı, nümerik olarak elde edilmektedir. Ayrıca, Laplace ve Steklov ÖDPleri, birim disk içine kaydedilmiş olan düzgün çokgenler üzerinde de ele alınmaktadır. Çokgen tanım bölgesi üzerindeki Laplace ÖDPnin hem tek hem de çoklu özdeğerlerinin, çokgenin kenar sayısının ters kuvvetlerindeki bir temsiline uyduğu sayısal olarak gösterilmektedir. Yazarın bilgisi dahilinde açık literatürde bulunmayan çeşitli karakteristik özellikler açısından Steklov ÖDP için de benzer sonuçlar sayısal olarak gösterilmektedir.

Anahtar Kelimeler: Laplace ÖDP, Steklov ÖDP, SEY, Sınır Pertürbasyonları.

ACKNOWLEDGEMENTS

I want to start by thanking my supervisor Assist. Prof. Dr. Önder Türk, who patiently and exhaustively guided me in every stage of this study. He provided me my thesis subject and encouraged me to do better research with his sincere guidance and informative advice. I appreciate that I had a chance to study with him and develop myself with his invaluable supervision.

Secondly, I would like to thank Aslı, Emine, Eren, Pınar, and Umut, who distracted my mind when I was exhausted from studying and making me never feel alone with their friendships for years. I would also like to thank Defne, Gamze, and Uğur for being with me whenever I needed it during my master's education.

I would also like to express my deepest thanks to my parents İlknur and Gürcan, who always supported and encouraged me with excitement and love to achieve my goals. Last but not least, thanks to my sister İlke, who put up with my stress during the thesis period and accompanied me in all circumstances throughout our life.

TABLE OF CONTENTS

LIST OF ABBREVIATIONS AND ACRONYMS

Abbreviations and Acronyms		Explanations
$\mathcal{L}$	:	Elliptic partial differential operator.
Δ	:	Laplace operator.
Ω	:	Domain.
$\partial\Omega$	:	Boundary of Ω.
Ω'	:	Perturbed domain.
$\partial\Omega'$	:	Boundary of Ω'.
δ	:	Perturbation parameter.
J_p	:	Bessel's function of order p.
$\rho^{(p,q)}$	:	qth root of Bessel's function of order p.
ϕ	:	Basis function.
$\mathcal{T}$	:	Mesh (triangulation).
Ω^e	:	Triangular element.
diam	:	Diameter.
K	:	Stiffness matrix.
K^e	:	Local stiffness matrix.
M	:	Mass matrix.
M^e	:	Local stiffness matrix.
R	:	Boundary mass matrix.
R^e	:	Local boundary mass matrix.
λ	:	Eigenvalues.
λ_h	:	Approximate eigenvalues.
λ'	:	Eigenvalues on perturbed domains.

λ'_h	:	Approximate eigenvalues on perturbed domains.
u	:	Eigenfunctions.
u_h	:	Approximate eigenfunctions.
u'	:	Eigenfunctions on perturbed domains.
u'_h	:	Approximate eigenfunctions on perturbed domains.
t	:	Time parameter.
C	:	Velocity.
BVP	:	Boundary value problem.
EVP	:	Eigenvalue problem.
FEM	:	Finite element method.
1D	:	One dimensional.
PDE	:	Partial differential equation.
2D	:	Two dimensional.

LIST OF FIGURES

LIST OF TABLES

Table No: **Page**

1. INTRODUCTION

Many problems in natural sciences, engineering, and economics involve partial differential equations (PDEs). In many cases, determining exact solutions of PDEs is either too complicated in closed form or even impossible. Therefore, their solutions must be approximated numerically using numerical methods such as finite difference, finite volume, finite element, boundary element, and spectral methods to provide accurate and reliable approaches to these exact solutions.

Finite element methods including conforming, non-conforming, mixed finite elements, standard, discontinuous, and weak Galerkin approximations, can be described as a family of procedures of approximating functions as discrete models. These procedures involve a set of finite number of points and subdomains in the domain where the given problem is defined. The most important advantage of finite element methods is that they achieve more accurate solutions than the finite difference method on geometrically complex domains. Another significant advantage is that finite element methods transform the governing differential equations into a system of algebraic equations that can be solved locally over each finite element.

In this thesis, the finite element method (FEM) that is based on the standard Galerkin approximation is considered to obtain the approximate solutions of the Laplace and Steklov eigenvalue problems (EVPs) involving the Laplace operator which is a second-order elliptic partial differential operator. In general, numerical integrations, boundary perturbations (variations, deformations), and approximate boundary conditions, can be the cause of various errors in finite element methods (one can refer to, for instance, [1] for more details). Based on this, a series of strategies on investigating the effect of boundary perturbations on the eigensolutions of the Laplace and Steklov EVPs are identified and discussed in this study.

1.1. Literature Survey

Approximation of EVPs is significant to many scientific and engineering applications, such as structural dynamics, quantum chemistry, electrical networks, magnetohydrodynamics, and control theory [2]. Due to the important features such as the ability to handle solution domains with arbitrary geometry and rigorous theoretical foundations, finite element methods have been studied extensively for EVPs, for instance, [2–12].

1.1.1. Finite Element Methods for the Laplace EVP

The Laplace eigenvalue is the fundamental problem resided in many physical phenomena such as fluid flows being modeled by Navier-Stokes equations, acoustic theory, problems of vibrating elastic membranes, electromagnetic waveguides, electron wave functions in quantum waveguides, nuclear magnetic resonance measurements of diffusive transport, construction of heat kernels in the theory of diffusion, etc. [2, 13]. For instance, vibration modes of a thin membrane are given by the Laplacian eigenfunctions under the Dirichlet boundary conditions for a fixed boundary with the drum frequencies proportional to the corresponding eigenvalues [13, 14]. Finite element methods including conforming, non-conforming, mixed finite elements, standard, discontinuous, and weak Galerkin approximations have been studied by many researchers for approximating the Laplace EVP. A review of them is given below.

Different types of non-conforming and conforming finite elements have been considered in [15, 16] to obtain and analyze the approximate solution of the Laplace EVP. In [15], Armentano and Duran have analyzed the approximation obtained for the Dirichlet eigenvalues of the Laplace operator by the piecewise linear non-conforming Crouzeix-Raviart finite element method. Later on, FuSheng and HeHu [16] have obtained the lower bound for the eigenvalues of the Laplace EVP using the two types of non-conforming finite elements which are Crouzeix-Raviart element and extended Q_1^{rot}. They have also provided an upper bounds using conforming finite elements for the eigenvalues. On the other hand, discontinuous and weak Galerkin finite element methods have been used to approximate the eigensolutions of the Laplace EVP in [17, 18]. Antonietti, Buffa, and Perugia [17] have presented and analyzed discontinuous Galerkin methods for computing the eigenvalues and eigenfunctions of the Laplace operator. In [18], Zhai, Xie, Zhang, and Zhang have analyzed the two-grid and two-space schemes for the approximation of the Laplace EVP by the weak Galerkin finite element method. Liu and Oishi [19] has applied the finite element method to bound leading Laplacian eigenvalues over polygonal domains and provided concrete eigenvalue bounds for domains of arbitrary geometry.

A comprehensive review of the standard Galerkin approximations, non-conforming approximations, and approximation of EVPs in mixed form have been given by Boffi in [12]. In this study, Boffi has also presented several examples about the approximations of the Laplace EVP using the finite element method in one-dimension, two-dimensions, and also in mixed forms. Besides, this study involves the direct proof of convergence and the Babuška-Osborn spectral theory [9], which are widely used methods for the convergence analysis of the finite element solutions of EVPs. A proof the convergence estimates for the eigensolutions of the Laplace EVP has been provided in [12] also using the direct method and the spectral theory. Later on, Xiao, Gong, Sun, and Zhang [20] have proposed a new finite element approach for the Dirichlet EVP using the abstract approximation theory for holomorphic operator functions. This new approach is different than the classic Babuška-Osborn spectral theory.

1.1.2. Finite Element Methods for the Steklov EVP

The Steklov EVP defined with the boundary condition involving the eigenvalue parameter has also various applications in many physical subjects. For instance, it is employed to model the dynamics of liquids in moving containers (sloshing problems) and problems involving a vibrating membrane with its mass concentrated along its boundary (see, e.g., [21–27]). A review of the studies about the approximation of the Steklov EVPs using finite elements methods is given below.

Bramble and Osborn [28] have studied the Galerkin method with the convergence estimates for the approximation of Steklov eigenvalues of a strongly elliptic, non-selfadjoint, second-order differential operator. Later on, Andreev and Todorov [29] has presented the isoparametric variant of the finite-element method to obtain an approximation of Steklov EVPs for second-order, selfadjoint, elliptic differential operators.

Different types of non-conforming and conforming finite elements are also used widely for finite element analysis of the Steklov EVP. Yang, Li, and Li [30] have investigated non-conforming finite element approximations of the Steklov EVP and derived the error estimates for eigenvalues and eigenfunctions. They have also provided the lower bounds for the eigenvalues using two different types of non-conforming elements. Then, Bi and Yang [31] have presented and analyzed a two-grid discretization scheme of non-conforming Crouzeix-Raviart finite element for the Steklov EVP. Later on, Li, Lin, and Xie [32] have considered four types of non-conforming finite elements and provided error estimates for the non-conforming finite element approximations of the Steklov eigenvalues both on convex and concave domains. Further, a multilevel correction scheme of non-conforming finite element has been given by Han, Li, and Xie in [33]. Besides, the conforming finite element approximation of a fourth-order Steklov EVP has been studied by Bi, Ren, and Yang in [34]. The accelerated two-grid algorithm has been presented and analyzed by Weng, Zhai, and Feng [35] to approximate the solution of the two-dimensional Steklov EVP using the finite element method.

It is of particular importance to note that, approximation of the Laplace and Steklov eigensolutions has also been studied by many researchers using other numerical methods. As on instance, Kuttler has analyzed the Laplace EVP given with Dirichlet boundary condition using the finite difference method in [36]. A boundary element method is presented and analyzed by Steinbach and Unger in [37] for solving the Dirichlet EVP for the Laplace operator. Meng, Zhang, and Mei [38] have studied the virtual element method to approximate the Laplace EVP in mixed form, and have provided the spectral approximation and the optimal convergence order for the eigenvalues using the spectral theory of compact operators. A virtual element method has also been presented and analyzed by Mora, Rivera, and Rodríguez [39] for the two-dimensional Steklov EVP. Türk [27] has proposed a dual reciprocity boundary element method to obtained and analyzed an approximate solution of the Steklov EVP.

1.1.3. Boundary Perturbations

There are numerous studies in the literature about boundary perturbations for BVPs and EVPs on smooth and non-smooth domains with several boundary conditions. A review of them is given below.

Strang and Berger [40] have considered Poisson's equation given with the Dirichlet boundary conditions on a convex plane domain and on a polygon which is inscribed the convex plane domain. They have investigated the difference between the solutions on the convex plane domain and the polygon.

Blair [41] has analyzed the difference between the solutions of second-order elliptic partial differential equations for Dirichlet boundary conditions when the boundary is perturbed. It has been considered the domain, where the given problem is originally defined, with the perturbed domain, which approximates the original domain, in this analysis. He has shown that the error between the solutions on the original domain and the perturbed domain depends only on the Euclidean distance between the original and perturbed domains.

Dauge and Helfer have investigated the variations of Neumann eigenvalues concerning a one-dimensional domain in [42]. They have derived the formula for the first variation of the eigenvalues concerning the Sturm-Liouville operators to obtain information about the variations of the eigenvalues when the width of the domain goes to zero or infinity. In [43], they have extended that formula for higher-dimensional domains. Such formulas, commonly referred to as shape derivative formulas, represent the rate of change of the eigenvalues as a given domain deforms and has been given first by Hadamard in [44] for the simple Laplacian eigenvalues under the Dirichlet boundary conditions.

In [45–47], Vanmaele and Ženíšek have investigated the effects of the boundary perturbations on the finite element analysis of second-order elliptic EVPs in the case where the approximate domains are not subdomains of the original domain. The optimum rate of convergence for the approximate eigenvalues and the approximate eigenfunctions are obtained for simple eigenvalues and corresponding eigenfunctions in [45]. The convergence of approximate eigenfunctions corresponding to the multiple eigenvalues is investigated in [46] for a second-order elliptic EVP on a concave bounded domain with homogeneous Dirichlet boundary conditions.

Kozlov has derived the formula for the first eigenvalue of the Laplace EVP, given with Dirichlet boundary condition, on arbitrary non-smooth domains in [48]. The formula has been derived for this eigenvalue considering an arbitrary perturbation of the domains in that study. It has been observed that the leading term of this formula is the same as in Hadamard's shape derivative formula, but the second term is new and is of the same order as the first one for arbitrary non-smooth domains. Besides, Kozlov and Nazarov have considered the eigenvalues of a second-order elliptic EVP given with Dirichlet boundary condition on a non-smooth domain, and have derived the formula for the eigenvalues in [49]. This formula contains terms that are not involved in Hadamard's formula.

In [50, 51], Grinfeld and Strang have shown that the eigenvalues of the Laplace EVP, given with Dirichlet boundary conditions, on N-sided regular polygon, which is inscribed in the unit disc, are represented as a series in terms of the inverse powers of sides N. This series has been obtained for the lowest simple eigenvalues using Hadamard's formula in [51]. A similar application of Hadamard's formula to the Laplace eigenvalues on an ellipse with semi-axes $1 + a$ and $1 + b$, which is a perturbation of the unit disc, also given by Fiore and Grinfeld in [52]. It has been shown that the eigenvalues on the ellipse can be given as a series in terms of powers of a and b. Besides, Grinfeld has derived shape derivative formulas for Neumann, and mixed boundary conditions, multiple eigenvalues, and second-order derivatives in [53]. The theoretical background of these studies can be found in [54]. Bandle and Wagner [55] have been interested in how functionals related to elliptic boundary and EVPs with Robin boundary conditions are affected by domain variations. They have computed the first and second domain variations for these functionals and also for the eigenvalues. The shape derivative formulas have been derived in [56] for both simple and multiple eigenvalues of the EVP with Wentzell boundary conditions. Besides, the formulas for the simple and multiple eigenvalues of the Steklov and Laplace-Beltrami EVPs are given in Appendix E of [56]. The formula has also been derived in [57, 58] for the simple eigenvalues of the Steklov EVP.

1.2. Plan of the Thesis

As a prelude, basic FEM principles are introduced for boundary value problems (BVPs) in Chapter 2. FEM analysis of the Laplace and Steklov EVPs that is provided in Chapter 3 and Chapter 4 is based on these principles.

In Chapter 3, FEM is introduced for the Laplace EVP, and this problem is analyzed on various one- and two-dimensional domains. In the one-dimensional case, the convergence the FEM solution computed using piecewise linear and quadratic basis functions to the exact solution is investigated with respect to the mesh parameter. As in the one-dimensional domain, the convergence behaviors of the FEM solutions are investigated on the square domain and the unit disc which are discretized by linear elements. Since the FEM solutions are actually obtained on discretized domains inscribed in the original domains, the influence of the boundary perturbations to the eigensolutions is investigated. Based on the study [41], the Laplace EVP is considered on the perturbed domain assumed to be placed within the original domain and approximately close to the boundary of the original domain. The convergence between the solutions of the Laplace EVP on the original domain and the perturbed domain is investigated both analytically and numerically with respect to the perturbation parameter by introducing a set of differing perturbations on a one-dimensional domain. Besides, the convergence properties of the approximate eigenvalues of the perturbed problem, which can be obtained analytically using FEM with piecewise linear basis functions to the analytical solution of the original (unperturbed) problem on a one-dimensional domain, are investigated for a fixed mesh. The computations concerning the eigenvalues are extended to two-dimensional settings by analytical considerations when the problem is considered on square and disc domains. Taylor's series expansions of the errors between the solution on the original domain and the solution on the perturbed domain are used to obtain these convergence behaviors. Moreover, based on the fact that the FEM solution of the Laplace EVP on a disc is actually obtained by discretizing a polygon inscribed in this disc, the Laplace EVP is considered on regular polygons, which are inscribed in the unit disc with an increasing number of sides. Then, it is numerically shown that both simple and multiple eigenvalues of the Laplace EVP on the polygon can be represented in terms of inverse powers of the number of its sides, as given in [51] (see also [50]) for the simple eigenvalues. Note that numerical results about the boundary perturbations are obtained using FEM on domains discretized by linear elements.

In Chapter 4, the FEM approximation of the Steklov EVP is analyzed. The convergence of the FEM solution computed using linear elements to the exact solution is investigated, considering the Steklov EVP on the unit disc. In addition, in analogy with the Laplace EVP case, a series representation in terms of inverse powers of the sides of the polygon is investigated numerically for the Steklov EVP.

Finally, Chapter 5 includes a summary of the studies carried out in the thesis and ideas for future studies.

1.3. Contributions in the Thesis

In this thesis, FEM is considered to obtain approximate solutions of both the Laplace and Steklov EVPs. It is known that the double eigenvalues are approximated by two distinct discrete ones, and the direct sum of the eigenspaces corresponding to the discrete eigenvalues should be compared to the two-dimensional eigenspace associated with the continuous eigenvalue [12]. In the present study, a procedure is proposed to obtain the linear combinations of the approximate eigenfunctions corresponding to the multiple eigenvalues. As a consequence, the convergence behavior of the linear combinations to the exact eigenfunctions is provided numerically.

Several forms of the Steklov EVP have been studied by finite element methods in the literature (e.g., in [59, 60]). On the other hand, FEM for a Steklov EVP in which the differential operator is the Laplace operator and the associated bilinear form is not coercive, has been analyzed for the first time in this thesis to the best of the author's knowledge.

The influence of the boundary perturbations on the solutions of the Laplace and Steklov EVP is also investigated in the present study. It is known that the solutions of the second-order elliptic BVPs on the perturbed domain converge to the corresponding ones on the original domain as the boundary of the perturbed domain approaches to the boundary of the original domain [41]. An analogous investigation is conducted for both FEM and exact solutions of the Laplace EVP, considering the problem on various one- and two- dimensional perturbed domains in this thesis. Theoretically, the convergence together with its order of the perturbed solution to the original solution is explored in terms of a characteristic perturbation parameter.

Furthermore, the Laplace and Steklov EVPs are considered on regular polygons which are assumed to be variations of the unit disc. In [51], it has been theoretically shown that the eigenvalues of the Laplace EVP on regular polygons corresponding to the simple eigenvalues on the unit disc can be represented as a series in terms of the inverse powers of the number of the sides. In this thesis, analogous results are numerically shown to hold for the multiple eigenvalues of the Laplace and Steklov EVPs, which are not available in the open literature to the best of the author's knowledge.

2. THE FINITE ELEMENT METHOD

In this chapter, the principles of FEM are presented for BVPs. Specifically, the function spaces where the solutions are sought, the variational formulation of BVPs, the Galerkin approach, the approximation properties of piecewise polynomials, and some theoretical results of convergence analysis are introduced.

In general, the finite element methodology consists of three basic components:

i) The given problem is converted into an equivalent form, known as the weak or variational form.

ii) Piecewise polynomials are used as trial functions to discretize the variational form.

iii) The discrete problem is represented as an algebraic form, and the solution of this form gives the approximate solution.

To begin with, the function space that have fundamental importance in the analysis of PDEs with FEM and norms on these spaces are presented. The following definitions and theorems on these spaces can be found in standard texts on finite element methods for instance [2, 61–66].

2.1. Function Spaces

2.1.1. Normed and Banach Spaces

A vector space X is called a normed space if it is defined with a norm on it. A norm on a vector space X is a mapping such that $\|\cdot\| : X \to \mathbb{R}$ with the following properties:

- $\|u + v\| \leq \|u\| + \|v\|$,
- $\|\alpha \cdot u\| = |\alpha| \cdot \|u\|$,
- $\|u\| \geq 0$, with equality if and only if $u = 0$

for all $u, v \in X$ and $\alpha \in \mathbb{R}$.

Let $\{u_i\}_{i=0}^{\infty}$ be a sequence in a normed space X. A sequence $\{u_i\}_{i=0}^{\infty}$ is called a

Cauchy sequence in a normed space X, if for all $\epsilon > 0$ there exists a positive integer n such that

$$\|u_i - u_j\| \leq \epsilon, \quad \forall i, j \geq n, \tag{2.1}$$

A sequence $\{u_i\}_{i=0}^{\infty}$ is said to be convergent if there exists $u \in X$ such that

$$\|u - u_i\| \leq \epsilon, \quad \forall i \geq n, \tag{2.2}$$

for all $\epsilon > 0$, and n is a positive integer. A normed space X is called complete if every Cauchy sequence defined in X is convergent. A Banach space is a complete normed vector space.

2.1.2. Inner Product and Hilbert Spaces

Let X and Y be normed vector spaces with the norms $\|\cdot\|_X$ and $\|\cdot\|_Y$ respectively. A linear mapping L is called a linear operator if it is defined from the normed space X into the normed space Y. The linear operator $L(\cdot)$ is bounded if there is a real number c such that

$$\|Lu\| \leq c\,\|u\|, \tag{2.3}$$

for all $u \in X$. The norm of the linear operator L is defined as

$$\|L\| = \sup_{u \in X} \frac{\|Lu\|}{\|u\|}, \tag{2.4}$$

for $u \neq 0$. A linear functional or linear form on the normed space X is a linear operator from the normed space X into the scalar field $\mathbb{R}$, and is commonly denoted by $l(\cdot) : X \to \mathbb{R}$.

A bilinear form on the normed space X is defined as a mapping from $X \times X$ to $\mathbb{R}$. A bilinear form $B(\cdot, \cdot)$ satisfies the following properties:

- $B(u + v, w) = B(u, v) + B(v, w)$,
- $B(u, v + w) = B(u, v) + B(u, w)$,
- $B(\alpha \cdot u, v) = \alpha \cdot B(u, v)$,
- $B(u, \alpha \cdot v) = \alpha \cdot B(u, v)$,

for all $u, v, w \in X$ and $\alpha \in \mathbb{R}$. A bilinear form is symmetric if

$$B(u, v) = B(v, u), \tag{2.5}$$

for all $u, v \in X$. An inner product is a symmetric bilinear form which satisfies the condition $B(u, u) \geq 0$, with equality if and only if $u = 0$ for all $u \in X$. Inner products are commonly denoted as $(\cdot, \cdot)$. An inner product defines a norm as

$$\|u\| = \sqrt{(u, u)}, \tag{2.6}$$

for all $u \in X$. Also, a bilinear form $B(\cdot, \cdot)$ defines the so called energy norm $\|u\|_E = \sqrt{B(u, u)}$. The vector space X is called an inner product space if it is defined with an inner product on it. A Hilbert space is a complete inner product space.

2.1.3. L^p Spaces

The space of p-times integrable functions L^p in a given domain Ω is defined as

$$L^p(\Omega) = \left\{ u : \Omega \to \mathbb{R} : \|u\|_{L^p(\Omega)} < \infty \right\}, \tag{2.7}$$

where

$$\|u\|_{L^p(\Omega)} = \left(\int_\Omega |u|^p \, d\Omega \right)^{1/p}, \quad 1 \leq p < \infty, \tag{2.8}$$

and

$$\|u\|_{L^\infty(\Omega)} = \sup_{x \in \Omega} |u(x)| \,. \tag{2.9}$$

The function spaces $L^p(\Omega)$ are Banach spaces for all $1 \leq p < \infty$.

2.1.4. Weak Derivatives

Let $C^k(\Omega)$ be the space of k times continuously differentiable functions on a given domain Ω. Also, let $\mathcal{D}(\Omega)$ be the space of all infinitely differentiable functions which vanish on the boundary of a given domain Ω. Space $\mathcal{D}(\Omega)$ is also named as the space of test functions.

The partial derivative is defined as

$$D^\alpha \varphi = \frac{\partial^{|a|} \varphi}{\partial x_1^{a_1} \ldots \partial x_N^{a_N}}, \quad \forall \varphi \in \mathcal{D}(\Omega), \tag{2.10}$$

where $\alpha = (\alpha_1, ..., \alpha_N)$ is a multi-index, and $|\alpha| = \sum_{i=1}^{N} \alpha_i$ is the length of α.

For $u \in C^1(\Omega)$, using integration by part gives the following identity

$$\int_\Omega \frac{\partial u}{\partial x_i} \varphi dx = -\int_\Omega \frac{\partial \varphi}{\partial x_i} u dx, \ \ \forall \varphi \in \mathcal{D}(\Omega), \tag{2.11}$$

since the test function φ vanishes on the boundary of Ω. Repeating this process yields

$$\int_\Omega D^\alpha u \varphi dx = (-1)^{|\alpha|} \int_\Omega u D^\alpha \varphi dx, \ \ \forall \varphi \in \mathcal{D}(\Omega), \tag{2.12}$$

for $u \in C^{|\alpha|}(\Omega)$.

A function is called locally integrable when it is integrable on every compact subset of its domain. In other words, a locally integrable function f is a measurable function such that $\int_K |f|$ is finite for every compact subspace K of a given domain. The space of locally integrable function is denoted by $L_{loc}(\Omega)$ and is defined as

$$L_{loc}(\Omega) = \left\{ v : v \in L^1(K), \text{ for all compact } K \subset \Omega \right\}, \tag{2.13}$$

for a given domain Ω. A given function $f \in L_{loc}(\Omega)$ has a weak derivative $D^\alpha f$ if there exists a function $g \in L_{loc}(\Omega)$ such that

$$\int_\Omega g \varphi dx = (-1)^{|\alpha|} \int_\Omega f D^\alpha \varphi dx, \ \ \forall \varphi \in \mathcal{D}(\Omega). \tag{2.14}$$

The function g is called as a weak derivative of the function f.

2.1.5. Sobolev Spaces

Sobolev spaces are essential in finite element analysis because they provide the norms to deal with the solutions of PDEs, and to be able to measure the approximation errors. Let k be a positive integer and $u \in L_{loc}(\Omega)$. Assume that all weak derivatives $D^\alpha u$ exist for $|\alpha| \leq k$. Then, the Sobolev space is defined as

$$W_k^p(\Omega) = \left\{ u \in L_{loc}(\Omega) : \|u\|_{W_k^p(\Omega)} < \infty \right\}, \tag{2.15}$$

where $\|u\|_{W_k^p(\Omega)}$ is the Sobolev norm of u defined as

$$\|u\|_{W_k^p(\Omega)} = \left(\sum_{|\alpha| \leq k} \|D^\alpha u\|_{L^p(\Omega)}^p \right)^{1/p}, \tag{2.16}$$

and for the case $p = \infty$,

$$\|u\|_{W_k^p(\Omega)} = \max_{|\alpha|\leq k} \|D^\alpha u\|_{L^\infty(\Omega)} . \tag{2.17}$$

The case $p = 2$ is the most common one encountered in finite element analysis. For this case, $\|u\|_{W_k^2(\Omega)} = \|u\|_{L^2(\Omega)}$. Since $\|u\|^2_{L^2(\Omega)} = (u, u)_{L^2(\Omega)}$, where $(u, v)_{L^2(\Omega)} = \int_\Omega uv d\Omega$, the Sobolev spaces $W_k^2(\Omega)$ are Hilbert spaces. These spaces are denoted by $H^k = W_k^2(\Omega)$. The Hilbert space $H^k(\Omega)$ denotes the space of functions that have kth derivatives and are square integrable in $L^2(\Omega)$, and is defined as

$$H^k(\Omega) = \left\{u \in L^2(\Omega) : D^k u \in L^2(\Omega)\right\} . \tag{2.18}$$

In particular, the space $H^1(\Omega)$ is defined as

$$H^1(\Omega) = \left\{u \in L^2(\Omega) : D^1 u \in L^2(\Omega)\right\} , \tag{2.19}$$

and is given with the norm

$$\|u\|_{H^1} = \left(\int_\Omega |u|^2 d\Omega + \int_\Omega |\nabla u|^2 d\Omega\right)^{1/2} , \ \forall u \in H^1(\Omega), \tag{2.20}$$

associated to the following inner product

$$(u, v)_{H^1} = \int_\Omega (uv + \nabla u \cdot \nabla v) d\Omega, \ \forall u, v \in H^1(\Omega). \tag{2.21}$$

The norm and the inner product on H^1 will be denoted as $\|\cdot\|_1$ and $(u, v)_1$ respectively. Also, the norm and the inner product on L^2 will be denoted as $\|\cdot\|$ and (u, v), respectively. The space $H_0^1(\Omega)$ denotes the space of functions in $H^1(\Omega)$ vanishing along the boundary $\partial\Omega$. The inner product and norm on H_0^1 are defined as

$$(u, v)_{H_0^1(\Omega)} = \int_\Omega (\nabla u \cdot \nabla v) d\Omega, \qquad \forall u, v \in H_0^1(\Omega), \tag{2.22}$$

$$\|u\|_{H_0^1(\Omega)} = \left(\int_\Omega |\nabla u|^2 d\Omega\right)^{1/2} , \ \forall u \in H_0^1(\Omega). \tag{2.23}$$

2.2. Variational Formulation

The variational formulation of a BVP is the starting point to discretize the problem with finite elements. As a beginning, some prerequisites and theorems about the existence and uniqueness of the solution of a variational problem are given below. Then, it is described with examples how the variational formulation of a second order elliptic PDE is obtained.

Let V be a Hilbert space and $B(\cdot,\cdot) : V \times V \to \mathbb{R}$ be a bilinear form. If there exists a positive constant c_1 such that

$$|B(u,v)| \leq c_1 \|u\|_H \|v\|_V, \ \ \forall u, v \in V, \tag{2.24}$$

then the bilinear form $B(\cdot,\cdot)$ is said to be continuous. If there exists a constant $c_2 > 0$ such that

$$B(v,v) \geq c_2 \|v\|_V^2, \ \ \forall v \in V, \tag{2.25}$$

then the bilinear form $B(\cdot,\cdot)$ is said to be coercive on V, or V-elliptic.

Let $l(\cdot) : V \to \mathbb{R}$ be a continuous linear functional. Since a continuous linear functional satisfies

$$l(v) \leq c \|v\|_V, \ \ \forall u, v \in V, \tag{2.26}$$

for a constant c, the variational form of a given BVP takes the following form: find $u \in V$ such that

$$B(u,v) = l(v), \ \ \forall v \in V. \tag{2.27}$$

The Riesz representation theorem is necessary to analyze the variational problem (2.27). A proof of this theorem is provided in [67].

Theorem 2.1: Riesz Representation Theorem: Every continuous linear functional $l(\cdot)$ *on a Hilbert space* V *can be uniquely represented as*

$$l(v) = (u,v), \ \ \forall v \in V, \tag{2.28}$$

for some $u \in V$*, where* $(\cdot,\cdot)$ *denotes the inner product on* V*.*

Since the symmetric, continuous, and coercive bilinear form is an inner product, the existence and uniqueness of a solution to variational problem (2.27) follow from the Riesz representation theorem. Hence, there is a unique solution to variational problem (2.27) for symmetric bilinear form. The extension of the Riesz representation theorem known as Lax-Milgram Lemma is required for non-symmetric bilinear forms. The Lax-Milgram Lemma and its proof can be found in many texts about finite element methods such as [67].

Theorem 2.2: Lax-Milgram Lemma: Let V be a Hilbert space with inner product $(\cdot,\cdot)$, and $B : V \times V \to \mathbb{R}$ be a bounded and coercive bilinear form on V, and $l(\cdot)$ be a linear functional on V. The following variational problem has a unique solution: find $u \in V$ such that

$$B(u,v) = l(v), \ \ \forall v \in V. \tag{2.29}$$

2.2.1. Variational Formulations of Second Order Elliptic PDEs

Assume that $\Omega \subset \mathbb{R}^d$ is an open, bounded set with boundary $\partial\Omega$. Consider the following second order elliptic partial differential equations in the general form

$$-\sum_{i,j=1}^{d} \frac{\partial}{\partial x_i}\left(a_{ij}\frac{\partial u}{\partial x_j}\right) + \sum_{i=1}^{d} b_i \frac{\partial u}{\partial x_i} + cu = f \quad \text{in}\ \Omega, \tag{2.30}$$

where a_{ij}, b_i and c are coefficients for $i, j = 1, 2, ..., d$. In the compact form, the differential equation can be written as

$$-\nabla \cdot (A\nabla u) + b \cdot \nabla u + cu = f, \tag{2.31}$$

where A is the $d \times d$ matrix with entries a_{ij}, and b is the $d \times 1$ vector with entries b_i.

The differential equation has to be considered with boundary conditions such as

- Homogenous Dirichlet boundary conditions: $u = 0$ on $\partial\Omega$,
- Inhomogeneous Neumann boundary conditions: $A\dfrac{\partial u}{\partial n} = g$ on $\partial\Omega$,
- Mixed boundary conditions: $u = 0$ on Γ_D and $A\dfrac{\partial u}{\partial n} = g$ on Γ_N.

Note that $\partial u/\partial n = n \cdot \nabla u$ is the outward normal derivative of u, and assume that $\Gamma_D \cap \Gamma_N = \emptyset$ and $\Gamma_D \cup \Gamma_N = \partial\Omega$.

Let u be the solution of (2.31) with homogenous Dirichlet boundary conditions. Multiplying (2.31) by a test function $v \in H_0^1$ and integrating by parts using Green's identity yield

$$\begin{aligned}
\int_\Omega f v d\Omega &= -\int_\Omega \nabla \cdot (A\nabla u)\, v d\Omega + \int_\Omega b \cdot \nabla u v d\Omega + \int_\Omega c u v d\Omega \\
&= -\int_\Omega A\nabla u \cdot \nabla v d\Omega + \int_\Omega b \cdot \nabla u v d\Omega + \int_\Omega c u v d\Omega \\
&= -\int_\Omega (A\nabla u \cdot \nabla v + b \cdot \nabla u v + c u v)\, d\Omega + \int_{\partial\Omega} v \cdot A\frac{\partial u}{\partial n} d\partial\Omega \\
&= -\int_\Omega A\nabla u \cdot \nabla v d\Omega + \int_\Omega b \cdot \nabla u v d\Omega + \int_\Omega c u v d\Omega.
\end{aligned} \tag{2.32}$$

The variational formulation of (2.31) is obtained as $B(u,v)=l(v)$, where

$$B(u,v)=(A\nabla u,\nabla v)+(b\cdot\nabla u,v)+(cu,v), \tag{2.33a}$$
$$l(v)=(f,v). \tag{2.33b}$$

Note that $(\cdot,\cdot)$ stands for the inner product in $L^2(\Omega)$.

If the equation (2.31) is considered with inhomogeneous Neumann boundary conditions, the variational formulation is obtained by multiplying (2.31) by a test function $v\in H^1$ and integrating by parts:

$$\begin{aligned}\int_\Omega fvd\Omega &= -\int_\Omega \nabla\cdot(A\nabla u)\,vd\Omega+\int_\Omega b\cdot\nabla uvd\Omega+\int_\Omega cuvd\Omega\\ &=-\int_\Omega A\nabla u\cdot\nabla vd\Omega+\int_\Omega b\cdot\nabla uvd\Omega\\ &+\int_\Omega cuvd\Omega+\int_{\partial\Omega} v\cdot A\frac{\partial u}{\partial n}d\partial\Omega\\ &=-\int_\Omega A\nabla u\cdot\nabla vd\Omega+\int_\Omega b\cdot\nabla uvd\Omega\\ &+\int_\Omega cuvd\Omega+\int_{\partial\Omega} gvd\partial\Omega\end{aligned} \tag{2.34}$$

for $v\in H^1$. For mixed boundary condition, same procedures result in

$$\begin{aligned}\int_\Omega fvd\Omega &= -\int_\Omega \nabla\cdot(A\nabla uv)\,d\Omega+\int_\Omega b\cdot\nabla uvd\Omega+\int_\Omega cuvd\Omega\\ &=-\int_\Omega (A\nabla u\cdot\nabla v+b\cdot\nabla uv+cuv)\,d\Omega+\int_{\partial\Omega} v\cdot A\frac{\partial u}{\partial n}d\partial\Omega\\ &=-\int_\Omega (A\nabla u\cdot\nabla v+b\cdot\nabla uv+cuv)\,d\Omega\\ &+\int_{\Gamma_D} v\cdot A\frac{\partial u}{\partial n}d\Gamma_D+\int_{\Gamma_N} v\cdot A\frac{\partial u}{\partial n}d\Gamma_N\\ &=-\int_\Omega (A\nabla u\cdot\nabla v+b\cdot\nabla uv+cuv)\,d\Omega+\int_{\Gamma_N} gvd\Gamma_N,\end{aligned} \tag{2.35}$$

where $v\in H_D^1=\{\varphi\in H^1(\Omega):\varphi|_{\Gamma_D}=0\}$.

Example 2.1: Consider Poisson's equation

$$-\Delta u=f \quad \textit{in}\ \Omega, \tag{2.36a}$$
$$u=0 \quad \textit{on}\ \partial\Omega. \tag{2.36b}$$

The variational formulation of this problem is obtained by multiplying the equation $-\Delta u=f$ *by a test function* $v\in H_0^1(\Omega)$*, and integrating by parts using the boundary* *conditions:*

$$\begin{aligned}\int_{\Omega} f v d\Omega &= -\int_{\Omega} \Delta u v d\Omega \\ &= \int_{\Omega} \nabla u \cdot \nabla v d\Omega - \int_{\partial\Omega} v \cdot \frac{\partial u}{\partial n} d\partial\Omega \\ &= \int_{\Omega} \nabla u \cdot \nabla v d\Omega.\end{aligned} \tag{2.37}$$

The variational formulation of this problem is stated as $B(u, v) = l(f, v)$*, where* $B(u, v) = (\nabla u, \nabla v)$ *and* $l(f, v) = (f, v)$ *for all* $u, v \in H_0^1$*. The coercivity of bilinear for* $B(\cdot, \cdot)$ *follows as*

$$\begin{aligned}a(u, u) &= \int_{\Omega} \nabla u \cdot \nabla u d\Omega \\ &\geq C \left\|\nabla u\right\|^2 \\ &= C \left\|u\right\|_{H_0^1}^2,\end{aligned} \tag{2.38}$$

where C *is a positive constant. The continuity of* $B(\cdot, \cdot)$ *follows from the Cauchy-Schwarz inequality as*

$$\begin{aligned}a(u, v) &= \int_{\Omega} \nabla u \cdot \nabla v d\Omega \\ &\leq \left\|\nabla u\right\| \left\|\nabla v\right\| \quad \textit{(Cauchy-Schwarz inequality)} \\ &\leq \left\|u\right\|_{H_0^1} \left\|v\right\|_{H_0^1}.\end{aligned} \tag{2.39}$$

The continuity of $l(\cdot)$ *follows from the Cauchy-Schwarz and Poincaré inequalities as*

$$\begin{aligned}l(f, v) &= \int_{\Omega} f v d\Omega \\ &\leq \left\|f\right\| \left\|\nabla v\right\| \qquad \textit{(Cauchy-Schwarz inequality)} \\ &\leq C \left\|f\right\| \left\|\nabla v\right\| \quad \textit{(Poincaré inequality)} \\ &\leq C \left\|f\right\| \left\|v\right\|_{H_0^1},\end{aligned} \tag{2.40}$$

where C *is a positive constant. Thus, it is concluded that the variational problem has a unique solution according to the Lax-Milgram lemma.*

2.3. Galerkin Method

The Galerkin method is used for converting a given BVP into a discrete problem based on the variational form of the problem. From the Lax-Milgram Lemma, it is known that the solution $u \in V$ to the variational form (2.27) exists and is unique. Let V_h be a finite- dimensional subspace of V. Since V_h is finite- dimensional, it has a basis $\{\phi_1, \phi_2, \ldots \phi_n\}$ such that $V_h = \text{span}\,\{\phi_1, \phi_2, \ldots \phi_n\}$, and $v_h \in V_h$ can be represented as

$$v_h = \sum_{i=1}^{n} \alpha_i \phi_i, \quad i = 1, 2, \ldots, n, \tag{2.41}$$

where α is an unknown vector. The aim of the Galerkin method is to solve a given equation in V_h. Consider the following aforementioned variational form

$$B(u, v) = l(v), \quad \forall v \in V, \tag{2.42}$$

where B is a bilinear form on the Hilbert space V, and l is a continuous linear functional on V. The variational form becomes

$$B(u_h, v_h) = l(v_h), \quad \forall v_h \in V_h \tag{2.43}$$

in V_h. Since $\{\phi_1, \phi_2, \ldots \phi_n\}$ is a basis for V, the discrete form (2.43) can be represented as

$$B(u_h, \phi_i) = l(\phi_i), \quad \forall v_h \in V_h. \tag{2.44}$$

Inserting the linear combination (2.41) into the discrete form (2.44) results in

$$\sum_{i=1}^{n} \alpha_i B(\phi_i, \phi_j) = l(\phi_j), \quad i = 1, 2, \ldots, n, \tag{2.45}$$

which is a system of n linear algebraic equations for the unknowns $\alpha_i, i = 1, 2, \ldots, n$.

In the matrix form (2.45) can be written as

$$K\alpha = b, \tag{2.46}$$

where K is the so called stiffness matrix with the entries $k_{i,j} = B(\phi_i, \phi_j)$, and b is the load vector with the entries $b_j = l(\phi_j)$. Solving the linear system (2.46) for the unknown vector α gives the approximate solution $u_h = \sum_{i=1}^{n} \alpha_i \phi_i$.

2.3.1. Galerkin Orthogonality

It is known that the solution u satisfies the conditions (2.27) and in particular,

$$B(u, v_h) = l(v_h), \quad \forall v_h \in V_h. \tag{2.47}$$

The Galerkin approximation $u_h \in V_h$ also satisfies the conditions (2.43). Subtracting (2.43) from (2.47) yields

$$B(u - u_h, v_h) = 0, \quad \forall v_h \in V_h. \tag{2.48}$$

This means that the error $e = u - u_h$ is orthogonal to V_h. The Galerkin orthogonality gives the best approximation result in the energy norm a result known as Cea's lemma. This results known as Cea's lemma and its proof can be found e.g., in [67].

Theorem 2.3: Cea's Lemma: The error e satisfies the best approximation result

$$\|e\|_E \leq \frac{C_a}{m} \|u - v\|_E, \quad \forall v \in V_h. \tag{2.49}$$

2.4. Piecewise Polynomials

FEM is stated as the Galerkin method with a subspace of piecewise polynomial functions. In this section, piecewise polynomials used as a basis functions to discretize a variational form are introduced.

2.4.1. One Dimensional Piecewise Polynomials

A polynomial in one-dimension with degree n has the following form

$$p(x) = \alpha_0 + \alpha_1 x + \alpha_2 x^2 + \cdots + \alpha_n x^n, \tag{2.50}$$

where α_i are constants for $i = 0, 1, \ldots, n$. The space of the nth degree polynomials is denoted as $P^n(\Omega)$ on an interval Ω, and is defined as

$$P^n(\Omega) = \{p : p(x) = \alpha_0 + \alpha_1 x + \cdots + \alpha_n x^n, \; x \text{ on } \Omega, \; \alpha_i \in \mathbb{R}\}. \tag{2.51}$$

The space of linear polynomials and quadratic polynomials are denoted as

$$P^1(\Omega) = \{p : p(x) = \alpha_0 + \alpha_1 x, \; x \text{ on } \Omega, \; \alpha_i \in \mathbb{R}\}, \tag{2.52}$$

$$P^2(\Omega) = \left\{p : p(x) = \alpha_0 + \alpha_1 x + \alpha_2 x^2, \; x \text{ on } \Omega, \; \alpha_i \in \mathbb{R}\right\}. \tag{2.53}$$

To define piecewise polynomials over a domain, it is necessary to partition the domain into subdomains. The polynomials defined on each subdomain are called piecewise polynomials. The collection of subdomains is commonly referred as a mesh.

Let $\Omega = [a, b]$ be an interval. A partition of Ω into n subintervals $I_i = [x_{i-1}, x_i]$ with length $h_i = x_i - x_{i-1}$ is defined as

$$I : a = x_0 < x_1 < x_2 < \cdots < x_{n-1} < x_n = b, \tag{2.54}$$

with $n+1$ nodal points $\{x_i\}_{i=0}^{n}$. The space of continuous piecewise linear functions is defined as

$$P_h^1(\Omega) = \left\{ v : v \in C^0(I),\;\; v|_{I_i} \in P^1(I_i) \right\}, \tag{2.55}$$

where C^0 is the space of all continuous functions on I. Any function v can be determined by its nodal values $\{v(x_i)\}_{i=0}^{n}$. A basis ϕ_i for P_h^1 satisfies the condition

$$\phi_i(x_j) = \begin{cases} 1; & i = j \\ 0; & i \neq j \end{cases} \qquad i, j = 0, 1, \ldots, n, \tag{2.56}$$

and is called a Lagrange basis or a nodal basis. These basis functions are also called as hat functions or shape functions, because of their shapes, see Figure 2.1.

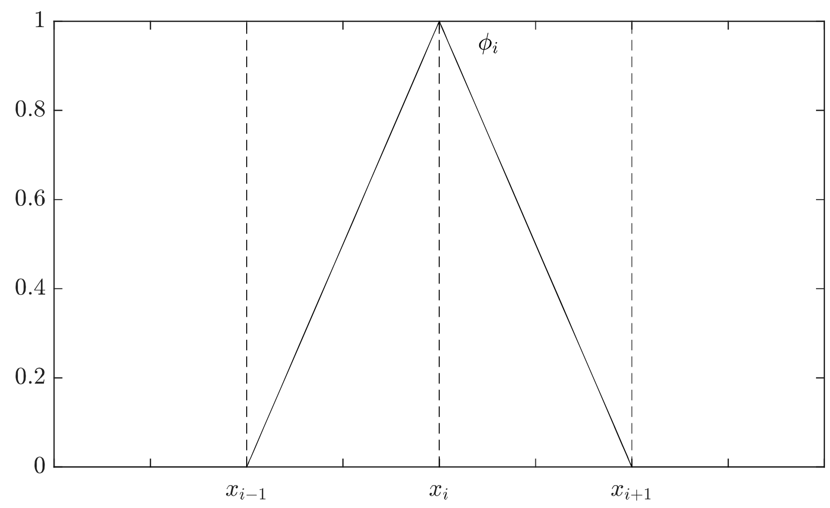

Figure 2.1: Hat function ϕ_i.

Each hat function takes a unit value at its own node x_i whereas zero at other nodes. So, the hat function ϕ_i has non-zero value only on the intervals I_i and I_{i+1} which contain the node x_i. Besides, the hat functions have the following explicit expression

$$\phi_i(x) = \begin{cases} \dfrac{(x - x_{i-1})}{(x_i - x_{i-1})} & \text{if} \quad x_{i-1} \leq x < x_i, \\ \dfrac{(x_{i+1} - x)}{(x_{i+1} - x_i)} & \text{if} \quad x_i \leq x < x_{i+1}, \\ 0 & \text{otherwise}, \end{cases} \tag{2.57}$$

for $i, j = 0, 1, \ldots, n$.

The quadratic basis function is defined as the following two types of basis functions:

$$\phi_i(x) = \begin{cases} 1 + 3\left(\dfrac{x - x_i}{h_i}\right) + 2\left(\dfrac{x - x_i}{h_i}\right)^2 & \text{if} \quad x \in [x_{i-1}, x_i], \\ 1 - 3\left(\dfrac{x - x_i}{h_i}\right) + 2\left(\dfrac{x - x_i}{h_i}\right)^2 & \text{if} \quad x \in [x_i, x_{i-1}], \end{cases} \tag{2.58}$$

and,

$$\phi_{i+1/2}(x) = 4\left[\frac{x - x_i}{h_i} - \left(\frac{x - x_i}{h_i}\right)^2\right]. \tag{2.59}$$

The first type (2.58) is a piecewise-quadratic polynomial, and it satisfies the usual condition (2.56), also vanishes at two interior points $x_{i\pm1/2}$. The second type (2.59) is a quadratic polynomial which takes on the value one at $x_{i+1/2}$ and vanishes at the other nodes. Figure 2.2 illustrates a quadratic basis function.

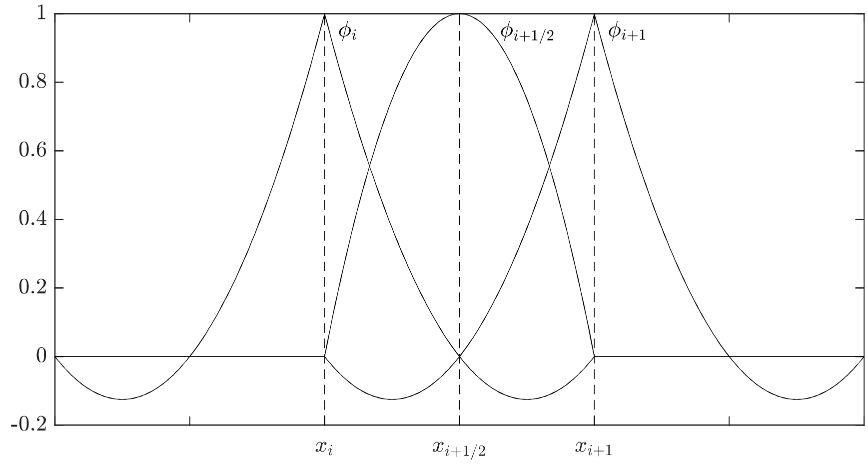

Figure 2.2: Piecewise quadratic basis function.

2.4.2. Two Dimensional Piecewise Polynomials

A polynomial in two-dimension with degree n has the following form

$$p(x, y) = \alpha_{00} + \alpha_{10}x + \alpha_{01}y + \alpha_{20}x^2 + \alpha_{11}xy + \alpha_{02}y^2 + \cdots + \alpha_{0n}y^n, \quad (2.60)$$

where α_{ij} are constants for $i, j = 0, 1, \ldots, n$. The space of the nth degree polynomials is denoted as $\tilde{P}^n(\Omega)$ on a given domain Ω, and is defined as

$$\tilde{P}^n(\Omega) = \{p : p(x, y),\ x, y \text{ on } \Omega,\ \alpha_{ij} \in \mathbb{R}\}. \quad (2.61)$$

The space of linear polynomials is defined as

$$\tilde{P}^1(\Omega) = \{p : p(x, y) = \alpha_{00} + \alpha_{10}x + \alpha_{01}y,\ x, y \text{ on } \Omega,\ \alpha_{ij} \in \mathbb{R}\}, \quad (2.62)$$

on a domain Ω. The most common meshes in two-dimension are triangulations. Let $\Omega \subset \mathbb{R}^2$ be a bounded two-dimensional domain with smooth boundary $\partial\Omega$, and let $\mathcal{T}$ be a triangulation or mesh of Ω. $\mathcal{T}$ is a set of triangles T_i which are called finite elements. The domain Ω is expressed as the union of triangles such that $\Omega = \bigcup_{i=1}^{N_e} T_i$, where N_e denotes the number of triangles (elements) in the mesh. Every edge of T_i is either a part of the boundary $\partial\Omega$, or the edge of another element. The corners of the triangles are called the nodes. These nodes will be denoted as P_i. Figure 2.3 illustrates triangular meshes of two polygonal domains, namely, a square and a hexagon.

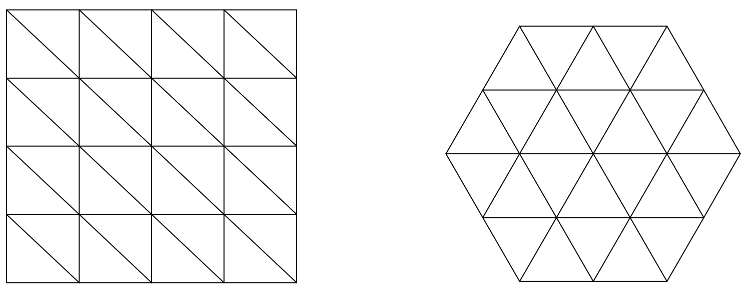

(a) Triangulation of a square. (b) Triangulation of a hexagon.

Figure 2.3: Triangular meshes of two polygonal domains.

To describe the shape of a triangle T_i, the largest disc contained in T_i can be compared with the diameter of T_i. The diameter of a set S defined as [63]

$$\text{diam}(S) = \sup\{d(z_1, z_2) : \ z_1, z_1 \in S\}, \quad (2.63)$$

where $d(z_1, z_2)$ denotes the all distances between z_1 and z_2. For a triangle T_i, diam(T_i) states the length of the longest side of T_i. The diameter of the largest disc involved in T_i is denoted by d_T. The triangulation $\mathcal{T}$ is called non-degenerate if there exists a positive constant ϵ supplying the following condition

$$\frac{d_T}{\text{diam}(T_i)} \geq \epsilon, \forall T_i \in \mathcal{T} \text{ for all } h, \tag{2.64}$$

where h is the maximum diameter of any triangle in $\mathcal{T}$, and will be denoted as h_{max} in the Chapter 3 and Chapter 4.

Let $\tilde{P}_h^1$ be the space of all continuous piecewise linear polynomials, defined as

$$\tilde{P}_h^1(\Omega) = \left\{ v : v \in C^0(\Omega),\ v|_{T_i} \in P^1(T_i) \right\}. \tag{2.65}$$

The polynomial v can be determined by its nodal values $\{v(P_i)\}_{i=1}^{n_p}$, where n_p denotes the number of nodes. The basis ϕ_i satisfying the condition given in (2.56) at the nodes P_i is a basis for P_h^1 as in one-dimensional case. The linear polynomial can be given as

$$\phi_i = 1 - \frac{x}{h} - \frac{y}{h}, \quad \phi_{i+1} = \frac{x}{h}, \quad \phi_{i+2} = \frac{y}{h}, \tag{2.66}$$

for the standard triangle given in Figure 2.4a.

The space of quadratic functions is defined as

$$\begin{aligned} \tilde{P}^2(\Omega) = \{ p : p(x,y) = \alpha_{00} + \alpha_{10}x + \alpha_{01}y + \alpha_{20}x^2 + \alpha_{11}xy + \alpha_{02}y^2 \ , \\ x, y \text{ on } \Omega,\ \alpha_{ij} \in \mathbb{R} \} \end{aligned} \tag{2.67}$$

on a two dimensional domain Ω. If three more nodes are added to the triangle T, the quadratic function can be determined. These nodes are commonly located at the midpoints of the three edges of the triangle T. Figure 2.4b and Figure 2.4c illustrate the triangular meshes which are constructed by linear and quadratic elements, respectively.

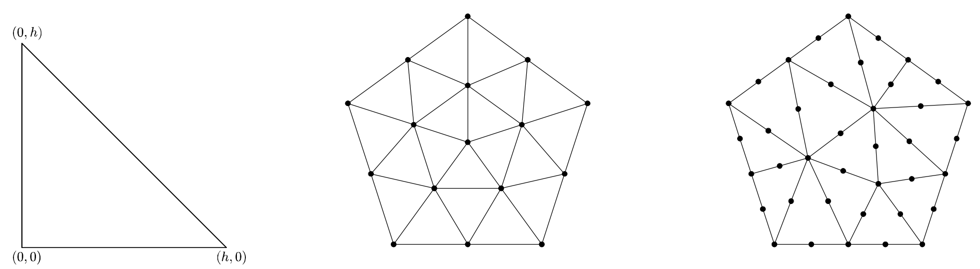

(a) The standard triangle. (b) Linear elements. (c) Quadratic elements.

Figure 2.4: The standard triangle and triangular meshes constructed by linear and quadratic elements.

2.5. Convergence Analysis of FEM

From Cea's Lemma, it is known that FEM gives the best approximation in the energy norm to the exact solution of the given BVP. As the mesh size goes to zero, to prove that the approximate solution converges to the exact solution, it is necessary to understand how well piecewise polynomials can approximate a given function. For this purpose, fundamental theorems about the approximation with finite elements are given in this section. These theorems and their proofs can be found in standard texts for instance [62, 63, 67].

2.5.1. Approximation by Linear Elements

Consider the use of continuous piecewise linear polynomials. Let u_I be the piecewise linear interpolant of u such that

$$u_I = \sum_{i=1}^{n_p} u(P_i)\phi_i, \tag{2.68}$$

where P_i and n_p denotes the nodal points and number of the nodal points respectively.

Since the function u_I has the same nodal values with u at the nodes N_i, is called as interpolant of u. If u_h is the best approximation to u from the approximating subspace in FEM, then it satisfies

$$\|u - u_h\|_E \leq \|u - u_I\|_E \, . \tag{2.69}$$

The following theorem introduces bounds on the approximation errors in $L^2(\Omega)$ and $H^1(\Omega)$ defined by the L^2- and H^1-norms. A proof of this theorem is provided in [62] (see also [63]).

Theorem 2.4: Let $\mathcal{T}$ be a non-degenerate family of triangulation of a polygonal domain $\Omega \subset \mathbb{R}^2$, and suppose $u \in H^2(\Omega)$. Then there exists a constant C depending on Ω and the value ρ in (2.64) *such that*

$$\|u - u_I\| \leq Ch^2 \, |u|_{H^2(\Omega)} \, , \tag{2.70}$$

and

$$\|u - u_I\|_1 \leq Ch \, |u|_{H^2(\Omega)} \, , \tag{2.71}$$

where $|u|_{H^2(\Omega)}$ *is the semi-norm defined as*

$$|u|^2_{H^2(\Omega)} = \int_\Omega \left(\left|\frac{\partial^2 u}{\partial x^2}\right|^2 + 2\left|\frac{\partial^2 u}{\partial x \partial y}\right|^2 + \left|\frac{\partial^2 u}{\partial y^2}\right|^2 \right). \tag{2.72}$$

2.5.2. Approximation by Higher-Order Elements

Consider the use of nth degree piecewise polynomials. Let u_I be the piecewise polynomial interpolant of degree n of u which satisfies (2.68).

The following theorem introduces bounds on the approximation errors in $L^2(\Omega)$ and $H^1(\Omega)$ defined by the L^2- and H^1-norms. A proof of this theorem is provided in [62] (see also [63]).

Theorem 2.5: Let $\mathcal{T}$ *be a non-degenerate family of triangulation of a polygonal domain* $\Omega \subset \mathbb{R}^2$, *and suppose* $u \in H^{n+1}(\Omega)$. *Then there exists a constant* C *depending on* Ω *and the value* ρ *in* (2.64) *such that*

$$\|u - u_I\| \leq Ch^{n+1} |u|_{H^{n+1}(\Omega)}, \tag{2.73}$$

and

$$\|u - u_I\|_1 \leq Ch^{n} |u|_{H^{n+1}(\Omega)}, \tag{2.74}$$

where $|u|_{H^{n+1}(\Omega)}$ *is the semi-norm defined as*

$$|u|^2_{H^2(\Omega)} = \sum_{i+j=n+1} \int_\Omega \left|\frac{\partial^{n+1} u}{\partial x^i \partial y^j}\right|^2. \tag{2.75}$$

3. LAPLACE EIGENVALUE PROBLEM

In this chapter, the Laplace EVP given by Dirichlet boundary conditions is analyzed using FEM on one-dimensional, square, and disc domains. Since FEM solutions of the EVPs are obtained on discretized domains replaced within these original domains, the Laplace EVP is considered on the perturbed domains which are assumed to be inscribed into these original domains and whose boundaries are approximately close to the boundaries of the original domains. In this way, the effects of this boundary perturbation on the exact and the FEM solutions of the Laplace EVP are investigated both analytically and numerically.

Assume that Ω is a domain in $\mathbb{R}^d$ where $d = 1, 2, 3$, with boundary $\partial\Omega$. The Laplace EVP is defined as: find eigenvalues $\lambda \in \mathbb{R}$, and eigenfunctions $u \neq 0$ such that

$$-\Delta u = \lambda u \quad \text{in } \Omega, \tag{3.1a}$$

$$u = 0 \qquad \text{on } \partial\Omega, \tag{3.1b}$$

where Δ is the Laplace operator. Here u and λ comprise the eigensolution of (3.1), which can be obtained analytically on one-dimensional, square, and disc domains. Since the convergence behavior of the FEM solution to the exact solution of the Laplace EVP will be investigated in this chapter, it is explained how exact solutions are obtained on these domains.

1D- Case

Assume that the first original domain Ω_1 is the interval $[0, \pi]$. For this one-dimensional domain, the Laplace EVP is written as

$$-u'' = \lambda u \quad \text{in} \quad \Omega_1, \tag{3.2a}$$

$$u(0) = u(\pi) = 0. \tag{3.2b}$$

Let σ_i, $i = 1, 2$, be the roots of the characteristic polynomial of (3.2a) such that

$$\sigma^2 + \lambda = 0 \Rightarrow \sigma_{1,2} = \mp\sqrt{\lambda} i. \tag{3.3}$$

When $\lambda \leq 0$, the Laplace EVP has the trivial solution. Indeed, if it is assumed that $\lambda < 0$, the general solution of (3.2a) is written as

$$u(x) = c_1 e^{\sqrt{\lambda}x} + c_2 e^{-\sqrt{\lambda}x}, \tag{3.4}$$

and the only solution that satisfies the boundary conditions (3.2b) is $u(x) = 0$, which corresponds to the values of $c_1 = c_2 = 0$. In the case of $\lambda = 0$, the general solution of (3.2a) is $u(x) = c_1 + c_2 x$, and the trivial solution $u(x) = 0$ is obtained when the boundary conditions are applied. On the other hand, when $\lambda > 0$, the general solution of (3.2a) is written as

$$u(x) = c_1 \cos(\sqrt{\lambda}x) + c_2 \sin(\sqrt{\lambda}x), \tag{3.5}$$

and the condition $u(0) = 0$ requires $c_1 = 0$. From the condition $u(\pi) = 0$, it is obtained that

$$c_2 \sin(\sqrt{\lambda}x) = 0. \tag{3.6}$$

The eigenvalues different from zero that satisfy (3.6) are

$$\lambda^{(k)} = k^2, \tag{3.7}$$

and the corresponding eigenfunctions are

$$u^{(k)}(x) = c \sin(kx), \tag{3.8}$$

where $k \in \mathbb{Z}^+$, and c is an arbitrary constant.

2D- Case: Square

Assume that the second original domain Ω_2 is the square $[0, \pi] \times [0, \pi]$. For this two-dimensional domain, the Laplace EVP is written as

$$-u_{xx} - u_{yy} = \lambda u \quad \text{in } \Omega_2, \tag{3.9a}$$

$$u(0, y) = 0, \tag{3.9b}$$

$$u(\pi, y) = 0, \tag{3.9c}$$

$$u(x, 0) = 0, \tag{3.9d}$$

$$u(x, \pi) = 0. \tag{3.9e}$$

Suppose that the solution of (3.9a) is in the form of

$$u(x, y) = X(x)Y(y). \tag{3.10}$$

Substituting the partial derivatives of u obtained from (3.10) into (3.9a) and dividing both sides by XY yield

$$\frac{X''}{X}+\frac{Y''}{Y}+\lambda=0. \tag{3.11}$$

If it is assumed that $\lambda=\lambda_x+\lambda_y$ such that $\lambda_x=-\frac{X''}{X}$ and $\lambda_y=-\frac{Y''}{Y}$, two ordinary differential equations are obtained as

$$X''+\lambda_x X=0, \tag{3.12a}$$

$$Y''+\lambda_y Y=0. \tag{3.12b}$$

From the 1D-Case, it is known that (3.12a) and (3.12b) have trivial solutions, when $\lambda_x\leq 0$ and $\lambda_y\leq 0$. This means that (3.9a) has trivial solution in the cases of $\lambda_x\leq 0$ and $\lambda_y\leq 0$. When $\lambda_x>0$ and $\lambda_y>0$, the general solutions of (3.12a) and (3.12b) are written as

$$X(x)=c_1\cos(\sqrt{\lambda_x}x)+c_2\sin(\sqrt{\lambda_x}x), \tag{3.13a}$$

$$Y(y)=c_3\cos(\sqrt{\lambda_y}y)+c_4\sin(\sqrt{\lambda_y}y), \tag{3.13b}$$

respectively. From the conditions (3.9b) and (3.9d), it is obtained that $c_1=c_3=0$. On the other hand, applying the conditions (3.9c) and (3.9e) to (3.13a) and (3.13b) results in

$$c_2\sin(\sqrt{\lambda_x}x)=0, \tag{3.14a}$$

$$c_4\sin(\sqrt{\lambda_y}y)=0, \tag{3.14b}$$

where c_2 and c_4 are arbitrary constants. Thus, the non-zero values of λ_x and λ_y are obtained as $\lambda_x=m^2$ and $\lambda_y=n^2$, where m and n are positive integers. Since $\lambda=\lambda_x+\lambda_y$, and $u(x,y)=X(x)Y(y)$, the eigenvalues and the corresponding eigenfunctions of (3.9) are obtained as $\lambda^{(m,n)}=m^2+n^2$ and $u^{(m,n)}(x,y)=c\sin(mx)\sin(ny)$ respectively, where $m,n\in\mathbb{Z}^+$ and c is an arbitrary constant.

2D- Case: Disc

Assume that the third original domain Ω_3 is a disc with radius a. The two-dimensional Laplace EVP must be written in the polar coordinates (r,θ) to obtain its solution on the disc. Using the transformations $x=r\cos\theta$, $y=r\sin\theta$, and the chain rule gives

$$\frac{\partial^2 u}{\partial r^2} = \cos^2\theta \frac{\partial^2 u}{\partial x^2} + 2\cos\theta\sin\theta \frac{\partial^2 u}{\partial x \partial y} + \sin^2\theta \frac{\partial^2 u}{\partial y^2}, \tag{3.15a}$$

$$\begin{aligned}\frac{\partial^2 u}{\partial \theta^2} &= -r\left(\cos\theta \frac{\partial u}{\partial x} + \sin\theta \frac{\partial u}{\partial y}\right) \\ &\quad + r^2\left(\sin^2\theta \frac{\partial^2 u}{\partial x^2} + 2\cos\theta\sin\theta \frac{\partial^2 u}{\partial x \partial y} + \cos^2\theta \frac{\partial^2 u}{\partial y^2}\right),\end{aligned} \tag{3.15b}$$

where $r = \sqrt{x^2+y^2}$ and $\theta = \arctan \frac{y}{x}$. Dividing both sides of (3.15b) by r^2 and summation with (3.15a) side by side yields

$$u_{xx} + u_{yy} = u_{rr} + \frac{1}{r}u_r + \frac{1}{r^2}u_{\theta\theta}. \tag{3.16}$$

Thus, the two-dimensional Laplace EVP is written as

$$-u_{rr} - \frac{1}{r}u_r - \frac{1}{r^2}u_{\theta\theta} = \lambda u. \tag{3.17}$$

As in the square case, separation of variables gives the solution of the Laplace EVP in polar coordinates. Assume that $u(r,\theta) = R(r)\Theta(\theta)$ is the solution of (3.17). Substitution of partial derivatives into (3.17) and dividing both sides by $R\Theta$ yield

$$-\frac{R''}{R} - \frac{1}{r}\frac{R'}{R} - \frac{1}{r^2}\frac{\Theta''}{\Theta} = \lambda. \tag{3.18}$$

Multiplying both sides of (3.18) by r^2 and moving all of the terms dependent on R to one side and all of the terms dependent on Θ to the other side yields

$$\lambda r^2 + \frac{r^2 R''}{R} + \frac{rR'}{R} = -\frac{\Theta''}{\Theta}. \tag{3.19}$$

Both sides of (3.19) must be equal a constant μ for these two expressions to be equal for all possible values of r and θ. Thus, it is obtained that

$$\Theta'' + \mu\Theta = 0, \tag{3.20a}$$

$$R'' + \frac{1}{r}R' + \left(\lambda - \frac{\mu}{r^2}\right)R = 0. \tag{3.20b}$$

First, consider the equation that depends on θ. The boundary conditions to be applied to (3.20a) state that the function $\Theta(\theta)$ and its first derivative with respect to θ are periodic such that

$$\Theta(0) = \Theta(2\pi), \tag{3.21a}$$

$$\Theta'(0) = \Theta'(2\pi). \tag{3.21b}$$

Let σ_i, $i = 1, 2$, be the roots of the characteristic polynomial of (3.20a) such that

$$\sigma^2 + \mu = 0 \Rightarrow \sigma_{1,2} = \mp\sqrt{\mu}i. \tag{3.22}$$

In the case of $\mu < 0$, the general solution of (3.20a) is obtained as

$$\Theta(\theta) = c_1 e^{\sqrt{\mu}\theta} + c_2 e^{-\sqrt{\mu}\theta}. \tag{3.23}$$

Applying the conditions (3.21a) and (3.21b) gives the trivial solution $\Theta(\theta) = 0$, which corresponds to the values of $c_1 = c_2 = 0$. If it is assumed that $\mu \geq 0$ and $\mu = p^2$, the solution of (3.20a) is written as

$$\Theta(\theta) = c_1 \cos(p\theta) + c_2 \sin(p\theta), \tag{3.24}$$

where $p = 0, 1, 2, \ldots$.

Now, consider Equation (3.20b) dependent on radius r. By changing the variables such that $\rho = \sqrt{\lambda}r$, Equation (3.20b) is written in terms of a function $S(\rho) = R(\rho/\sqrt{\lambda})$. Thus, the derivatives of $R(r)$ are obtained as $R' = \sqrt{\lambda}S'$ and $R'' = \lambda S''$. Substituting of these derivatives into (3.20b) and multiplying both sides of (3.20b) by r^2 gives

$$\rho^2 S'' + \rho S' + \left(\rho^2 - p^2\right)\rho = 0, \tag{3.25}$$

where $p^2 = \mu$. Equation (3.25) is a well-known ordinary differential equation, and is called as Bessel's equation of order p. To solve this equation, it is assumed that there is a solution such that

$$S(\rho) = \rho^\alpha \sum_{k=0}^{\infty} a_k \rho^k, \tag{3.26}$$

where $a_0 \neq 0$. Substituting (3.26) and its derivatives into (3.25) results in

$$\begin{aligned}\rho^2 \sum_{k=0}^{\infty} a_k(k+\alpha)(k+\alpha-1)\rho^{k+\alpha-2} &+ \rho \sum_{k=0}^{\infty} a_k(k+\alpha)\rho^{k+\alpha-1} \\ &+ (\rho^2 - p^2)\sum_{k=0}^{\infty} a_k s^{k+\alpha} \equiv 0.\end{aligned} \tag{3.27}$$

After the necessary index shifting and simplification process, (3.27) is written as

$$\begin{aligned}(\alpha^2 - p^2)a_0 s^\alpha &+ \left[(\alpha+1)^2 - p^2\right] a_1 s^{\alpha+1} \\ &+ \sum_{k=2}^{\infty}\left[\left((\alpha+k)^2 - p^2\right) a_k + a_{k-2}\right]\rho^{\alpha+k} = 0.\end{aligned} \tag{3.28}$$

Since $a_0 \neq 0$, Equation (3.28) requires $\alpha^2 - p^2 = 0$. When the roots of this equation are considered, a_1 must be zero since the coefficient of a_1 is not zero. The other coefficients are computed by using the recurrence relation

$$a_k = \frac{-1}{(\alpha + k)^2 - p^2} a_{k-2}, \quad k \geq 2, \tag{3.29}$$

that is obtained by equating the coefficient of $\rho^{\alpha+k}$ to zero. Since $a_1 = 0$, a_k must be zero for all odd k according to the recurrence relation. The sequence corresponding to the even k is obtained as

$$a_{2j} = \frac{(-1)^j}{j! \cdot 2^j (p+1)(p+2) \cdots (p+j)} a_0, \tag{3.30}$$

where $j = 1, 2, \ldots$. If it is assumed that $a_0 = \frac{1}{2^p p!}$ for convenience, (3.30) is written as

$$a_{2j} = \frac{(-1)^j}{2^{2j+p} j! \, (p+j)!}, \tag{3.31}$$

where $j = 1, 2, \ldots$. Substituting (3.31) into (3.26) yields

$$S(\rho) = \rho^\alpha \sum_{j=0}^{\infty} \frac{(-1)^j}{j! \, (p+j)!} \left(\frac{\rho}{2}\right)^{2j+p}. \tag{3.32}$$

Function (3.32) is known as Bessel's function of order p, and is denoted by $J_p(\rho)$. Thus, the solution of Equation (3.20b) is obtained as $R(r) = S(\rho) = J_p(\rho)$. The boundary condition to be applied to (3.20b) is $R(a) = 0$, where a is the radius of the disc. This means that $J_p(\rho) = 0$. Assume that $\rho^{(p,q)}$ is the qth root of $J_p(\rho)$. Since $\rho = \sqrt{\lambda} r$ and $u(r,\theta) = R(r)\Theta(\theta)$, the eigenvalues and the corresponding eigenfunctions of the Laplace EVP are obtained as

$$\lambda^{(p,q)} = \left(\frac{\rho^{(p,q)}}{a}\right)^2, \tag{3.33a}$$

$$u^{(p,q)}(r,\theta) = J_p\left(\frac{\rho^{(p,q)} r}{a}\right) \left[c_1 \cos(p\theta) + c_2 \sin(p\theta)\right], \tag{3.33b}$$

where c_1 and c_2 are arbitrary constants.

3.1. The Finite Element Method for the Laplace EVP

In general, it may be difficult or even impossible to obtain the exact solution of the Laplace EVP, unlike the cases given in the previous section. In such cases, the solution must be approximated numerically. To this end, FEM is introduced for the Laplace EVP in this section. As described in Chapter 2, the basic idea of FEM is to obtain the variational formulation of the Laplace EVP and the approximate solution, which is an approximation to the exact solution from the finite-dimensional subspace constructed by piecewise polynomials.

The variational formulation of the Laplace EVP is obtained by multiplying Equation (3.1a) by a test function v, and integrate by parts using the boundary conditions (3.1b) such that

$$\begin{aligned} \lambda \int_\Omega uv d\Omega &= -\int_\Omega \Delta uv d\Omega \\ &= \int_\Omega \nabla u \cdot \nabla v d\Omega - \int_{\partial\Omega} uv d\partial\Omega \\ &= \int_\Omega \nabla u \cdot \nabla v d\Omega \end{aligned} \tag{3.34}$$

for all $u, v \in H_0^1(\Omega)$. Thus, the variational formulation of the Laplace EVP (3.1) is obtained as

$$\int_\Omega \nabla u \cdot \nabla v d\Omega = \lambda \int_\Omega uv d\Omega. \tag{3.35}$$

Let $V_h = \text{span}\{\phi_1, \phi_2, \ldots \phi_N\}$ be a finite dimensional subspace of H_0^1, where ϕ_i are piecewise polynomials for $i = 1, 2, \ldots, N$. The discretization of (3.35) is stated as

$$\int_\Omega \nabla u_h \cdot \nabla v_h d\Omega = \lambda_h \int_\Omega u_h v_h d\Omega \tag{3.36}$$

for all $v_h \in V_h$. According to the Galerkin method, we seek the eigenvalues $\lambda_h \in \mathbb{R}$, and the eigenfunctions $u_h = \sum_{i=1}^N \alpha_i \phi_i \in V_h$, where α_i are the unknowns, of the system

$$\int_\Omega \nabla u_h \cdot \nabla \phi_i d\Omega = \lambda_h \int_\Omega u_h \phi_i d\Omega. \tag{3.37}$$

Inserting $u_h = \sum_{i=1}^N \alpha_i \phi_i \in V_h$ into Equation (3.37) results in

$$\sum_{i=1}^N \alpha_i \int_\Omega \nabla \phi_i \cdot \nabla \phi_j d\Omega = \lambda_h \sum_{i=1}^N \alpha_i \int_\Omega \phi_i \phi_j d\Omega, \quad i, j = 1, 2, \ldots, N, \tag{3.38}$$

which consists of N linear algebraic equations for the unknowns α_i. In the matrix form, (3.38) can be written as

$$K\alpha = \lambda_h M\alpha, \tag{3.39}$$

which is an $N \times N$ linear system for the unknown vector $\alpha = [\alpha_1, \alpha_2, \ldots, \alpha_N]$, where K and M are stiffness and mass matrices respectively, with the entries

$$K_{ij} = \int_\Omega \nabla\phi_i \cdot \nabla\phi_j d\Omega, \quad i, j = 1, 2, \ldots, N, \tag{3.40a}$$

$$M_{ij} = \int_\Omega \phi_i\phi_j d\Omega, \quad i, j = 1, 2, \ldots, N. \tag{3.40b}$$

Solution of the linear system of equations (3.39) gives the FEM solution of the Laplace EVP. The analytically known FEM solution of the Laplace EVP on a one-dimensional domain is given in the following case to illustrate FEM.

1D-FEM Case

Consider the first original domain $\Omega_1 = [0, \pi]$, and assume that Ω_1 is partitioned into N equally spaced subintervals. Each subintervals written as $I = [x_{i-1}, x_i]$ such that

$$I : 0 = x_0 < x_1 < x_2 < \cdots < x_N < x_N = \pi, \tag{3.41}$$

where $x_i = ih$, $h = \pi/N$, for $i = 0, 1, \ldots, N$. If the piecewise linear polynomial given as

$$\phi_i(x) = \begin{cases} (x - x_{i-1})/h & \text{if} \quad x_{i-1} \leq x < x_i, \\ (x_{i+1} - x)/h & \text{if} \quad x_i \leq x < x_{i+1}, \\ 0 & \text{otherwise}, \end{cases} \tag{3.42}$$

is considered as a basis function to construct the finite dimensional subspace V_h, then the entries of the stiffness matrix are obtained by computing the explicit expressions of (3.40a) such that

$$K_{i,i+1} = \int_{x_i}^{x_{i+1}} -\frac{1}{h}\frac{1}{h} dx = -\frac{1}{h}, \tag{3.43a}$$

$$K_{i+1,i} = \int_{x_i}^{x_{i+1}} -\frac{1}{h}\frac{1}{h} dx = -\frac{1}{h}, \tag{3.43b}$$

$$K_{ii} = \int_{x_{i-1}}^{x_{i+1}} \left(\frac{1}{h}\right)^2 dx = \frac{2}{h}, \tag{3.43c}$$

$$K_{ij} = 0, \quad \text{for} \ \ |i - j| > 1, \tag{3.43d}$$

for $i, j = 1, 2, \ldots, N-1$. In the same way, the entries of the mass matrix are obtained as

$$M_{i,i+1} = \int_{x_i}^{x_{i+1}} \frac{x_{i+1} - x}{h} \frac{x - x_i}{h} dx = \frac{h}{6}, \tag{3.44a}$$

$$M_{i+1,i} = \int_{x_i}^{x_{i+1}} \frac{x - x_i}{h} \frac{x_{i+1} - x}{h} dx = \frac{h}{6}, \tag{3.44b}$$

$$M_{ii} = \int_{x_{i-1}}^{x_i} \left(\frac{x - x_i}{h}\right)^2 dx + \int_{x_i}^{x_{i+1}} \left(\frac{x_{i+1} - x}{h}\right)^2 dx = \frac{4h}{6}, \tag{3.44c}$$

$$M_{ij} = 0, \quad \text{for } \ |i - j| > 1, \tag{3.44d}$$

for $i, j = 1, 2, \ldots, N-1$. Thus, the stiffness and the mass matrices are written as

$$K = \frac{1}{h} \cdot \begin{bmatrix} 2 & -1 & & \\ -1 & 2 & \ddots & \\ & \ddots & \ddots & -1 \\ & & -1 & 2 \end{bmatrix}, \text{ and } M = \frac{h}{6} \cdot \begin{bmatrix} 4 & 1 & & \\ 1 & 4 & \ddots & \\ & \ddots & \ddots & 1 \\ & & 1 & 4 \end{bmatrix}. \tag{3.45}$$

It is known that the eigenvectors and eigenfunctions of a tridiagonal matrix

$$K = \frac{1}{h} \cdot \begin{bmatrix} a & b & & \\ c & a & \ddots & \\ & \ddots & \ddots & b \\ & & c & a \end{bmatrix} \in \mathbb{C}^{(N-1)\times(N-1)}, \tag{3.46}$$

given as

$$\lambda = a + 2\sqrt{bc} \cos\left(\frac{k\pi}{N}\right), \tag{3.47a}$$

$$w = (c/b)^{(k/2)} \sin\left(\frac{ki\pi}{N}\right), \tag{3.47b}$$

respectively, where $k, i = 1, 2, \ldots, N-1$ [68]. Now, assume that λ_K and λ_M are the eigenvalues of K and M respectively. From (3.47a), the eigenvalues of K and M are obtained as

$$\lambda_K = \frac{1}{h}\left(2 - 2\cos\left(\frac{k\pi}{N}\right)\right), \tag{3.48a}$$

$$\lambda_M = \frac{h}{6}\left(4 + 2\cos\left(\frac{k\pi}{N}\right)\right). \tag{3.48b}$$

From (3.47b), the eigenvectors of the both matrices are obtained as

$$u_h = \sin\left(\frac{ki\pi}{N}\right), \tag{3.49}$$

for $k, = 1, 2, \ldots, N-1$. Since the both matrices has the same eigenvector, the eigenvalues of the system $Ku_h = \lambda_h M u_h$ are obtained by dividing λ_K by λ_M such that

$$
\begin{aligned}
Ku_h = \lambda_K u_h, \quad Mu_h = \lambda_M u_h \quad & \Rightarrow Ku_h = \lambda_h \lambda_M u_h \\
& \Rightarrow \lambda_K u_h = \lambda_h \lambda_M u_h \\
& \Rightarrow \lambda_h = \frac{\lambda_K}{\lambda_M} = \frac{1 - \cos\left(\dfrac{k\pi}{N}\right)}{2 + \cos\left(\dfrac{k\pi}{N}\right)}.
\end{aligned} \tag{3.50}
$$

Thus, the FEM solution of the Laplace EVP is derived as

$$u_h = \sin(kih), \tag{3.51a}$$

$$\lambda_h = \left(\frac{6}{h^2}\right)\frac{1 - \cos(kh)}{2 + \cos(kh)}, \tag{3.51b}$$

where $h = \pi/N$, and $k, i = 1, 2, \ldots, N-1$.

3.1.1. Assembly of Stiffness and Mass Matrices

Although, in 1D- FEM Case, the entries of the stiffness and mass matrices are obtained directly with computing the integrals in (3.43), and (3.44), assembly procedure is required to obtain these entries on higher dimensional domains or in the case of using the quadratic elements. Therefore, the assembly procedure is described in this section.

Assumed that $\mathcal{T}$ is a mesh described by the union of disjoint domains $\Omega^e \subset \Omega$, where e denotes the label of the elements in the mesh. Let K^e and M^e denote the local stiffness and mass matrices respectively. For each element Ω^e, the entries of the local stiffness and mass matrices is obtained by computing the integrals

$$K^e_{ij} = \int_{\Omega^e} \nabla\phi_i \cdot \nabla\phi_j d\Omega^e, \tag{3.52a}$$

$$M^e_{ij} = \int_{\Omega^e} \phi_i \phi_j d\Omega^e. \tag{3.52b}$$

The assembly procedure can be defined as the summation of the local matrices over all elements in the mesh, and gives the entries of the global stiffness and mass matrices as

$$K_{ij} = \sum_{e=1}^{N_e} \int_{\Omega^e} \nabla\phi_i \cdot \nabla\phi_j d\Omega^e = \sum_{e=1}^{N_e} K^e, \tag{3.53a}$$

$$M_{ij} = \sum_{e=1}^{N_e} \int_{\Omega^e} \phi_i\phi_j d\Omega^e = \sum_{e=1}^{N_e} M^e, \tag{3.53b}$$

where N_e denotes the number of elements in the mesh. The following example is given to illustrate the idea of this procedure.

Example 3.1: Consider the domain $\Omega_2 = [0, \pi] \times [0, \pi]$*, and the mesh of this square given in Figure 3.1 with the linear basis function*

$$\phi_i = 1 - \frac{x}{h} - \frac{y}{h}, \quad \phi_{i+1} = \frac{x}{h}, \quad \phi_{i+2} = \frac{y}{h}, \tag{3.54}$$

where $h = \pi/N$.

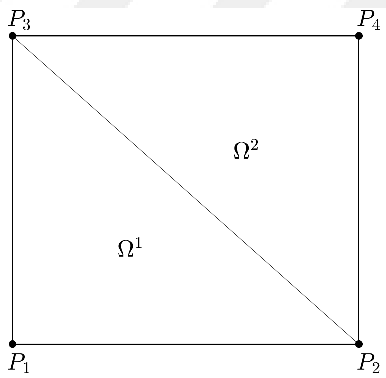

Figure 3.1: A mesh for the square $[0, \pi] \times [0, \pi]$ for $N = 1$.

Note that Ω^e *and* P_n *denote the elements and nodal points of the mesh respectively for* $e = 1, 2$ *and* $n = 1, 2, 3, 4$. *For each linear triangular element, the integral in* (3.52a) *can be computed with the quadrature formula [1]*

$$\begin{aligned} K^e_{ij} &= \int_{\Omega^e} \nabla\phi_i \cdot \nabla\phi_j d\Omega^e, \\ &= (b_i b_j + c_i c_j)|\Omega^e|, \end{aligned} \tag{3.55}$$

where $|\Omega^e|$ *is the area of the linear triangular element* Ω^e*, and* $\nabla\phi_i = [b_i \;\; c_i]^T$. *The following formula is used for computing the entries of the local mass matrix [67]*

$$\int_{\Omega^e} \phi_1^m \phi_2^n \phi_3^p d\Omega^e = \frac{2m!n!p!}{(m+p+n+2)!} |\Omega^e|, \tag{3.56}$$

where $|\Omega^e|$ is the area of the linear triangular element Ω^e, and m, n, and p are positive integers. Thus, the entries of the local mass matrices are obtained as

$$M_{ij}^e = \int_{\Omega^e} \phi_i \phi_j = \frac{1}{12}|\Omega^e| \quad \textit{for } i \neq j, \tag{3.57a}$$

$$M_{ij}^e = \int_{\Omega^e} \phi_i \phi_j = \frac{1}{6}|\Omega^e| \quad \textit{for } i = j, \tag{3.57b}$$

and the local stiffness and mass matrices are obtained as

$$K^e = \frac{1}{2}\begin{bmatrix} 2 & -1 & -1 \\ -1 & 1 & 0 \\ -1 & 0 & 1 \end{bmatrix} \quad \textit{and} \quad M^e = \frac{h^2}{24}\begin{bmatrix} 2 & 1 & 1 \\ 1 & 2 & 1 \\ 1 & 1 & 2 \end{bmatrix} \tag{3.58}$$

with using the formulas (3.55) *and* (3.56). *Hence, the global stiffness matrix is assembled as*

Table 3.1: The entries of the local and global stiffness matrices.

	P_1	P_2	P_3
P_1	1	$-\frac{1}{2}$	$-\frac{1}{2}$
P_2	$-\frac{1}{2}$	$\frac{1}{2}$	0
P_3	$-\frac{1}{2}$	0	$\frac{1}{2}$

(a) Local stiffness matrix K^e on Ω^1.

	P_4	P_2	P_3
P_4	1	$-\frac{1}{2}$	$-\frac{1}{2}$
P_2	$-\frac{1}{2}$	$\frac{1}{2}$	0
P_3	$-\frac{1}{2}$	0	$\frac{1}{2}$

(b) Local stiffness matrix K^e on Ω^2.

	P_1	P_2	P_3	P_4
P_1	1	$-\frac{1}{2}$	$-\frac{1}{2}$	0
P_2	$-\frac{1}{2}$	$\frac{1}{2}+\frac{1}{2}$	$0+0$	$-\frac{1}{2}$
P_3	$-\frac{1}{2}$	$0+0$	$\frac{1}{2}+\frac{1}{2}$	$-\frac{1}{2}$
P_4	0	$-\frac{1}{2}$	$-\frac{1}{2}$	1

(c) Global stiffness matrix K on Ω.

The global mass matrix is obtained in a similar way. Thus, the global matrices are written as

$$K = \frac{1}{2}\begin{bmatrix} 2 & -1 & -1 & 0 \\ -1 & 2 & 0 & -1 \\ -1 & 0 & 2 & -1 \\ 0 & -1 & -1 & 2 \end{bmatrix}, \quad \textit{and} \quad M = \frac{h^2}{24}\begin{bmatrix} 2 & 1 & 1 & 0 \\ 1 & 4 & 2 & 1 \\ 1 & 2 & 4 & 1 \\ 0 & 1 & 1 & 2 \end{bmatrix}. \tag{3.59}$$

3.1.2. Convergence Analysis

In this section, two widely used methods that are critical for the convergence analysis of FEM solutions of EVPs are considered. One is the direct proof approach to show convergence and based on fundamental aspects of the Rayleigh quotient [1] (see also [12]). The direct proof of convergence is mentioned for the elliptic EVPs $\mathcal{L}u = \lambda u$, where $\mathcal{L}$ is an elliptic operator. The other one is the Babuška-Osborn spectral theory [9] (see also [2], and [12]) defined by a compact solution operator on a Hilbert space where the solution of the EVP is defined. The Babuška-Osborn spectral theory is introduced in order to give the convergence estimates for the eigenvalues and the eigenfunctions of the Laplace EVP approximated with the use of piecewise polynomials.

3.1.2.1. Direct Proof of Convergence

In this section, direct proof of convergence is introduced for the elliptic EVP $\mathcal{L}u = \lambda u$ of order $2m$, where is $\mathcal{L}$ is an elliptic operator.

Let V be a Hilbert space and B is the bilinear form associated to $\mathcal{L}$. The variational form of the problem $\mathcal{L}u = \lambda u$ is obtained as

$$B(u, v) = \lambda(u, v), \quad \forall u, v \in V, \tag{3.60}$$

where $(\cdot, \cdot)$ stands for the inner product in $L^2(\Omega)$. As mentioned in Section 2.2.1, the variational formulation is produced by multiplying the problem $\mathcal{L}u = \lambda u$ by a function $v \in V$, and integrate by parts. The Galerkin discretization of problem (3.60) is given as: find eigenvalues $\lambda_h \in \mathbb{R}$ and eigenfunctions $0 \neq u_h \in V_h$ such that

$$B(u_h, v_h) = \lambda_h(u_h, v_h), \quad \forall v_h \in V_h, \tag{3.61}$$

on the finite dimensional subspace $V_h \subset V$ constructed by piecewise polynomials.

The direct proof is based on the Rayleigh quotient given as

$$R(v) = \frac{B(v, v)}{(v, v)}, \quad \forall v \neq 0 \in V, \tag{3.62}$$

and the corresponding eigenvalues are obtained as $\lambda = R(v)$. Moreover, the first and kth eigenvalues of problem (3.60) satisfy

$$\lambda^{(1)} = \min_{v \in V} R(v), \tag{3.63a}$$

$$\lambda^{(k)} = \min_{v \perp E^{(k-1)}} R(v), \tag{3.63b}$$

where $E^{(k-1)}$ denotes the space spanned by the eigenfunctions $u^{(i)}$, $i = 1, \ldots, k-1$ [1] (see also [12]). The kth eigenvalue is also obtained by the min-max principle which does not required knowing the eigenfunctions $u^{(i)}$, $i = 1, \ldots, k-1$. This principle is defined as

$$\lambda^{(k)} = \min_{E \subset V^{(k)}} \max_{v \in E} R(v), \tag{3.64}$$

where $V^{(k)}$ denotes the set of all subspaces of V, and E denotes the any subspace of $V^{(k)}$. The proof of this principle can be found in [1] and [12].

On the finite dimensional subspace V_h, the Rayleigh quotient is given as

$$R(v_h) = \frac{B(v_h, v_h)}{(v_h, v_h)}, \quad \forall v_h \neq 0 \in V_h. \tag{3.65}$$

The properties of the Rayleigh quotient given in (3.63) are satisfied by the eigenvalues of discrete problem (3.61) such that

$$\lambda_h^{(1)} = \min_{v_h \in V_h} R(v_h), \tag{3.66a}$$

$$\lambda_h^{(k)} = \min_{v_h \perp E_h^{(k-1)}} R(v_h). \tag{3.66b}$$

Besides, the analogous min-max principle is valid for the discrete problem (3.61) such that

$$\lambda_h^{(k)} = \min_{E_h \subset V_h^{(k)}} \max_{v_h \in E_h} R(v_h), \tag{3.67}$$

where $V_h^{(k)}$ denotes the set of all subspaces of V_h, and E_h denotes the any subspace of $V_h^{(k)}$. As a result of the min-max principles (3.64) and (3.67), all eigenvalues satisfy [1] (see also [12])

$$\lambda^{(k)} \leq \lambda_h^{(k)}, \quad \forall k \in \mathbb{Z}^+. \tag{3.68}$$

Before giving the error estimate of the eigenvalues and eigenfunctions of the elliptic EVPs, assume that $P : V \to V_h$ is an elliptic projection such that

$$B(u - Pu, v_h) = 0 \quad \forall v_h \in V_h. \tag{3.69}$$

This means that Pu is the closest function to the eigenfunction u in V_h. Thus, the projection Pu satisfies the best approximation property given as [1]

$$\|u - Pu\| \leq C \left[h^{s+1} + h^{2(s+1-m)} \right] \|u\|_{H^{s+1}(\Omega)}, \tag{3.70}$$

where s is the degree of the piecewise polynomial which is used to construct the finite dimensional subspace V_h [1].

Now, the following theorems give the error estimate of the eigenvalues and eigenfunctions of the elliptic EVPs $\mathcal{L}u = \lambda u$ of order $2m$. The proofs of these theorems can be found in [1], and based on the min-max principles (3.64), (3.67), and the best approximation property (3.70).

Theorem 3.1: Let V_h be a finite element space constructed by a piecewise polynomial of degree s, and $\lambda_h^{(k)}$ be an eigenvalues converging to $\lambda^{(k)}$. Then there is a constant C such that the approximate eigenvalues $\lambda_h^{(k)}$ are satisfy

$$\lambda^{(k)} \leq \lambda_h^{(k)} \leq \lambda^{(k)} + Ch^{s+1-m}, \tag{3.71}$$

for a small h.

Theorem 3.2: Let V_h be a finite element space constructed by a piecewise polynomial of degree s, and $u_h^{(k)}$ be an eigenfunction converging to $u^{(k)}$ associated with the eigenvalue $\lambda^{(k)}$. Then there exists a constant C such that the approximate eigenfunctions $u_h^{(k)}$ satisfy

$$\left\| u^{(k)} - u_h^{(k)} \right\| \leq C \left[h^{s+1} + h^{2(s+1-m)} \right] \lambda^{(k)^{(s+1)/2m}}. \tag{3.72}$$

3.1.2.2. Babuška-Osborn Theory

In this section, the Babuška-Osborn spectral theory is introduced for the Laplace EVP. As mentioned before, the variational form of the Laplace EVP is to find eigenvalues $\lambda \in \mathbb{R}$ and eigenfunctions $0 \neq u \in H_0^1(\Omega)$ such that

$$B(u, v) = \lambda(u, v), \quad \forall v \in H_0^1(\Omega), \tag{3.73}$$

and the discrete problem is to find eigenvalues $\lambda_h \in \mathbb{R}$ and eigenfunctions $\neq u_h \in V_h$ such that

$$B(u_h, v_h) = \lambda_h(u_h, v_h), \quad \forall v_h \in V_h \tag{3.74}$$

in the finite dimensional subspace $V_h \subset H_0^1(\Omega)$. Assume that X is a Hilbert space, and $T : X \to X$ is a solution operator such that

$$B(Tf, v) = (f, v), \quad \forall f, v \in X \tag{3.75}$$

and $T_h : X \to X$ is a discrete solution operator such that [12]

$$\|T - T_h\|_X \to 0 \quad \text{as} \quad h \to 0. \tag{3.76}$$

Let $T_V : H_0^1 \to H_0^1$ and $T_H : L^2 \to L^2$ denote the operators which are underlying the corresponding spaces. Assume that V_h provides the best approximation

$$\inf_{v \in V_h} \|u - v\| \leq Ch^{\min\{s+1,r\}} \|u\|_{H^r(\Omega)}, \tag{3.77}$$

$$\inf_{v \in V_h} \|u - v\|_1 \leq Ch^{\min\{s,r-1\}} \|u\|_{H^r(\Omega)}, \tag{3.78}$$

where s is the degree of the piecewise polynomial which is used to construct the finite dimensional subspace V_h, and r is the regularity of the eigenspace E spanned by the eigenfunctions associated with λ in other words $E \subset H^r$. Such convergence results are standard in the case of V_h contains the piecewise polynomials.

Consider the first case of $T_V : H_0^1 \to H_0^1$, and assume that $T = T_V$. The discrete solution operator $T_h : H_0^1 \to H_0^1$ can be defined as

$$B(T_h f, v) = (f, v), \quad \forall v \in V_h, \tag{3.79}$$

and satisfies the estimate

$$\|Tf - T_h f\|_1 \leq Ch^{\epsilon} \|f\|_1, \tag{3.80}$$

where $\epsilon > 0$. This implies that

$$\|T - T_h\|_1 = O\left(h^{\min\{s,r-1\}}\right). \tag{3.81}$$

The following theorems present the estimates for the eigenfunctions and eigenvalues and are given in [12].

Theorem 3.3: Let V_h be a finite element space constructed by a piecewise polynomial of degree s, and u be an unit eigenfunction associated with the eigenvalue λ of multiplicity m. Assume that $w_h^{(1)}, w_h^{(2)}, \ldots, w_h^{(m)}$ denote eigenfunctions associated with the m discrete eigenvalues converging to λ. Then there exists $u_h \in \text{span}\left\{w_h^{(1)}, w_h^{(2)}, \ldots, w_h^{(m)}\right\}$ such that

$$\|u - u_h\|_1 \leq Ch^{\tau} \|u\|_{H^{1+\tau}(\Omega)}, \tag{3.82}$$

where τ denotes the value $\min\{s, r-1\}$.

Theorem 3.4: Let V_h be a finite element space constructed by a piecewise polynomial of degree s, and $\lambda_h^{(k)}$ be an eigenvalue converging to $\lambda^{(k)}$. Then, there is a constant C such that the approximate eigenvalues $\lambda_h^{(k)}$ are satisfy

$$\lambda^{(k)} \leq \lambda_h^{(k)} \leq \lambda^{(k)} + Ch^{2\tau}, \tag{3.83}$$

where τ denotes the value $\min\{s, r-1\}$.

Now, consider the second case of $T_H : L^2 \to L^2$, and assume that $T = T_V$. To obtain the estimate for the eigenfunctions on $L^2(\Omega)$, let $T_h : L^2 \to L^2$ be the discrete solution operator such that

$$B(T_h f, v) = (f, v), \quad \forall v \in V_h, \tag{3.84}$$

and satisfies the estimate

$$\|Tf - T_h f\| \leq Ch^{\epsilon+1} \|f\|. \tag{3.85}$$

The following theorem present the estimate for the eigenfunctions and are given in [12].

Theorem 3.5: Let u be an unit eigenfunction associated with the eigenvalue λ of multiplicity m, and let $w_h^{(1)}, w_h^{(2)}, \ldots, w_h^{(m)}$ denote eigenfunctions associated with the m discrete eigenvalues converging to λ. Then there exists $u_h \in \operatorname{span}\left\{w_h^{(1)}, \ldots, w_h^{(m)}\right\}$ such that

$$\|u - u_h\| \leq Ch^{\tau+1} \|u\|_{H^{1+\tau}(\Omega)}. \tag{3.86}$$

If Ω is a convex domain then the eigenspace E spanned by the eigenfunctions associated with λ is contained $H^2(\Omega)$ [12]. Thus, the approximate solution of the Laplace EVP provides

$$\|\lambda - \lambda_h\| = O(h^2), \;\; \|u - u_h\| = O(h^2), \text{ and } \|u - u_h\|_1 = O(h) \tag{3.87}$$

for linear elements. Also, the convergence estimates for quadratic elements are obtained as

$$\|\lambda - \lambda_h\| = O(h^4), \;\; \|u - u_h\| = O(h^3), \text{ and } \|u - u_h\|_1 = O(h^2) \tag{3.88}$$

for a convex domain Ω.

3.1.3. Numerical Results

In this section, the numerical results obtained by using FEM is presented. The Laplace EVP is considered on the following domains:

- $\Omega_1 : [0, \pi]$
- $\Omega_2 : [0, \pi] \times [0, \pi]$
- $\Omega_3 : x^2 + y^2 = 1$

The convergence behavior of the FEM solution to the exact solution is investigated as the number of elements is increasing; in other words, as the mesh size is decreasing. This investigation is carried out according to mesh size $h = \pi/N$ on uniform meshes of Ω_1 and Ω_2 for increasing values of N. Besides, the convergence behavior is investigated on non-uniform meshes of Ω_2 and Ω_3 when h_{max} goes to zero, where h_{max} denotes the maximum of the longest side of the triangles in the mesh. The numerical results for the convergence behavior are compared with the corresponding theoretical results given in the previous section. Also, note that linear and quadratic elements are used for the discretization of Ω_1. The computations concerning Ω_2 and Ω_3 involve linear triangular elements. All of the computations and figures are procured by means of a program written using MATLAB.

3.1.3.1. Linear Elements on Ω_1

First ten approximate eigenvalues $\lambda_h^{(k)}$ and exact eigenvalues $\lambda^{(k)} = k^2$ of the Laplace EVP on $\Omega_1 = [0, \pi]$ are given in Table 3.2 with the rates of convergence for $N = 8, 16, 32, \ldots, 256$.

Table 3.2: First ten exact and approximate eigenvalues with the rates of convergence for Section 3.1.3.1, and $N = 8, 16, 32, \ldots, 256$.

$\lambda^{(k)}$	$N = 8$	$N = 16$	$N = 32$	$N = 64$	$N = 128$	$N = 256$
1	1.0129	1.0032 (2.0)	1.0008 (2.0)	1.0002 (2.0)	1.0001 (2.0)	1.0000 (2.0)
4	4.2095	4.0517 (2.0)	4.0129 (2.0)	4.0032 (2.0)	4.0008 (2.0)	4.0002 (2.0)
9	10.0803	9.2631 (2.0)	9.0652 (2.0)	9.0163 (2.0)	9.0041 (2.0)	9.0010 (2.0)
16	19.4537	16.8382 (2.0)	16.2067 (2.0)	16.0515 (2.0)	16.0129 (2.0)	16.0032 (2.0)
25	33.2628	27.0649 (2.0)	25.5059 (2.0)	25.1257 (2.0)	25.0314 (2.0)	25.0078 (2.0)
36	51.3724	40.3212 (1.8)	37.0525 (2.0)	36.2610 (2.0)	36.0651 (2.0)	36.0163 (2.0)
49	69.5582	57.0672 (1.3)	50.9572 (2.0)	49.4840 (2.0)	49.1206 (2.0)	49.0301 (2.0)
64	-	77.8147	67.3528 (2.0)	64.8266 (2.0)	64.2059 (2.0)	64.0514 (2.0)
81	-	103.0473	86.3943 (2.0)	82.3258 (2.0)	81.3299 (2.0)	81.0824 (2.0)
100	-	133.0513	108.2597 (2.0)	102.0237 (2.0)	100.5030 (2.0)	100.1256 (2.0)

From Table 3.2, it is observed that the approximate eigenvalues $\lambda_h^{(k)}$ converge to the corresponding exact eigenvalues $\lambda^{(k)} = k^2$ as the number of elements is increasing. To illustrate this convergence behavior, the log-log scale plots of the errors between the exact eigenvalues $\lambda^{(k)}$ and the approximate eigenvalues $\lambda_h^{(k)}$ are given in Figure 3.2 for $k = 1, 2, \ldots, 6$, and $N = 8, 16, \ldots, 256$. Looking at Figure 3.2, it is clearly seen that the expected convergence behavior $\left|\lambda^{(k)} - \lambda_h^{(k)}\right| = O(h^2)$ given in Section 3.1.2 is provided. Also, the rates of convergence given in Table 3.2 are in well accordance with this behavior.

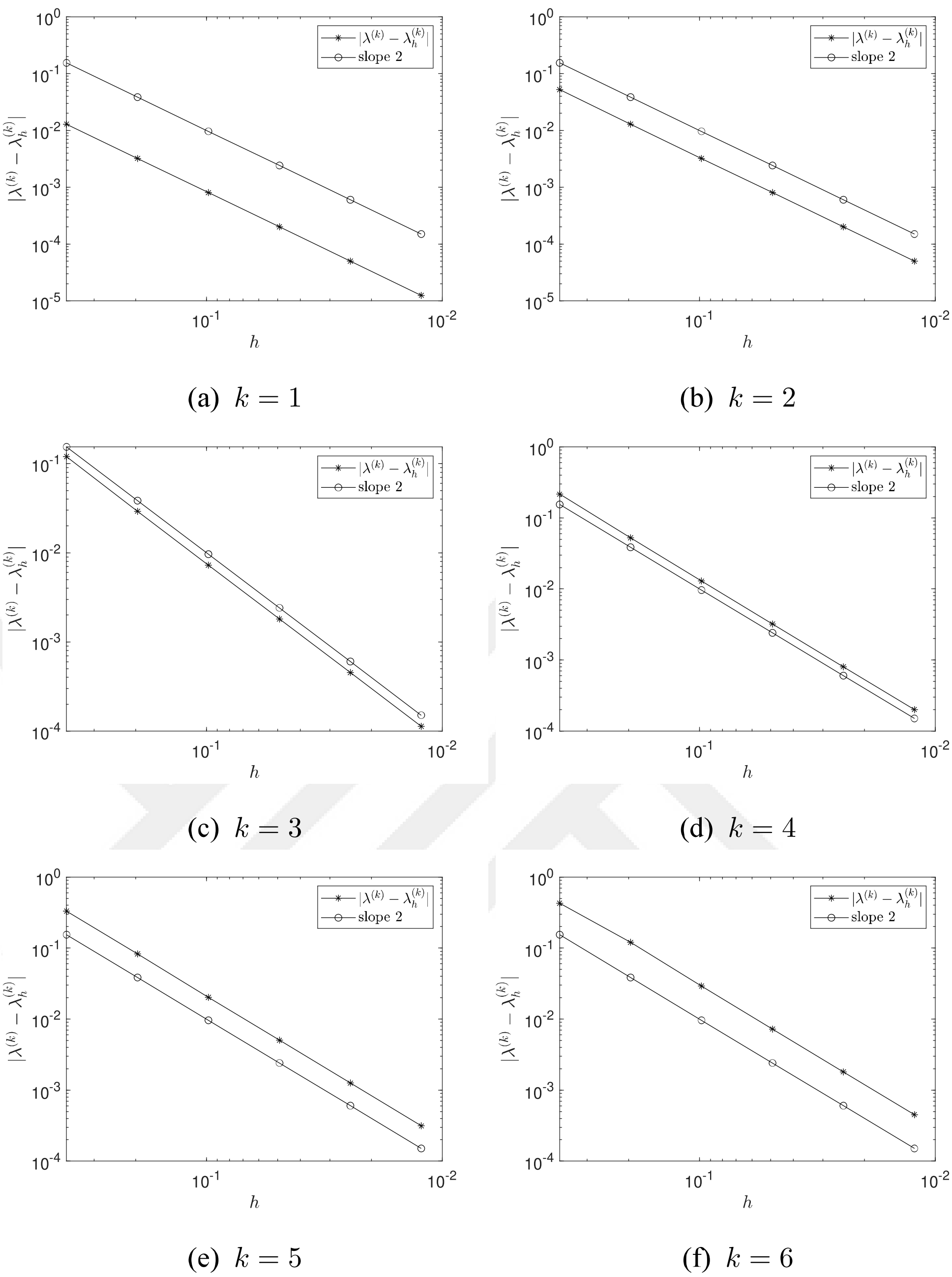

Figure 3.2: Log-log scale plot of $|\lambda^{(k)} - \lambda_h^{(k)}|/|\lambda^{(k)}|$ for Section 3.1.3.1, $k = 1, 2, \ldots, 6$, and $N = 8, 16, \ldots, 256$.

Since the approximate eigenfunction $u_h^{(k)} = \sin(kih)$ takes the same values with the corresponding exact eigenfunction $u^{(k)} = \sin(kx)$ at the interpolation points $x_i = ih$ for $i = 0, 1, \ldots, N$, the error between $u_h^{(k)}$ and $u^{(k)}$ is numerically obtained as zero. For this reason, to show that this is the case, Figure 3.3 is given for $k = 1, 2, \ldots, 6$, and $N = 32$.

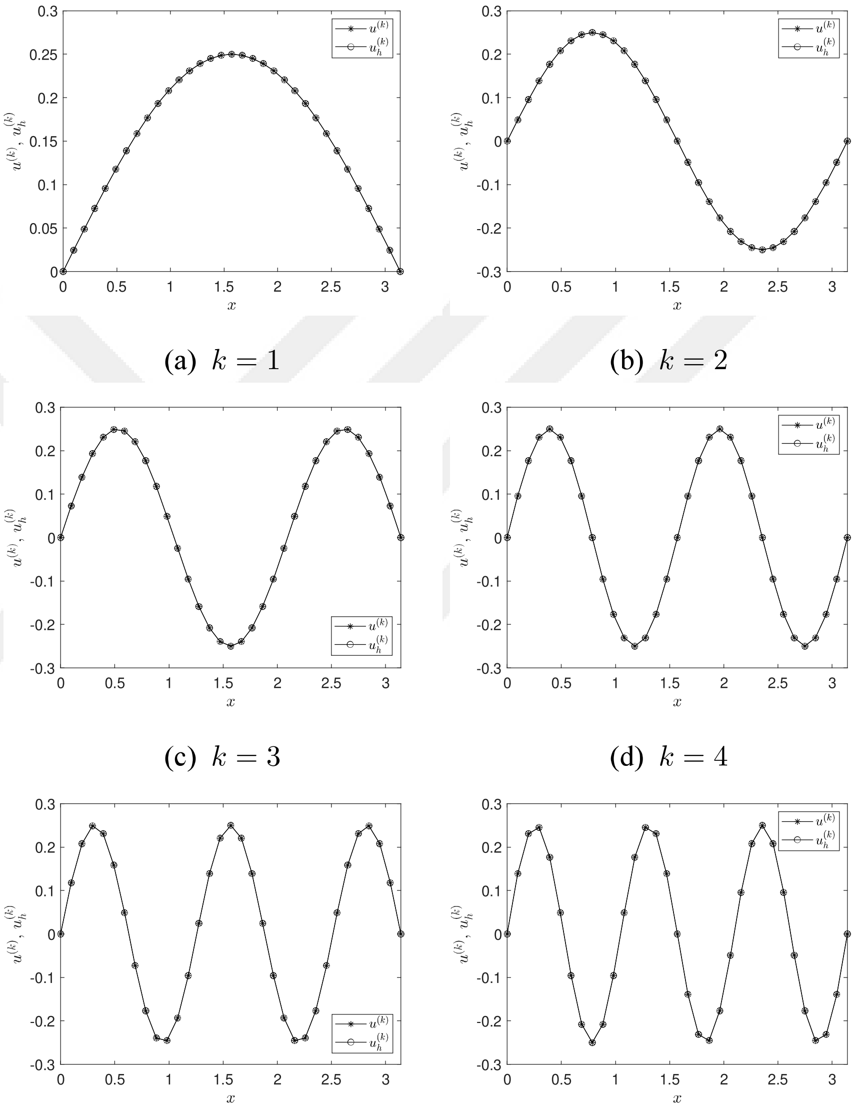

(a) $k = 1$ (b) $k = 2$

(c) $k = 3$ (d) $k = 4$

(e) $k = 5$ (f) $k = 6$

Figure 3.3: Plots of approximate eigenfunctions $u_h^{(k)}$ together with the corresponding exact eigenfunctions $u^{(k)}$ for Section 3.1.3.1, $k = 1, 2, \ldots, 6$, and $N = 32$.

3.1.3.2. Quadratic Elements on Ω_1

First ten approximate eigenvalues $\lambda_h^{(k)}$ and exact eigenvalues $\lambda^{(k)} = k^2$ of the Laplace EVP on $\Omega_1 = [0, \pi]$ are given in Table 3.3, with the rates of convergence for $N = 9, 27, \ldots, 729$. As seen in Table 3.3, the approximate eigenvalues $\lambda_h^{(k)}$ converge to the exact eigenvalues $\lambda^{(k)}$ as the number of elements is increasing.

Table 3.3: First ten exact and approximate eigenvalues with the rates of convergence for Section 3.1.3.2, and $N = 9, 27, \ldots, 729$.

$\lambda^{(k)}$	$N = 9$	$N = 27$	$N = 81$	$N = 243$	$N = 729$
1	1.0005	1.0000 (4.0)	1.0000 (4.0)	1.0000 (4.0)	1.0000 (3.6)
4	4.0301	4.0003 (3.9)	4.0000 (4.0)	4.0000 (4.0)	4.0000 (4.0)
9	9.2997	9.0034 (3.8)	9.0000 (4.0)	9.0000 (4.0)	9.0000 (4.0)
16	16.2114	16.0185 (2.1)	16.0002 (4.0)	16.0000 (4.0)	16.0000 (4.0)
25	31.2325	25.0689 (3.8)	25.0008 (3.9)	25.0000 (4.0)	25.0000 (4.0)
36	52.1694	36.1998 (3.7)	36.0024 (3.9)	36.0000 (4.0)	36.0000 (4.0)
49	80.5295	49.4874 (3.5)	49.0061 (3.9)	49.0001 (4.0)	49.0000 (4.0)
64	-	65.0463	64.0136 (3.9)	64.0002 (4.0)	64.0000 (4.0)
81	-	83.0329	81.0274 (3.8)	81.0003 (4.0)	81.0000 (4.0)
100	-	103.6337	100.0512 (3.8)	100.0006 (4.0)	100.0000 (4.0)

The log-log scale plots of the errors between the exact eigenvalues $\lambda^{(k)}$ and the approximate eigenvalues $\lambda_h^{(k)}$ are given in Figure 3.4 to illustrate the convergence behavior of the approximate eigenvalues $\lambda_h^{(k)}$ to the exact eigenvalues $\lambda^{(k)} = k^2$ according to $h = \pi/N$ for $N = 9, 27, \ldots, 729$. From Figure 3.4, it is observed that the expected convergence estimate $|\lambda^{(k)} - \lambda_h^{(k)}| = O(h^4)$ given with Theorem (3.4) is provided and the rates of convergence given in Table 3.3 are in well accordance with this behavior.

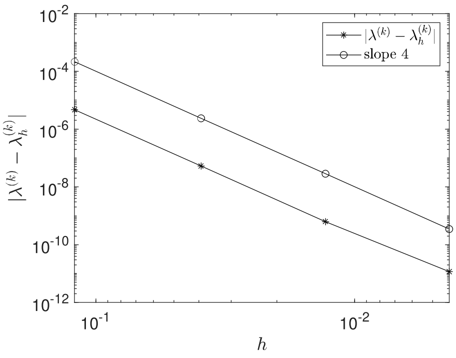

(a) $k = 1$

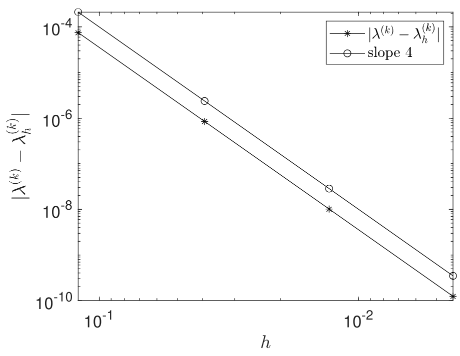

(b) $k = 2$

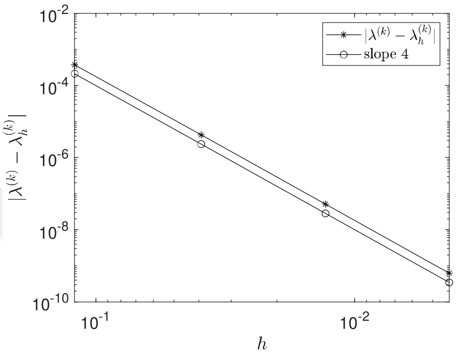

(c) $k = 3$

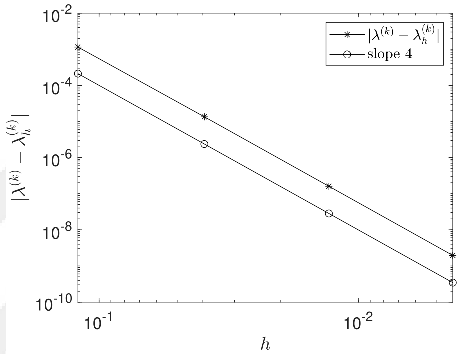

(d) $k = 4$

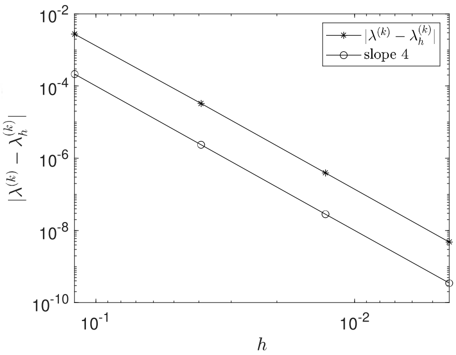

(e) $k = 5$

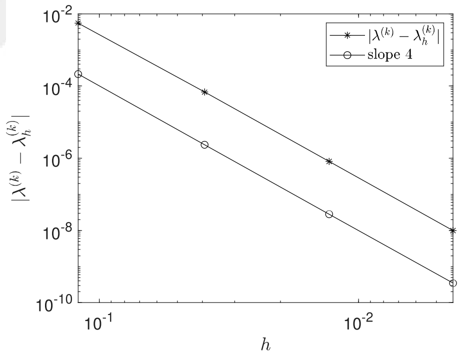

(f) $k = 6$

Figure 3.4: Log-log scale plot of $|\lambda^{(k)} - \lambda_h^{(k)}|/|\lambda^{(k)}|$ for Section 3.1.3.2, $k = 1, 2, \ldots, 6$, and $N = 27, 81, \ldots, 729$.

The convergence behaviors of the approximate eigenfunctions $u_h^{(k)}$ to the corresponding exact eigenfunctions $u^{(k)} = \sin(kx)$ are given in Figure 3.5 and Figure 3.6 with respect to the L^2- and H^1-norms, which are defined in (2.8) and (2.20).

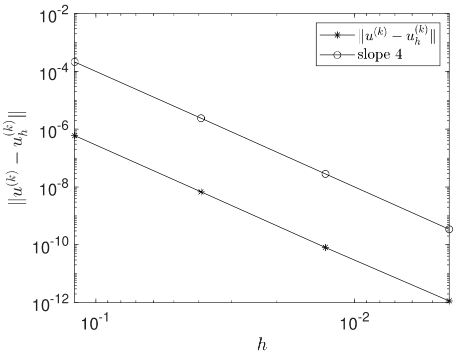

(a) $k = 1$

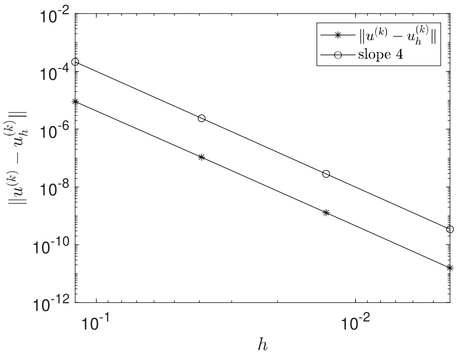

(b) $k = 2$

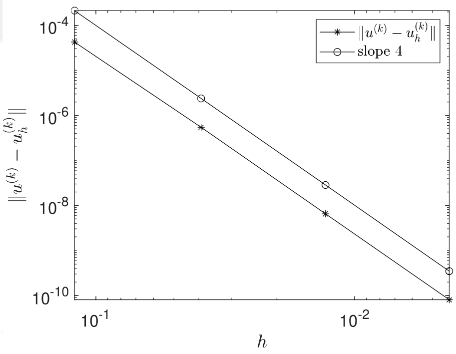

(c) $k = 3$

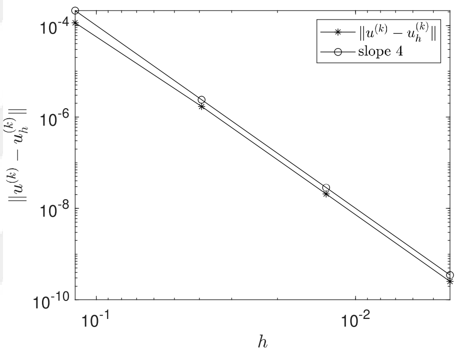

(d) $k = 4$

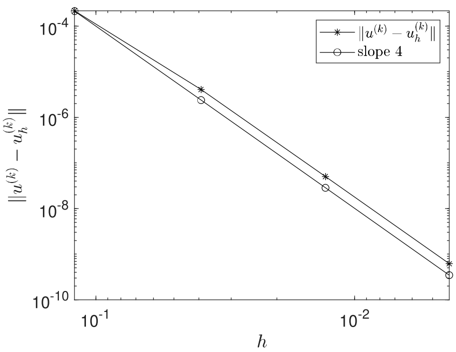

(e) $k = 5$

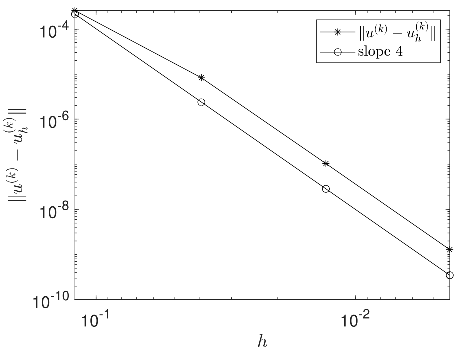

(f) $k = 6$

Figure 3.5: Log-log scale plot of $||u^{(k)} - u_h^{(k)}||/||u^{(k)}||$ for Section 3.1.3.2, $k = 1, 2, \ldots, 6$, and $N = 27, 81, 243, 729$.

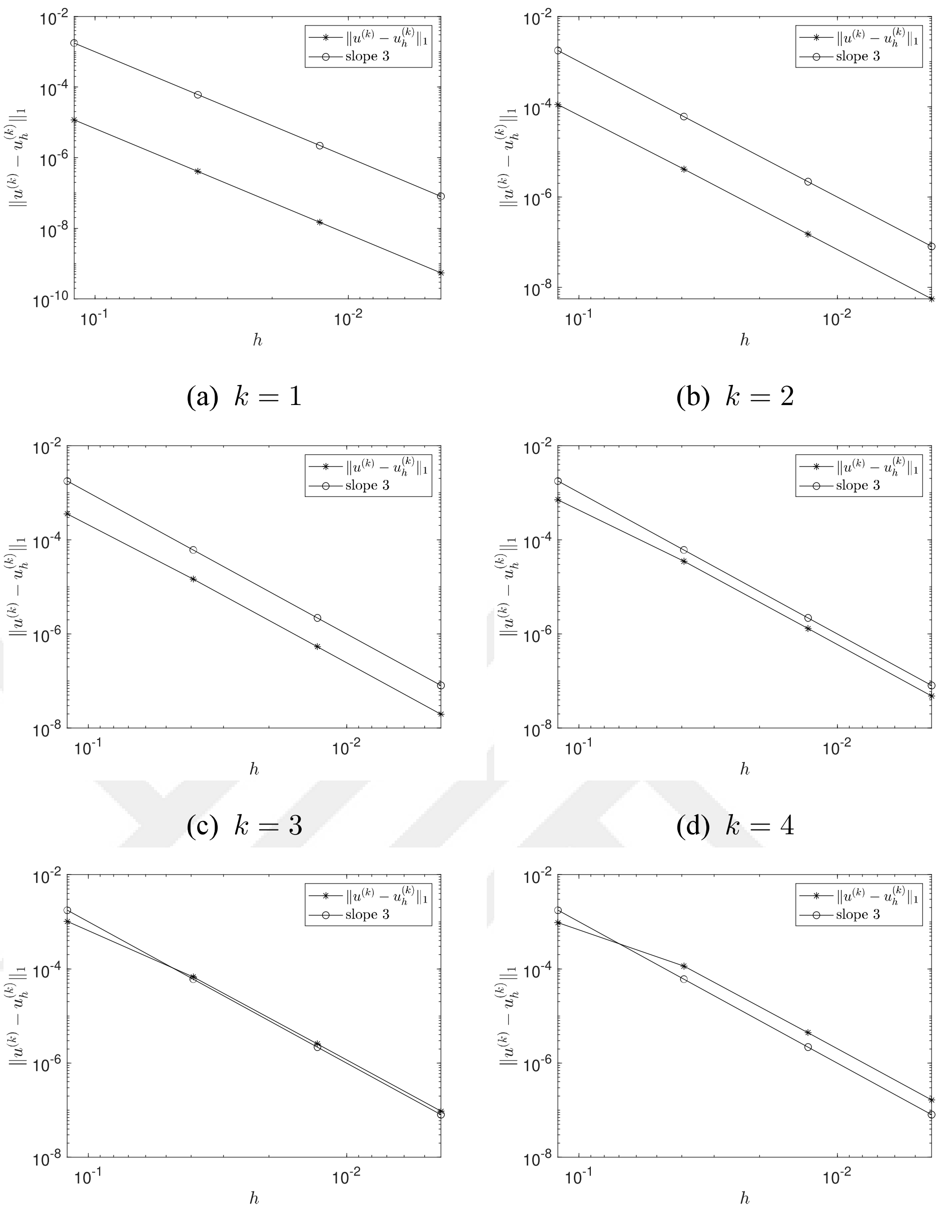

(a) $k = 1$ (b) $k = 2$

(c) $k = 3$ (d) $k = 4$

(e) $k = 5$ (f) $k = 6$

Figure 3.6: Log-log scale plot of $||u^{(k)} - u_h^{(k)}||_1/||u^{(k)}||_1$ for Section 3.1.3.2, $k = 1, 2, \ldots, 6$, and $N = 27, 81, 243, 729$.

From Figure 3.5 and Figure 3.6, it is observed that the approximate eigenfunctions $u_h^{(k)}$ converge to the exact eigenfunctions $u^{(k)}$ as $h = \pi/N$ goes to zero. Besides, it is clearly seen that these convergence behaviors are of order $O(h^4)$ and $O(h^3)$ with respect to L^2- and H^1-norms respectively. When the results obtained by using linear and quadratic elements are compared, it is seen that when linear elements are used, convergence behavior of the approximate eigenvalues $\lambda_h^{(k)}$ is of order $O(h^2)$, while quadratic elements are used, it is of order $O(h^4)$. This means that the approximate eigenvalues $\lambda_h^{(k)}$ obtained by using quadratic elements converge faster to the exact eigenvalues $\lambda^{(k)}$.

3.1.3.3. Linear Elements on Ω_2

In this section, convergence behaviors of the approximate eigenfunctions $u_h^{(m,n)}$ corresponding to the simple eigenvalues $\lambda^{(m,n)} = m^2+n^2$, where $m = n$, of the Laplace EVP on $\Omega_2 : [0,\pi] \times [0,\pi]$ are investigated on both uniform and non-uniform meshes constructed by linear triangular element as seen in Figure 3.7 and Figure 3.8. Besides, the eigenfunctions associated with the multiple eigenvalues $\lambda^{(m,n)} = m^2 + n^2$, where $m \neq n$, is also considered and the numerical results concerning these eigenfunctions are obtained on uniform meshes. The convergence behavior of the approximate eigenvalues $\lambda_h^{(m,n)}$ is investigated on both types of mesh.

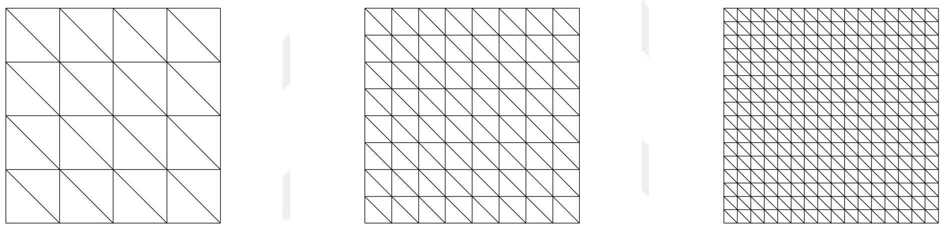

(a) $N = 4$ (b) $N = 8$ (c) $N = 16$

Figure 3.7: Uniform meshes of Ω_2 for Section 3.1.3.3 and $N = 4, 8, 16$.

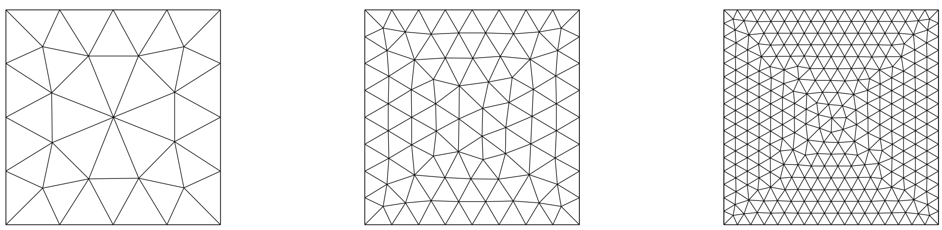

(a) $h_{max} = 0.8$ (b) $h_{max} = 0.4$ (c) $h_{max} = 0.2$

Figure 3.8: Non-uniform meshes of Ω_2 for Section 3.1.3.3 and $h_{max} = 0.8, 0.4, 0.2$.

First ten approximate eigenvalues $\lambda_h^{(m,n)}$ and exact eigenvalues $\lambda^{(m,n)} = m^2 + n^2$ of the Laplace EVP on Ω_2 are given in Table 3.4 and Table 3.5, together with the rates of convergence and the size S of the solved linear system of equations reduced by imposing the boundary conditions.

Table 3.4: First ten approximate and exact eigenvalues computed on uniform meshes with the rates of convergence for Section 3.1.3.3 and $N = 4, 8, 16, 32, 64$.

m,n	$\lambda^{(m,n)}$	$N=4$ $S: 9\times 9$	$N=8$ $S: 49\times 49$	$N=16$ $S: 225\times 225$	$N=32$ $S: 961\times 961$	$N=64$ $S: 3969\times 3969$
1,1	2	2.3168	2.0776 (2.0)	2.0193 (2.0)	2.0048 (2.0)	2.0012 (2.0)
1,2	5	6.3387	5.3325 (2.0)	5.0829 (2.0)	5.0207 (2.0)	5.0052 (2.0)
2,1	5	7.2502	5.5325 (2.1)	5.1302 (2.0)	5.0324 (2.0)	5.0081 (2.0)
2,2	8	12.2145	9.1826 (1.8)	8.3054 (2.0)	8.0769 (2.0)	8.0193 (2.0)
1,3	10	15.5629	11.5492 (1.8)	10.3814 (2.0)	10.0949 (2.0)	10.0237 (2.0)
3,1	10	16.7643	11.6879 (2.0)	10.3900 (2.1)	10.0955 (2.0)	10.0237 (2.0)
2,3	13	20.8965	15.2270 (1.8)	13.5716 (2.0)	13.1443 (2.0)	13.0362 (2.0)
3,2	13	26.0989	17.0125 (1.7)	13.9825 (2.0)	13.2432 (2.0)	13.0606 (2.0)
1,4	17	32.4184	21.3374 (1.8)	18.0416 (2.1)	17.2562 (2.0)	17.0638 (2.0)
4,1	17	-	21.5751	18.0705 (2.1)	17.2626 (2.0)	17.0653 (2.0)

Looking at Table 3.4 and Table 3.5, it is clearly seen that the approximate eigenvalues $\lambda_h^{(m,n)}$ approach to the exact eigenvalues $\lambda^{(m,n)}$ as the number of elements is increasing. When Table 3.4 and Table 3.5 are compared, it is observed that rates of convergence obtained on uniform meshes are more stable than the rates obtained on non-uniform meshes.

Table 3.5: First ten approximate and exact eigenvalues computed on non-uniform meshes with the rates of convergence for Section 3.1.3.3 and $h_{max} = 0.8, \ldots, 0.05$.

m, n	$\lambda^{(m,n)}$	$h_{max} = 0.8$ $S : 40 \times 40$	$h_{max} = 0.4$ $S : 148 \times 148$	$h_{max} = 0.2$ $S : 578 \times 578$	$h_{max} = 0.1$ $S : 2202 \times 2202$	$h_{max} = 0.05$ $S : 9076 \times 9076$
1,1	2	2.1424	2.0393 (1.9)	2.0102 (2.0)	2.0027 (1.9)	2.0006 (2.1)
1,2	5	6.0961	5.2495 (2.1)	5.0628 (2.0)	5.0163 (1.9)	5.0039 (2.0)
2,1	5	6.0986	5.2592 (2.1)	5.0636 (2.0)	5.0164 (2.0)	5.0040 (2.0)
2,2	8	10.2557	8.6427 (1.8)	8.1630 (2.0)	8.0422 (1.9)	8.0102 (2.0)
1,3	10	12.9564	11.0246 (1.5)	10.2560 (2.0)	10.0647 (2.0)	10.0158 (2.0)
3,1	10	12.9964	11.0850 (1.5)	10.2589 (2.1)	10.0660 (2.0)	10.0159 (2.1)
2,3	13	20.3752	14.7013 (2.1)	13.4310 (2.0)	13.1105 (2.0)	13.0266 (2.1)
3,2	13	20.4362	14.7766 (2.1)	13.4345 (2.0)	13.1110 (2.0)	13.0268 (2.1)
1,4	17	28.3108	20.0209 (1.9)	17.7467 (2.0)	17.1883 (2.0)	17.0456 (2.0)
4,1	17	29.7370	20.1168 (2.0)	17.7587 (2.0)	17.1917 (2.0)	17.0459 (2.1)

Figure 3.9 and Figure 3.10 are given to show that the convergence behavior of the approximate eigenvalues $\lambda_h^{(m,n)}$ to the exact eigenvalues $\lambda^{(m,n)}$. From Figure 3.9 and Figure 3.10, it is observed that the convergence behavior of the approximate eigenvalues $\lambda_h^{(m,n)}$ is of order $O(h^2)$.

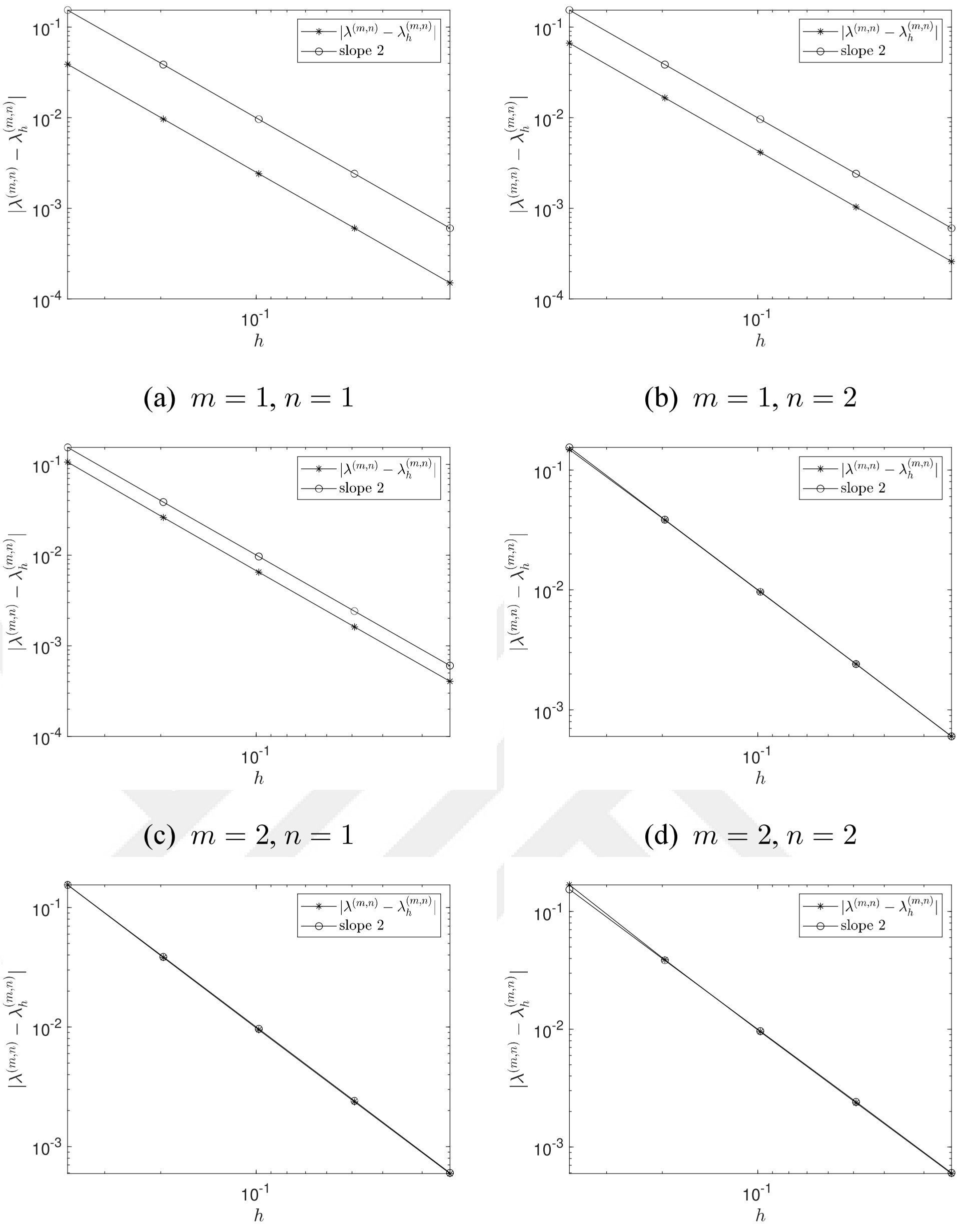

(a) $m = 1, n = 1$ (b) $m = 1, n = 2$

(c) $m = 2, n = 1$ (d) $m = 2, n = 2$

(e) $m = 1, n = 3$ (f) $m = 3, n = 1$

Figure 3.9: Log-log scale plot of $|\lambda^{(m,n)} - \lambda_h^{(m,n)}|/|\lambda^{(m,n)}|$ for Section 3.1.3.3 on uniform meshes and $N = 8, 16, \ldots, 128$.

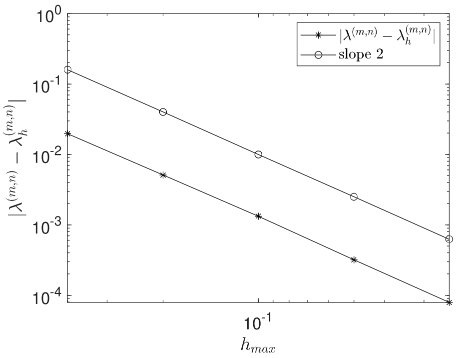

(a) $m = 1, n = 1$

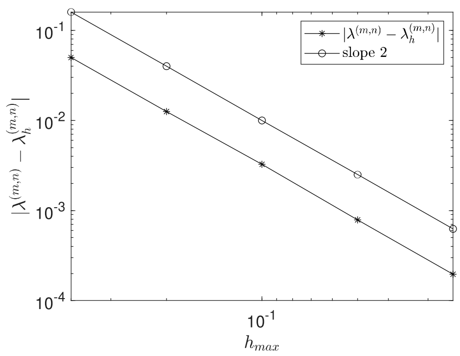

(b) $m = 1, n = 2$

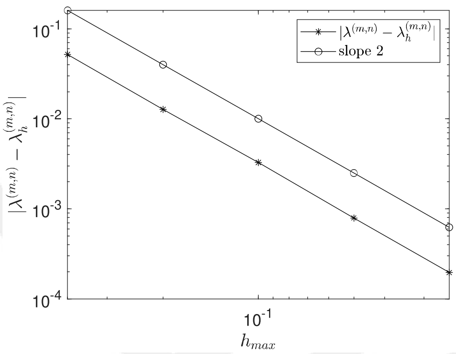

(c) $m = 2, n = 1$

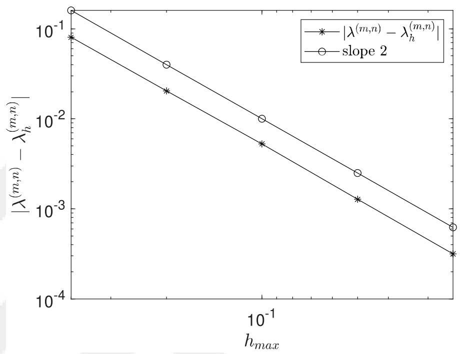

(d) $m = 2, n = 2$

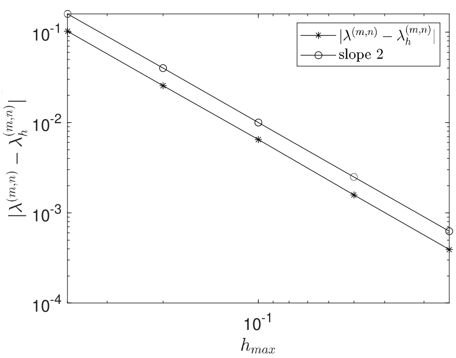

(e) $m = 1, n = 3$

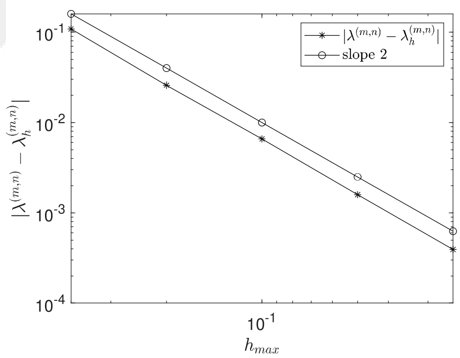

(f) $m = 3, n = 1$

Figure 3.10: Log-log scale plot of $|\lambda^{(m,n)} - \lambda_h^{(m,n)}|/|\lambda^{(m,n)}|$ for Section 3.1.3.3 on non-uniform meshes and $h_{max} = 0.4, 0.2, \ldots, 0.025$.

The convergence behavior of the approximate eigenfunctions $u_h^{(m,n)}$ to exact eigenfunctions $u^{(m,n)} = \sin(mx)\sin(ny)$ corresponding to the simple eigenvalues $\lambda^{(m,n)}$, where $m = n$, of the Laplace EVP on uniform meshes is given in Figure 3.11 and Figure 3.12 with respect to L^2- and H^1-norms respectively. Besides, the analogous behavior obtained on non-uniform meshes is also given in Figure 3.13 and Figure 3.14.

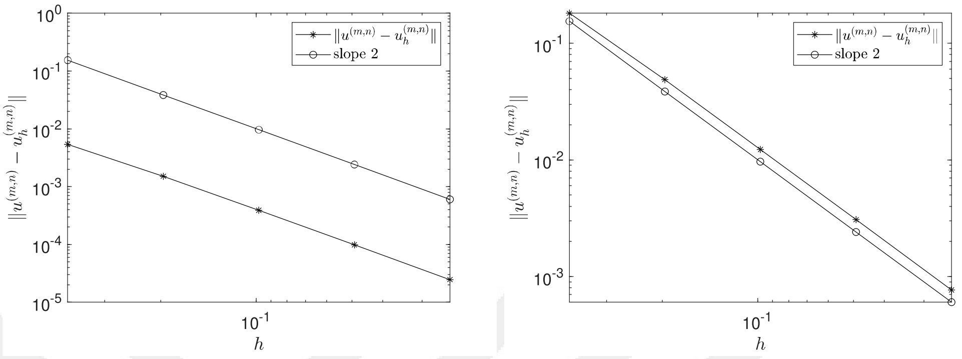

(a) $m = 1, n = 1$ (b) $m = 2, n = 2$

Figure 3.11: Log-log scale plot of $||u^{(m,n)} - u_h^{(m,n)}||/||u^{(m,n)}||$ for Section 3.1.3.3 on uniform meshes and $N = 8, 16, \ldots, 128$.

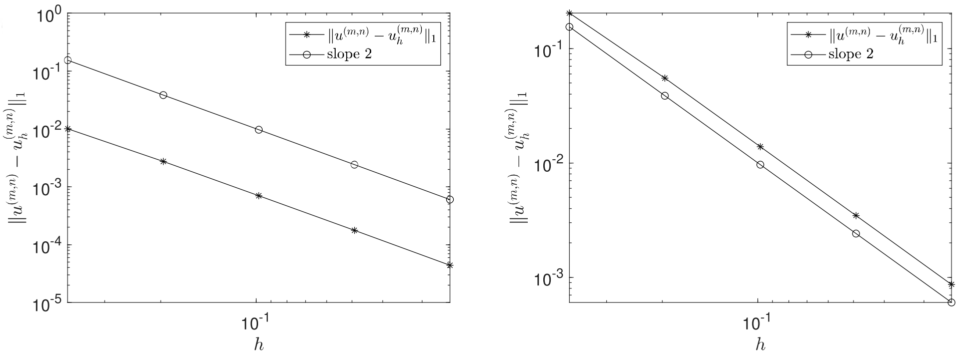

(a) $m = 1, n = 1$ (b) $m = 2, n = 2$

Figure 3.12: Log-log scale plot of $||u^{(m,n)} - u_h^{(m,n)}||_1/||u^{(m,n)}||_1$ for Section 3.1.3.3 on uniform meshes and $N = 8, 16, \ldots, 128$.

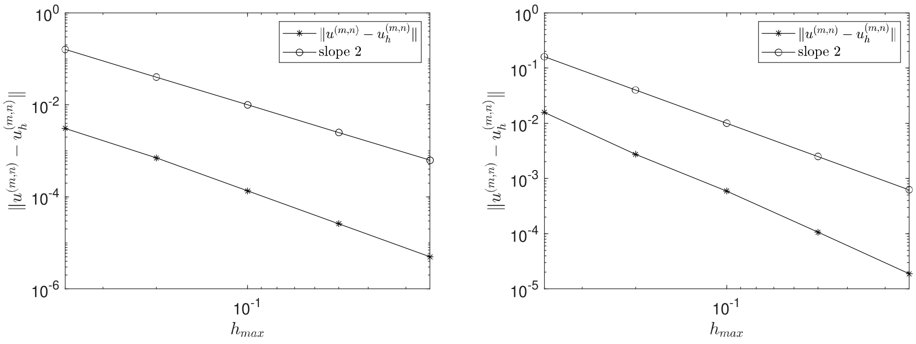

(a) $m = 1, n = 1$ (b) $m = 2, n = 2$

Figure 3.13: Log-log scale plot of $||u^{(m,n)} - u_h^{(m,n)}||/||u^{(m,n)}||$ for Section 3.1.3.3 on non-uniform meshes and $h_{max} = 0.4, 0.2, \ldots, 0.025$.

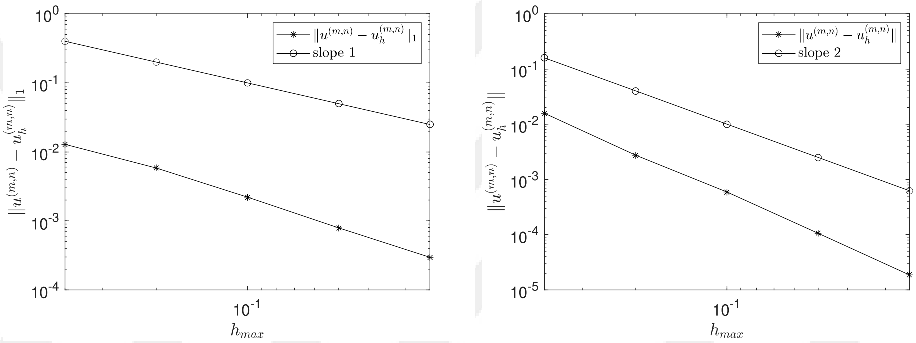

(a) $m = 1, n = 1$ (b) $m = 2, n = 2$

Figure 3.14: Log-log scale plot of $||u^{(m,n)} - u_h^{(m,n)}||_1/||u^{(m,n)}||_1$ for Section 3.1.3.3 on non-uniform meshes and $h_{max} = 0.4, 0.2, \ldots, 0.025$.

Compering Figure 3.11 and Figure 3.13, it is observed that the convergence behavior of the approximation eigenfunctions $u_h^{(m,n)}$ to the exact eigenfunctions $u^{(m,n)} = \sin(mx)\sin(ny)$ of the Laplace EVP is of order $O(h^2)$ with respect to L^2-norm on both uniform meshes and non-uniform meshes. In addition, while it is observed from Figure 3.12 that this convergence behavior on the uniform mesh with respect to H^1-norm is of order $O(h^2)$, it is clearly observed from Figure 3.14 that this behavior on non-uniform mesh is of order $O(h)$. Therefore, it is deduced that the approximate eigenfunctions $u_h^{(m,n)}$ behave more smoothly on uniform meshes.

While there is only one eigenfunction of the Laplace EVP on Ω_2 corresponding to a simple eigenvalue $\lambda^{(m,n)} = m^2 + n^2$, where $m = n$, there are two distinct eigenfunctions $u^{(m,n)} = \sin(mx)\sin(ny)$ and $u^{(n,m)} = \sin(nx)\sin(my)$ corresponding to double eigenvalues $\lambda^{(m,n)} = \lambda^{(n,m)} = m^2 + n^2$, where $m \neq n$. Therefore, the eigenfunctions corresponding to the double eigenvalues are considered separately.

When the approximate eigenvalues $\lambda_h^{(m,n)}$ given in Table 3.4 are considered, it is observed that there are two distinct eigenvalues $\lambda_h^{(m,n)}$ which are the approximations to the corresponding double eigenvalues $\lambda^{(m,n)} = \lambda^{(n,m)}$ for $m \neq n$. On the other hand, it is known that the dimension of the exact eigenspace is two and is spanned by the exact eigenfunctions $u^{(m,n)}$ and $u^{(n,m)}$ corresponding to the double eigenvalue for $m, n = 1, 2, \ldots$, and $m \neq n$. Since the approximate eigenvalues are distinct, the approximating eigenspace consists of two separate one-dimensional eigenspaces [12]. For this reason, in order to investigate the convergence behavior of approximate eigenfunctions corresponding to double eigenvalues, it is first assumed that

$$\alpha_{(m,n)} u^{(m,n)} + \alpha_{(n,m)} u^{(n,m)} = \beta_{(m,n)} u_h^{(m,n)} + \beta_{(n,m)} u_h^{(n,m)}, \tag{3.89}$$

where $u^{(m,n)}$, $u^{(n,m)}$, $u_h^{(m,n)}$, and $u_h^{(n,m)}$ denote the exact and approximate eigenfunctions corresponding to the double eigenvalues, and $\alpha_{(m,n)}$, $\alpha_{(n,m)}$, $\beta_{(m,n)}$, and $\beta_{(n,m)}$ are constants for $m, n = 1, 2, \ldots$, and $m \neq n$. Equation (3.89) can be written as

$$\begin{bmatrix} u^{(m,n)} & u^{(n,m)} \end{bmatrix} \begin{bmatrix} \alpha_{(m,n)} \\ \alpha_{(n,m)} \end{bmatrix} = \begin{bmatrix} u_h^{(m,n)} & u_h^{(n,m)} \end{bmatrix} \begin{bmatrix} \beta_{(m,n)} \\ \beta_{(n,m)} \end{bmatrix}. \tag{3.90}$$

When both sides of (3.90) are multiplied by $\begin{bmatrix} u^{(m,n)^T} & u^{(n,m)^T} \end{bmatrix}^T$ such that

$$\begin{bmatrix} u^{(m,n)^T} \\ u^{(n,m)^T} \end{bmatrix} \begin{bmatrix} u^{(m,n)} & u^{(n,m)} \end{bmatrix} \begin{bmatrix} \alpha_{(m,n)} \\ \alpha_{(n,m)} \end{bmatrix} = \begin{bmatrix} u^{(m,n)^T} \\ u^{(n,m)^T} \end{bmatrix} \begin{bmatrix} u_h^{(m,n)} & u_h^{(n,m)} \end{bmatrix} \begin{bmatrix} \beta_{(m,n)} \\ \beta_{(n,m)} \end{bmatrix}, \tag{3.91}$$

it is obtained that

$$\begin{bmatrix} u^{(m,n)^T} u^{(m,n)} & u^{(m,n)^T} u^{(n,m)} \\ u^{(n,m)^T} u^{(m,n)} & u^{(n,m)^T} u^{(n,m)} \end{bmatrix} \begin{bmatrix} \alpha_{(m,n)} \\ \alpha_{(n,m)} \end{bmatrix} = \begin{bmatrix} u^{(m,n)^T} u_h^{(m,n)} & u^{(m,n)^T} u_h^{(n,m)} \\ u^{(n,m)^T} u_h^{(m,n)} & u^{(n,m)^T} u_h^{(n,m)} \end{bmatrix} \begin{bmatrix} \beta_{(m,n)} \\ \beta_{(n,m)} \end{bmatrix}. \tag{3.92}$$

Let the matrix in the right hand side of (3.92) be denoted by B. Since the matrix in the left hand side of (3.92) is identity matrix as a result of the orthonormality, Equation (3.92) is reduced as

$$\begin{bmatrix} \alpha_{(m,n)} \\ \alpha_{(n,m)} \end{bmatrix} = B \begin{bmatrix} \beta_{(m,n)} \\ \beta_{(n,m)} \end{bmatrix}. \tag{3.93}$$

If B is a non-singular matrix, and $\begin{bmatrix}\alpha_{(m,n)} & \alpha_{(n,m)}\end{bmatrix}^T$ is a nonzero vector, then the existence of nonzero constants $\beta_{(m,n)}$, and $\beta_{(n,m)}$ is guaranteed. To show that B is a non-singular matrix numerically, its determinant is listed in Table 3.6 for $m, n = 1, 2, 3, 4$.

Table 3.6: Determinant of B and the corresponding double eigenvalues for Section 3.1.3.3 and $N = 64$.

$\lambda^{(m,n)}$	$u^{(m,n)},\ u^{(n,m)}$	$u_h^{(m,n)},\ u_h^{(n,m)}$	$\lvert B\rvert$
$\lambda^{(1,2)} = 5$	$u^{(1,2)} = \sin(x)\sin(2y),\ u^{(2,1)} = \sin(2x)\sin(y)$	$u_h^{(1,2)},\ u_h^{(2,1)}$	1.0000
$\lambda^{(1,3)} = 10$	$u^{(1,3)} = \sin(x)\sin(3y),\ u^{(3,1)} = \sin(3x)\sin(y)$	$u_h^{(1,3)},\ u_h^{(3,1)}$	1.0000
$\lambda^{(2,3)} = 13$	$u^{(2,3)} = \sin(2x)\sin(3y),\ u^{(3,2)} = \sin(3x)\sin(2y)$	$u_h^{(2,3)},\ u_h^{(3,2)}$	0.9978
$\lambda^{(1,4)} = 15$	$u^{(1,4)} = \sin(x)\sin(4y),\ u^{(4,1)} = \sin(4x)\sin(y)$	$u_h^{(1,4)},\ u_h^{(4,1)}$	0.9970

If it is assumed that $\begin{bmatrix}\alpha_{(m,n)} & \alpha_{(n,m)}\end{bmatrix} = \begin{bmatrix}1 & 0\end{bmatrix}$, then $\begin{bmatrix}\beta_{(m,n)} & \beta_{(n,m)}\end{bmatrix}$ is easily determined from (3.93). Moreover, (3.90) is reduced as

$$u^{(m,n)} = \beta_{(m,n)} u_h^{(m,n)} + \beta_{(n,m)} u_h^{(n,m)}. \tag{3.94}$$

In the case of $\begin{bmatrix}\alpha_{(m,n)} & \alpha_{(n,m)}\end{bmatrix} = \begin{bmatrix}0 & 1\end{bmatrix}$, it is similarly obtained that

$$u^{(n,m)} = \beta_{(m,n)} u_h^{(m,n)} + \beta_{(n,m)} u_h^{(n,m)}. \tag{3.95}$$

To validate this behavior qualitatively, the contour plots of the exact eigenfunctions $u^{(m,n)} = \sin(mx)\sin(ny)$, $u^{(n,m)} = \sin(nx)\sin(my)$ and the corresponding approximate eigenfunctions $u_h^{(m,n)}$ and $u_h^{(n,m)}$ obtained on uniform meshes are provided in Figure 3.15 and Figure 3.16 together with the linear combinations of the approximate eigenfunctions $u_h^{(m,n)}$ and $u_h^{(n,m)}$ given in the right hand sides of (3.94) and (3.95) for $m, n = 1, 2, 3$. It is important to note here that the same contour plots are also obtained on non-uniform meshes.

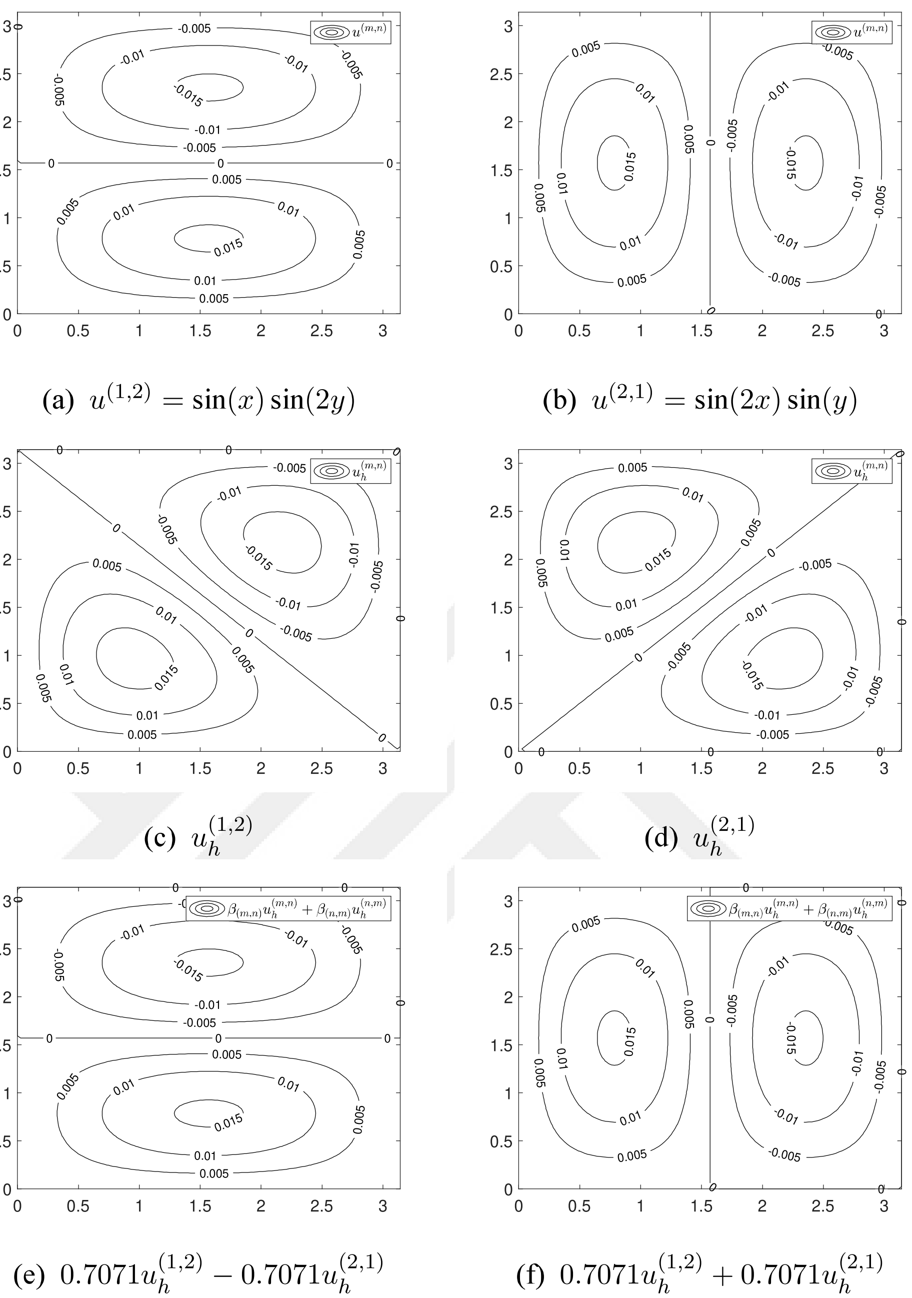

(a) $u^{(1,2)} = \sin(x)\sin(2y)$

(b) $u^{(2,1)} = \sin(2x)\sin(y)$

(c) $u_h^{(1,2)}$

(d) $u_h^{(2,1)}$

(e) $0.7071u_h^{(1,2)} - 0.7071u_h^{(2,1)}$

(f) $0.7071u_h^{(1,2)} + 0.7071u_h^{(2,1)}$

Figure 3.15: Contour plots of approximate and exact eigenfunctions corresponding to $\lambda^{(m,n)}$ and $\lambda^{(n,m)}$ for Section 3.1.3.3, $m, n = 1, 2$, and $N = 128$.

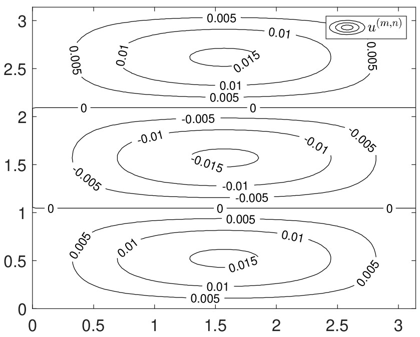

(a) $u^{(1,3)} = \sin(x)\sin(3y)$

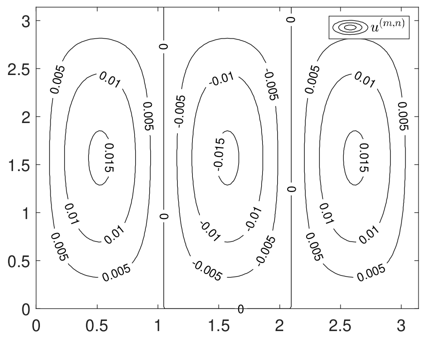

(b) $u^{(3,1)} = \sin(3x)\sin(y)$

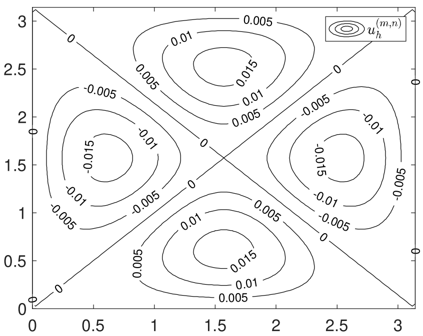

(c) $u_h^{(1,3)}$

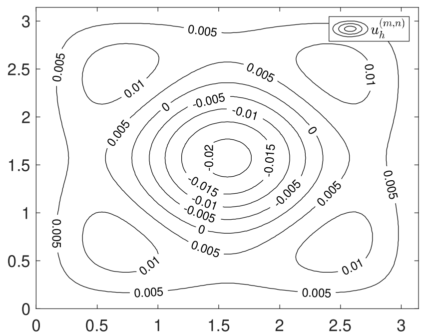

(d) $u_h^{(3,1)}$

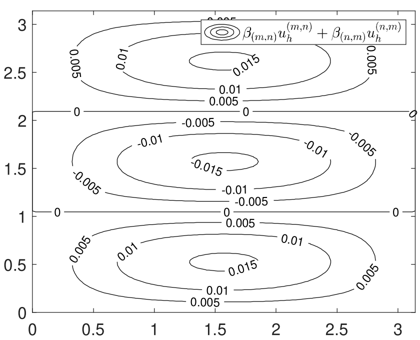

(e) $0.7071u_h^{(1,3)} + 0.7071u_h^{(3,1)}$

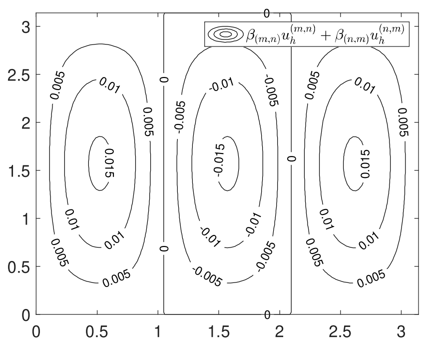

(f) $-0.7071u_h^{(1,3)} + 0.7071u_h^{(3,1)}$

Figure 3.16: Contour plots of approximate and exact eigenfunctions corresponding to $\lambda^{(m,n)}$ and $\lambda^{(n,m)}$ for Section 3.1.3.3, $m, n = 1, 3$, and $N = 128$.

From Figure 3.15 and Figure 3.16, it is observed that the linear combinations of the approximate eigenfunctions $u_h^{(m,n)}$ and $u_h^{(n,m)}$ are reasonable approximations to the exact eigenfunctions $u^{(m,n)} = \sin(mx)\sin(ny)$ and $u^{(n,m)} = \sin(nx)\sin(my)$. The convergence behavior of this linear combinations to exact eigenfunctions $u^{(m,n)}$ and $u^{(n,m)}$ corresponding to the multiple eigenvalues $\lambda^{(m,n)} = m^2 + n^2$ of the Laplace EVP for $m \neq n$ is given in Figure 3.17 and Figure 3.18 with respect to L^2- and H^1-norms respectively.

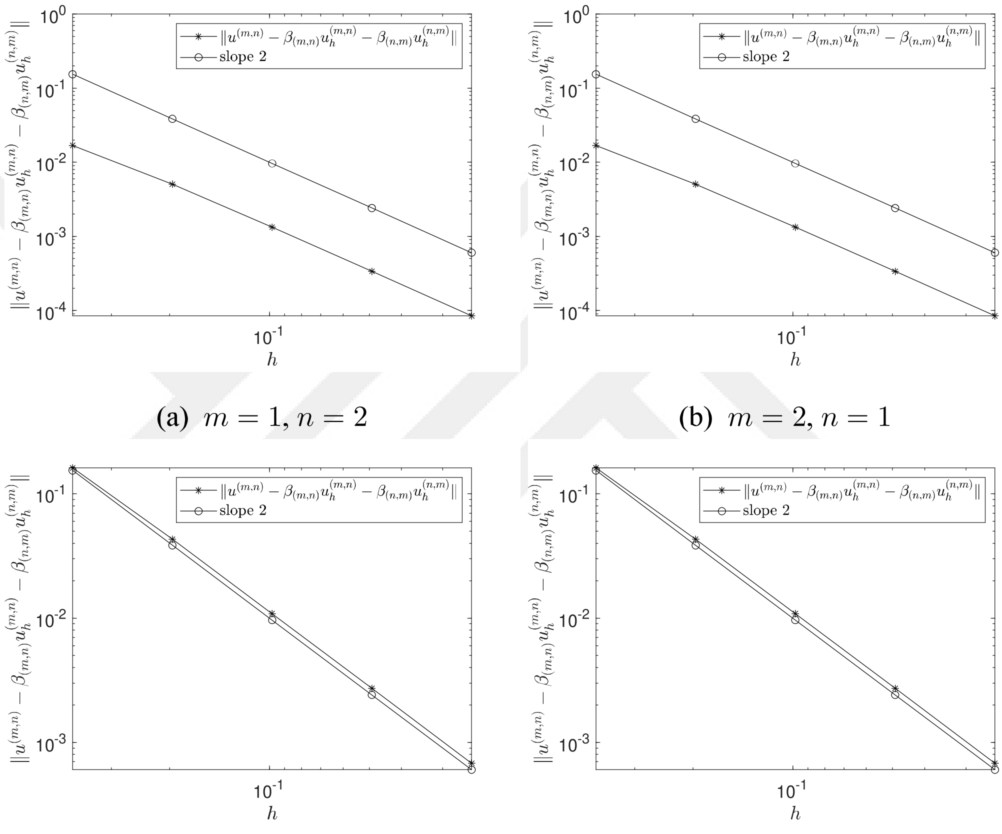

(a) $m = 1, n = 2$ (b) $m = 2, n = 1$

(c) $m = 1, n = 3$ (d) $m = 3, n = 1$

Figure 3.17: Log-log scale plot of $||u^{(m,n)} - \beta_{(m,n)}u_h^{(m,n)} - \beta_{(n,m)}u_h^{(n,m)}||/||u^{(m,n)}||$ on uniform meshes for Section 3.1.3.3 and $N = 8, 16, 32, 64, 128$.

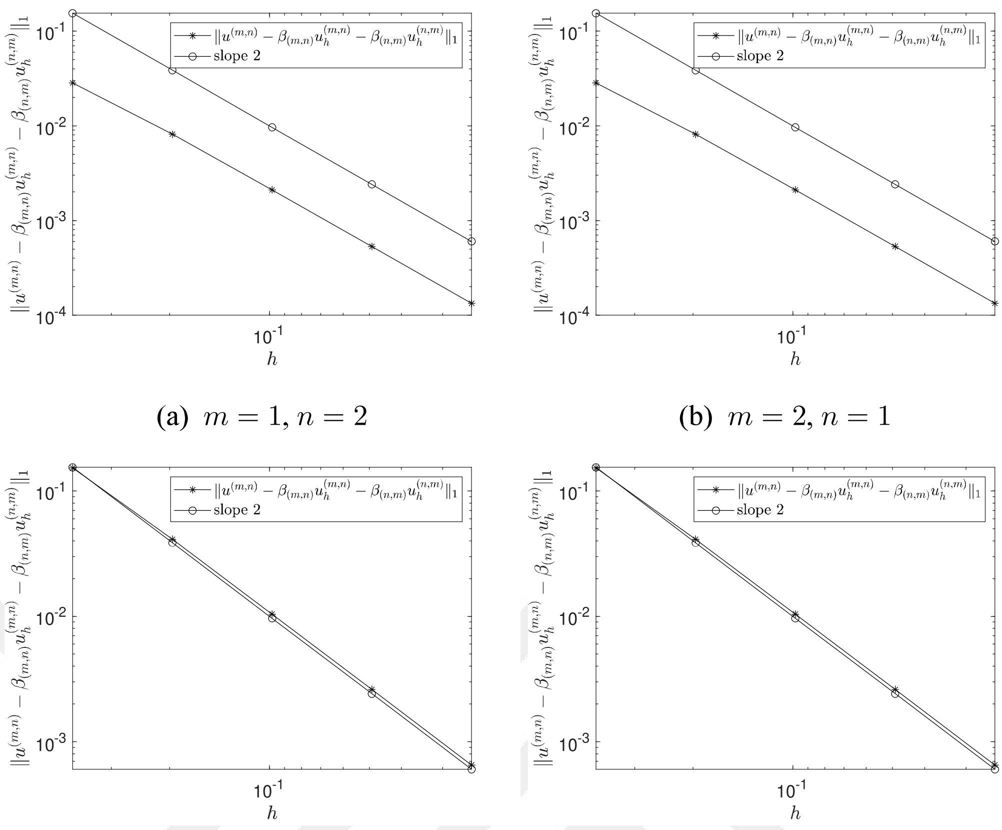

(a) $m = 1, n = 2$ (b) $m = 2, n = 1$

(c) $m = 1, n = 3$ (d) $m = 3, n = 1$

Figure 3.18: Log-log scale plot of $||u^{(m,n)} - \beta_{(m,n)}u_h^{(m,n)} - \beta_{(n,m)}u_h^{(n,m)}||_1/||u^{(m,n)}||_1$ on uniform meshes for Section 3.1.3.3 and $N = 8, 16, 32, 64, 128$.

From the Figure 3.17 and Figure 3.18, it is clearly seen that the linear combinations of $u_h^{(m,n)}$ and $u_h^{(n,m)}$ satisfy

$$||u^{(m,n)} - \beta_{(m,n)}u_h^{(m,n)} - \beta_{(n,m)}u_h^{(n,m)}|| \leq Ch^2, \tag{3.96a}$$

$$||u^{(m,n)} - \beta_{(m,n)}u_h^{(m,n)} - \beta_{(n,m)}u_h^{(n,m)}||_1 \leq Ch, \tag{3.96b}$$

where C is an arbitrary constant.

3.1.3.4. Linear Elements on Ω_3

In this section, convergence behavior of the approximate eigenfunctions $u_h^{(p,q)}$ to the exact eigenfunctions $u^{(p,q)} = J\left(\rho^{(p,q)} r\right)$ corresponding to the simple eigenvalues $\lambda^{(p,q)} = {\rho^{(p,q)}}^2$, where $p = 0$ and $\rho^{(p,q)}$ is the qth root of Bessel's function J_p of order p, are investigated on non-uniform meshes of the unit disc Ω_3. The numerical results concerning the eigenfunctions associated with the multiple eigenvalues $\lambda^{(p,q)} = {\rho^{(p,q)}}^2$, where $p \neq 0$, are obtained for linearly independent eigenfunctions $u^{(p,q)} = J\left(\rho^{(p,q)} r\right) \sin(p\theta)$ and $u^{(p,q)} = J\left(\rho^{(p,q)} r\right) \cos(p\theta)$ separately. Also, the convergence behavior of the approximate eigenvalues $\lambda_h^{(p,q)}$, corresponding to the both simple and multiple eigenvalues $\lambda^{(p,q)}$, are investigated.

The fist fifteen approximate eigenvalues $\lambda_h^{(p,q)}$ and exact eigenvalues $\lambda^{(p,q)}$ of the Laplace EVP on Ω_3 are given in Table 3.7, together with the rates of convergence and the size S of the solved linear system of equations reduced by imposing the boundary conditions. The errors between the approximate eigenvalues $\lambda_h^{(p,q)}$ and the exact eigenvalues $\lambda^{(p,q)}$ are shown in Figure 3.19 and Figure 3.20. From Table 3.7, Figure 3.19, and Figure 3.20, it is observed that the approximate eigenvalues $\lambda_h^{(p,q)}$ converge the exact eigenvalues $\lambda^{(p,q)}$ as h_{max} is decreasing, and this convergence behavior is observed to be of order $O(h^2)$ as expected from Theorem (3.4) as in Section 3.1.3.3.

Table 3.7: First fifteen approximate and exact eigenvalues on the unit disc for Section 3.1.3.4 and $h_{max} = 0.4, 0.2, \ldots, 0.025$.

p, q	$\lambda^{(p,q)}$	$h_{max} = 0.4$ $S : 12 \times 12$	$h_{max} = 0.2$ $S : 73 \times 73$	$h_{max} = 0.1$ $S : 316 \times 316$	$h_{max} = 0.05$ $S : 1370 \times 1370$	$h_{max} = 0.025$ $S : 6028 \times 6028$
$0, 1$	5.7832	6.1608	5.8698 (2.1)	5.8047 (2.0)	5.7886 (2.0)	5.7844 (2.1)
$1, 1$	14.6820	17.4675	15.2977 (2.1)	14.8351 (2.0)	14.7190 (2.0)	14.6907 (2.0)
$1, 1$	14.6820	17.5397	15.2991 (2.2)	14.8378 (2.0)	14.7194 (2.1)	14.6907 (2.1)
$2, 1$	26.3746	35.0387	28.3286 (2.1)	26.8612 (2.0)	26.4917 (2.1)	26.4024 (2.1)
$2, 1$	26.3746	35.9420	28.3436 (2.3)	26.8793 (2.0)	26.4936 (2.1)	26.4026 (2.1)
$0, 2$	30.4713	41.0836	33.1361 (2.0)	31.1656 (1.9)	30.6349 (2.1)	30.5094 (2.1)
$3, 1$	40.7065	60.3291	45.3231 (2.1)	41.8674 (2.0)	40.9838 (2.1)	40.7707 (2.1)
$3, 1$	40.7065	60.8080	45.3358 (2.1)	41.8730 (2.0)	40.9843 (2.1)	40.7709 (2.1)
$1, 2$	49.2185	75.8528	56.9692 (1.8)	50.9822 (2.1)	49.6436 (2.1)	49.3204 (2.1)
$1, 2$	49.2185	77.4468	57.0001 (1.9)	51.0280 (2.1)	49.6529 (2.1)	49.3207 (2.1)
$4, 1$	57.5829	84.1747	66.8191 (1.5)	59.8437 (2.0)	58.1247 (2.1)	57.7067 (2.1)
$4, 1$	57.5829	128.0208	67.1903 (2.9)	59.9110 (2.1)	58.1401 (2.1)	57.7082 (2.2)
$2, 2$	70.8500	-	86.0513	74.5781 (2.0)	71.7255 (2.1)	71.0590 (2.1)
$2, 2$	70.8500	-	86.3187	74.6803 (2.0)	71.7454 (2.1)	71.0596 (2.1)
$0, 3$	74.8870	-	91.8737	79.0550 (2.0)	75.8718 (2.1)	75.1237 (2.1)

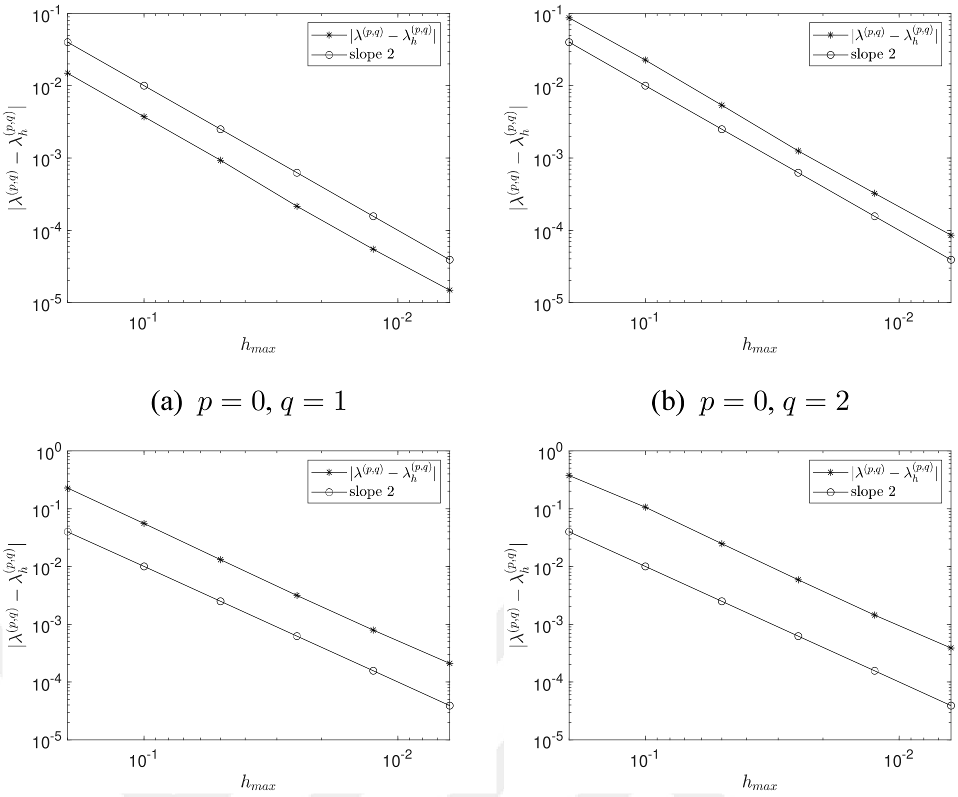

(a) $p = 0, q = 1$ (b) $p = 0, q = 2$

(c) $p = 0, q = 3$ (d) $p = 0, q = 4$

Figure 3.19: Log-log scale plot of $|\lambda^{(p,q)} - \lambda_h^{(p,q)}|/|\lambda^{(p,q)}|$ associated with the simple eigenvalues for Section 3.1.3.4 and $h_{max} = 0.2, 0.1, \ldots, 0.00625$.

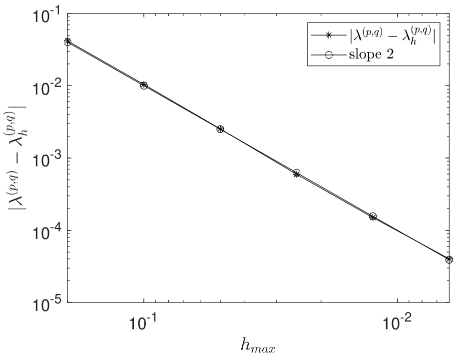

(a) $p = 1, q = 1$

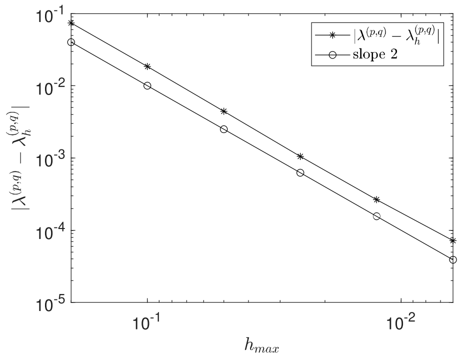

(b) $p = 2, q = 1$

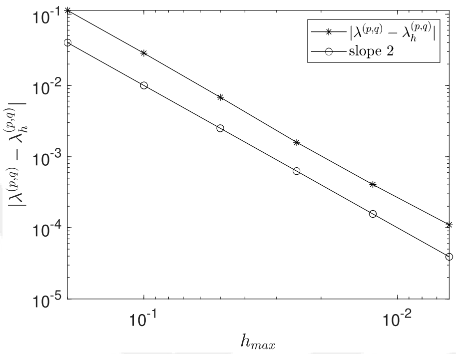

(c) $p = 3, q = 1$

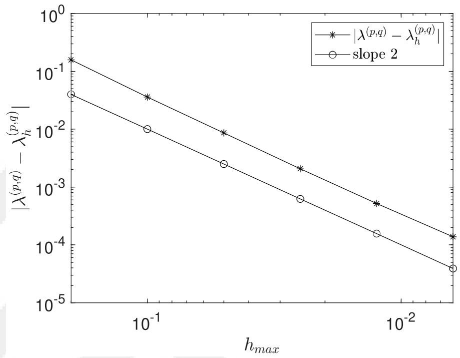

(d) $p = 1, q = 2$

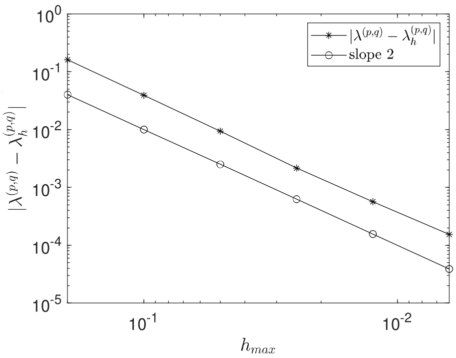

(e) $p = 4, q = 1$

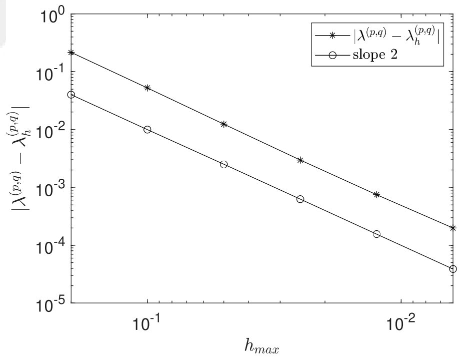

(f) $p = 2, q = 2$

Figure 3.20: Log-log scale plot of $|\lambda^{(p,q)} - \lambda_h^{(p,q)}|/|\lambda^{(p,q)}|$ associated with the multiple eigenvalues for Section 3.1.3.4 and $h_{max} = 0.2, 0.1, \ldots, 0.00625$.

The errors between approximate eigenfunctions $u_h^{(p,q)}$ and exact eigenfunctions $u^{(p,q)}$ corresponding to simple eigenvalues with respect to L^2- and H^1-norms are shown in Figure 3.21 and Figure 3.22 respectively.

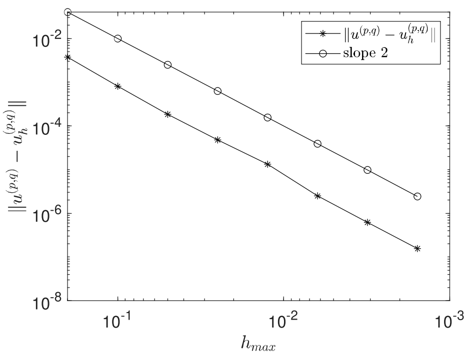

(a) $p = 0, q = 1$

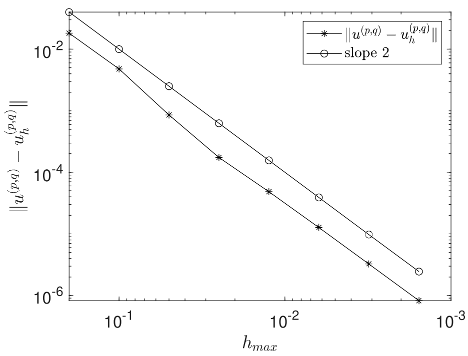

(b) $p = 0, q = 2$

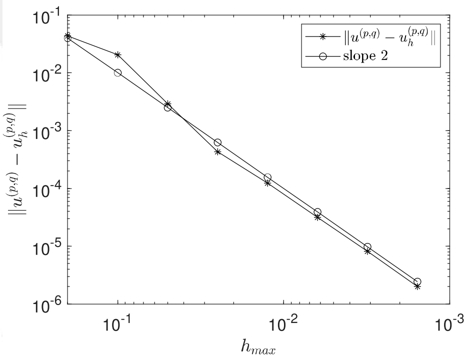

(c) $p = 0, q = 3$

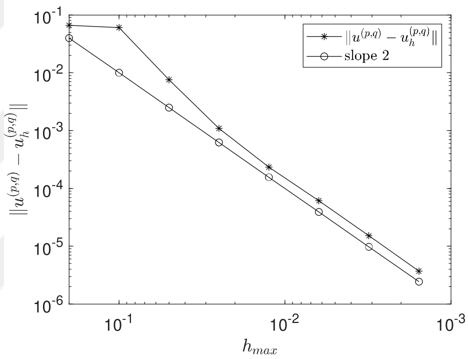

(d) $p = 0, q = 4$

Figure 3.21: Log-log scale plot of $||u^{(p,q)} - u_h^{(p,q)}||/||u^{(p,q)}||$ corresponding to the simple eigenvalues for Section 3.1.3.4 and $h_{max} = 0.2, 0.1, \ldots, 0.0015625$.

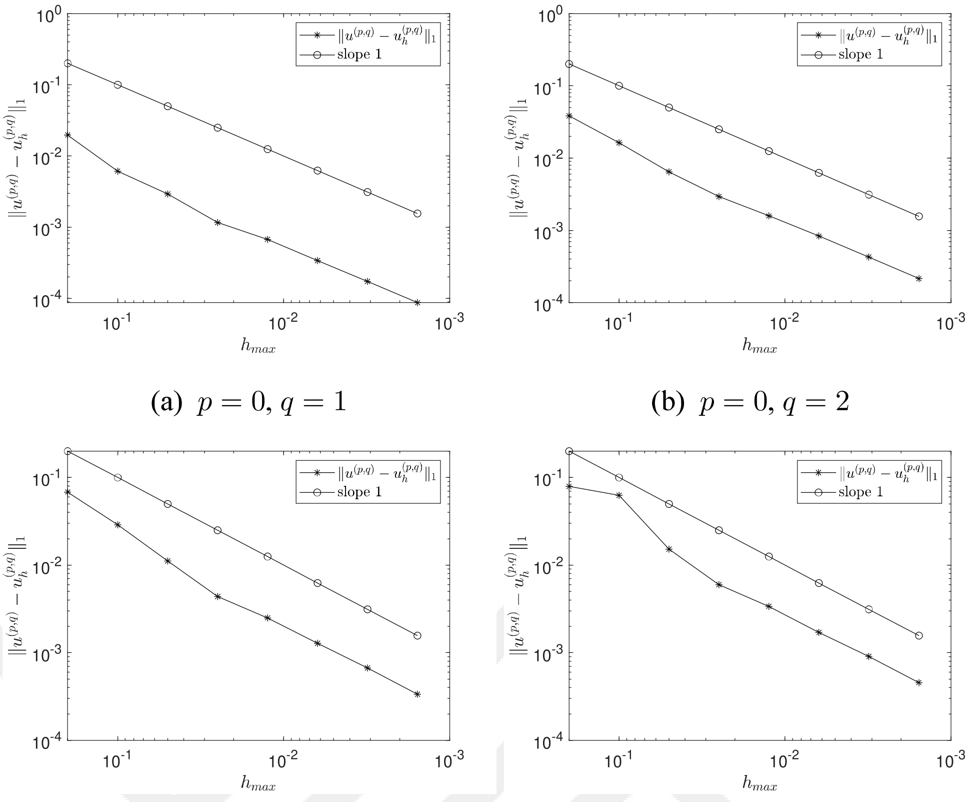

(a) $p = 0, q = 1$ (b) $p = 0, q = 2$

(c) $p = 0, q = 3$ (d) $p = 0, q = 4$

Figure 3.22: Log-log scale plot of $||u^{(p,q)} - u_h^{(p,q)}||_1/||u^{(p,q)}||_1$ corresponding to the simple eigenvalues for Section 3.1.3.4 and $h_{max} = 0.2, 0.1, \ldots, 0.0015625$.

From Figure 3.21 and Figure 3.22, it is observed that the convergence behavior of the approximation eigenfunctions $u_h^{(p,q)}$ to the exact eigenfunctions, corresponding to the simple eigenvalues, is of order $O(h^2)$ with respect to L^2-norm, while this convergence behavior with respect to H^1-norm is of order $O(h)$. On the other hand, it is known that the linear combinations of the approximate eigenfunctions corresponding to the multiple eigenvalues are reasonable approximations to the corresponding exact eigenfunctions from (3.96). To illustrate this behavior on Ω_3, the contour plots of the exact eigenfunctions $u^{(p,q)_1} = J\left(\rho^{(p,q)}r\right)\sin(p\theta)$, $u^{(p,q)_2} = J\left(\rho^{(p,q)}r\right)\cos(p\theta)$, and the approximate eigenfunctions $u_h^{(p,q)_1}$, $u_h^{(p,q)_2}$ are given in Figure 3.23 and Figure 3.23, together with the linear combinations of the approximate eigenfunctions $\beta_{(p,q)_1}u_h^{(p,q)_1} + \beta_{(p,q)_2}u_h^{(p,q)_2}$, where $i = 1, 2$ and $\beta_{(p,q)_1}$, $\beta_{(p,q)_2}$ are constants obtained in a similar way with (3.93).

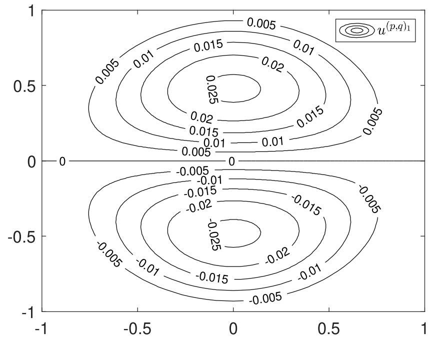

(a) $u^{(1,1)_1} = J_1(\rho^{(1,1)}r)\sin(\theta)$

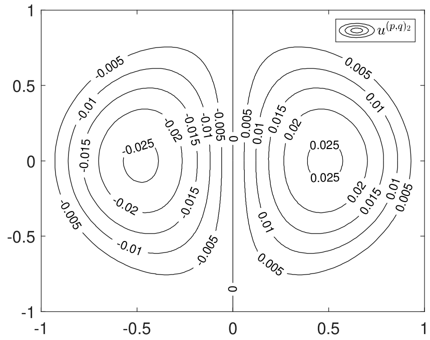

(b) $u^{(1,1)_2} = J_1(\rho^{(1,1)}r)\cos(\theta)$

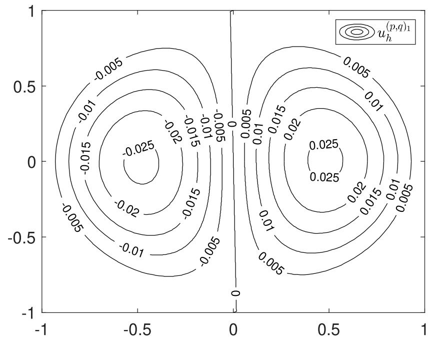

(c) $u_h^{(1,1)_1}$

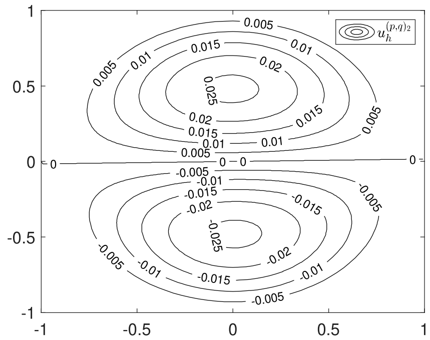

(d) $u_h^{(1,1)_2}$

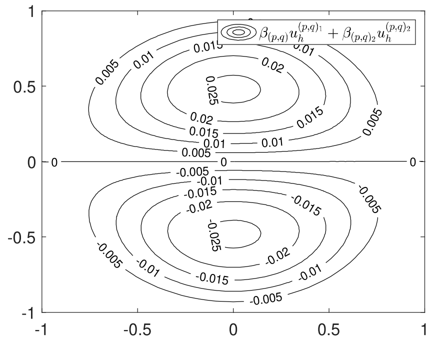

(e) $0.0146u_h^{(1,1)_1} - 0.9999u_h^{(1,1)_2}$

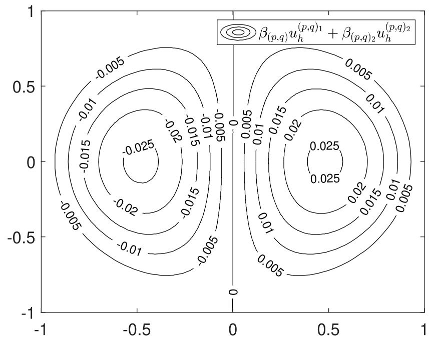

(f) $0.9999u_h^{(1,1)_1} - 0.0175u_h^{(1,1)_2}$

Figure 3.23: Contour plots of approximate and exact eigenfunctions corresponding to the multiple eigenvalues for Section 3.1.3.4, $p = 1$, $q = 1$, and $h_{max} = 0.025$.

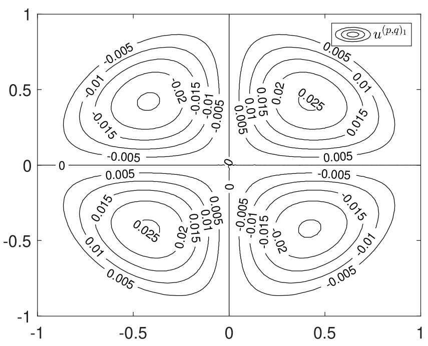

(a) $u^{(2,1)_1} = J_2(\rho^{(2,1)}r)\sin(2\theta)$

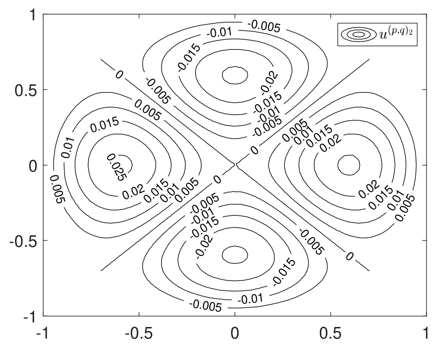

(b) $u^{(2,1)_2} = J_2(\rho^{(2,1)}r)\cos(2\theta)$

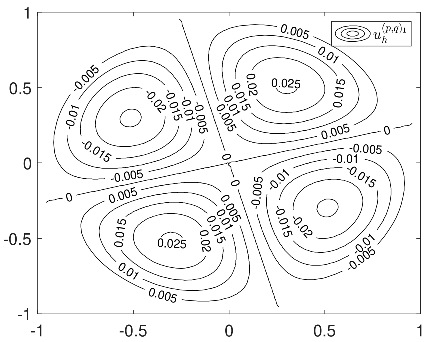

(c) $u_h^{(2,1)_1}$

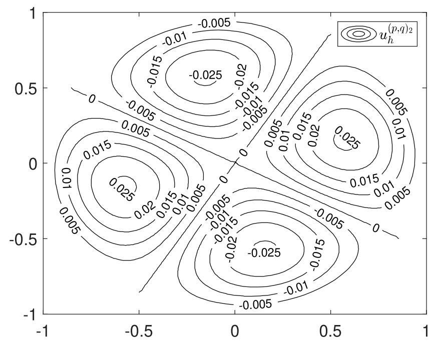

(d) $u_h^{(2,1)_2}$

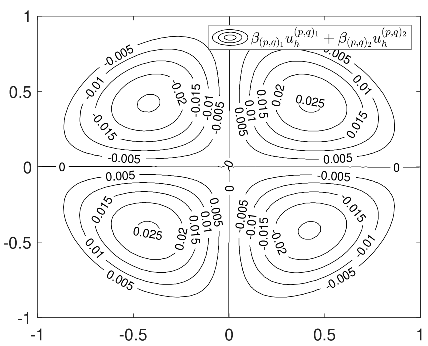

(e) $0.8660u_h^{(2,1)_1} + 0.4997u_h^{(2,1)_2}$

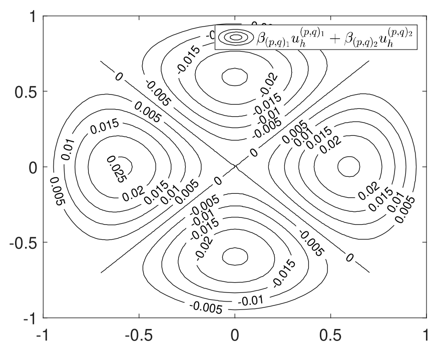

(f) $-0.4968u_h^{(2,1)_1} + 0.8681u_h^{(2,1)_2}$

Figure 3.24: Contour plots of approximate and exact eigenfunctions corresponding to the multiple eigenvalues for Section 3.1.3.4, $p = 2$, $q = 1$, and $h_{max} = 0.025$.

3.2. Boundary Perturbations

Based on the fact that FEM solutions of EVPs are obtained on discretized domains considered within the original domains where the problem is originally defined, the effects of boundary perturbations on the Laplace EVP are investigated both analytically and numerically in this section. To do this, it is assumed that the perturbed domain Ω' is placed within the original domain Ω and approximately represented by the boundary of the original domain. Then, the convergence behavior of both analytical and FEM solutions on Ω' to the analytical solution on Ω are investigated with respect to the perturbation parameter δ which is assumed to be approximately close to zero.

Let the Laplace EVP on the perturbed domain Ω' be defined as

$$-\Delta u' = \lambda' u' \quad \text{in } \Omega', \tag{3.97a}$$

$$u' = 0 \qquad \text{on } \partial\Omega'. \tag{3.97b}$$

The analytical solution of Problem (3.97) can be obtained in a similar way as is done for Ω_1, Ω_2, and Ω_3 in 1D-case and 2D-cases.

3.2.1. 1D Perturbation on an Interval

Assume that Ω_1' is the interval $[\delta_1, \pi - \delta_2]$, and δ_i, $i = 1, 2$, is close to zero. For this perturbed domain, the Laplace EVP is written as

$$\Delta u' = \lambda' u' \quad \text{in } \Omega, \tag{3.98a}$$

$$u'(\delta_1) = u'(\pi - \delta_2) = 0. \tag{3.98b}$$

Let σ_i, $i = 1, 2$, be the roots of the characteristic polynomial of (3.98a) so that

$$\sigma^2 + \lambda' = 0 \Rightarrow \sigma_{1,2} = \mp\sqrt{\lambda'} i. \tag{3.99}$$

When $\lambda' \leq 0$, the Laplace EVP has the trivial solution. If it is assumed that $\lambda' < 0$, the general solution of (3.98a) is written as

$$u'(x) = c_1 e^{\sqrt{\lambda'}x} + c_2 e^{-\sqrt{\lambda'}x}. \tag{3.100}$$

To satisfy the boundary conditions (3.98b), it must be either $\delta_1 + \delta_2 = \pi$ or $u'(x) = 0$. Since δ_i is close to zero, it cannot be so that $\delta_1 + \delta_2 = \pi$. Thus, the trivial solution $u'(x) = 0$ is obtained. In the case of $\lambda' = 0$, the general solution of (3.98a) is $u'(x) = c_1 + c_2 x$, and the same result in the case of $\lambda' < 0$ is obtained when the boundary conditions are applied. When $\lambda' > 0$, the general solution of (3.2a) is in the form

$$u'(x) = c_1 \cos(\sqrt{\lambda'}x) + c_2 \sin(\sqrt{\lambda'}x). \tag{3.101}$$

Applying the boundary conditions (3.98b) to (3.101) yields

$$\begin{aligned} 0 &= c_1 \cos(\sqrt{\lambda'}(\delta_1)) + c_2 \sin(\sqrt{\lambda'}(\delta_1)) \\ &\Rightarrow c_1 = -c_2 \tan(\sqrt{\lambda'}(\delta_1)), \end{aligned} \tag{3.102}$$

and

$$\begin{aligned} 0 &= c_1 \cos(\sqrt{\lambda'}(\pi - \delta_2)) + c_2 \sin(\sqrt{\lambda'}(\pi - \delta_2)) \\ &\Rightarrow c_1 = -c_2 \tan(\sqrt{\lambda'}(\pi - \delta_2)). \end{aligned} \tag{3.103}$$

From (3.102) and (3.103) it can be written

$$\tan(\sqrt{\lambda'}(\delta_1)) = \tan(\sqrt{\lambda'}(\pi - \delta_2)). \tag{3.104}$$

Taking the inverse tangent of the both sides of (3.104) results in the eigenvalue

$$\lambda'^{(k)} = \left(\frac{k\pi}{\pi - \delta_1 - \delta_2} \right)^2, \tag{3.105}$$

for $k \in \mathbb{Z}^+$. If c_1 is inserted into (3.101) in terms of c_2, the eigenfunction corresponding to $\lambda'^{(k)}$ is obtained as

$$u'^{(k)}(x) = \frac{\sin\left(\dfrac{k\pi}{\pi - \delta_1 - \delta_2}(x - \delta_1) \right)}{\cos\left(\dfrac{k\pi}{\pi - \delta_1 - \delta_2}\delta_1 \right)}, \tag{3.106}$$

for $k \in \mathbb{Z}^+$.

3.2.2. 2D Perturbation on a Rectangle

Assume that Ω_2' is the rectangle $[\delta_1, \pi - \delta_2] \times [\delta_3, \pi - \delta_4]$ which is inscribed in the domain $\Omega_2 = [0, \pi] \times [0, \pi]$ given in the 2D-case that is a square. On this two-dimensional perturbed domain, the Laplace EVP is written as

$$-u'_{xx} - u'_{yy} = \lambda' u' \quad \text{in } \Omega, \tag{3.107a}$$

$$u'(\delta_1, y) = 0, \tag{3.107b}$$

$$u'(\pi - \delta_2, y) = 0, \tag{3.107c}$$

$$u'(x, \delta_3) = 0, \tag{3.107d}$$

$$u'(x, \pi - \delta_4) = 0. \tag{3.107e}$$

As given in (3.10), separation of variables $u'(x, y) = X(x)Y(y)$ results in

$$X'' + \lambda'_x X = 0, \tag{3.108a}$$

$$Y'' + \lambda'_y Y = 0, \tag{3.108b}$$

where $\lambda' = \lambda'_x + \lambda'_y$ such that $\lambda'_x = -\frac{X''}{X}$ and $\lambda'_y = -\frac{Y''}{Y}$. From the 1D-case, it is known that (3.108a) and (3.108b) have the trivial solution when $\lambda'_x \leq 0$ and $\lambda'_y \leq 0$. If it is assumed that $\lambda_x > 0$ and $\lambda_y > 0$, the general solutions of (3.108a) and (3.108b) take the form

$$X(x) = c_1 \cos(\sqrt{\lambda'_x} x) + c_2 \sin(\sqrt{\lambda'_x} x), \tag{3.109a}$$

$$Y(y) = c_3 \cos(\sqrt{\lambda'_y} y) + c_4 \sin(\sqrt{\lambda'_y} y), \tag{3.109b}$$

respectively. In a similar way as in 1D perturbation on an interval, it is obtained that

$$X(x) = \frac{\sin\left(\dfrac{m\pi}{\pi - \delta_1 - \delta_3}(x - \delta_1)\right)}{\cos\left(\dfrac{m\pi}{\pi - \delta_1 - \delta_3}\delta_1\right)}, \tag{3.110a}$$

$$Y(y) = \frac{\sin\left(\dfrac{n\pi}{\pi - \delta_2 - \delta_4}(y - \delta_2)\right)}{\cos\left(\dfrac{n\pi}{\pi - \delta_2 - \delta_4}\delta_2\right)}, \tag{3.110b}$$

and

$$\lambda'_x = \left(\frac{m\pi}{\pi - \delta_1 - \delta_3}\right)^2, \tag{3.111a}$$

$$\lambda'_y = \left(\frac{n\pi}{\pi - \delta_2 - \delta_4}\right)^2, \tag{3.111b}$$

for $m, n \in \mathbb{Z}^+$. Since $u'(x,y) = X(x)Y(y)$ and $\lambda' = \lambda'_x + \lambda'_y$, the analytical solution of the Laplace EVP is obtained as

$$u'^{(m,n)}(x,y) = \frac{\sin\left(\dfrac{m\pi}{\pi-\delta_1-\delta_3}(x-\delta_1)\right)\sin\left(\dfrac{n\pi}{\pi-\delta_2-\delta_4}(y-\delta_2)\right)}{\cos\left(\dfrac{m\pi}{\pi-\delta_1-\delta_3}\delta_1\right)\cos\left(\dfrac{n\pi}{\pi-\delta_2-\delta_4}\delta_2\right)}, \tag{3.112a}$$

$$\lambda'^{(m,n)} = \left(\frac{m\pi}{\pi-\delta_1-\delta_3}\right)^2 + \left(\frac{n\pi}{\pi-\delta_2-\delta_4}\right)^2, \tag{3.112b}$$

where m and n are positive integers.

3.2.3. 2D Perturbation on a Disc

Assume that Ω'_3 is a disc with radius $a-\delta$, and has the same center with Ω_3 given in the 2D-case that is a disc with radius a. From (3.17), it is known that the Laplace EVP is written as

$$-u'_{rr} - \frac{1}{r}u'_r - \frac{1}{r^2}u'_{\theta\theta} = \lambda' u', \tag{3.113}$$

in the polar coordinates (r,θ). As before, separation of variables $u'(r,\theta) = R(r)\Theta(\theta)$ yields

$$\Theta'' + \mu\Theta = 0, \tag{3.114a}$$

$$R'' + \frac{1}{r}R' + \left(\lambda' - \frac{\mu}{r^2}\right) = 0. \tag{3.114b}$$

Since the perturbed domain Ω'_3 has same center with the original domain Ω_3, the solution of Equations (3.114a) and (3.20a), which depend on θ, are equal such that

$$\Theta(\theta) = c_1\cos(p\theta) + c_2\sin(p\theta), \tag{3.115}$$

where $p = 0, 1, 2, \cdots$. For Equation (3.114b), which depends on radius r, the boundary condition is $R(a-\delta) = 0$. This means that, the difference between the radius of the perturbed domain Ω'_3 and the radius of the original domain Ω_3 only effects the boundary condition to be applied to Equation (3.114b). In this way, the solution of (3.114b) can be obtained as

$$\lambda'^{(p,q)} = \frac{\left(\rho^{(p,q)}\right)^2}{(a-\delta)^2}, \tag{3.116a}$$

$$R(r) = J_p\left(\frac{\rho^{(p,q)}r}{a-\delta}\right), \tag{3.116b}$$

where $\rho^{(p,q)}$ is the qth zero of the pth Bessel function J_p. Thus, the eigenvalues and the corresponding eigenfunction of the Laplace EVP on Ω_3' are obtained as

$$\lambda'^{(p,q)} = \frac{\left(\rho^{(p,q)}\right)^2}{(a-\delta)^2}, \tag{3.117a}$$

$$u'^{(p,q)}(\theta, r) = J_p\left(\frac{\rho^{(p,q)}}{a-\delta} r\right) \left[c_1 \sin(p\theta) + c_2 \cos(p\theta)\right]. \tag{3.117b}$$

3.2.4. FEM Solutions on Perturbed Domains

The only difference between obtaining FEM solution on the original domain and the perturbed domain is the domain discretization. Since this situation changes only the mesh parameter, the stiffness and mass matrices are affected from the perturbation. The following one-dimensional case is given to illustrate this difference.

FEM Solution on 1D-Perturbed Domain Ω_1'

Consider the perturbed domain $\Omega_1' = [\delta_1, \pi - \delta_2]$. Assume that Ω_1' is partitioned into N subinterval $I = [x_{i-1}, x_i]$ with the same length $h = (\pi - \delta_1 - \delta_2)/N$ such that

$$I : \delta_1 = x_0 < x_1 < x_2 < \cdots < x_{n-1} < x_N = \pi - \delta_2, \tag{3.118}$$

where $x_i = ih$. If the linear basis function (3.42) is considered, the entries of the stiffness matrix are obtained as

$$K_{i,i+1} = -\int_{x_i}^{x_{i+1}} \frac{N}{\pi - \delta_1 - \delta_2} \frac{N}{\pi - \delta_1 - \delta_2} dx = -\frac{N}{\pi - \delta_1 - \delta_2}, \tag{3.119a}$$

$$K_{i+1,i} = -\int_{x_i}^{x_{i+1}} \frac{N}{\pi - \delta_1 - \delta_2} \frac{N}{\pi - \delta_1 - \delta_2} dx = -\frac{N}{\pi - \delta_1 - \delta_2}, \tag{3.119b}$$

$$K_{ii} = \int_{x_{i-1}}^{x_{i+1}} \left(\frac{N}{\pi - \delta_1 - \delta_2}\right)^2 dx = \frac{2N}{\pi - \delta_1 - \delta_2}, \tag{3.119c}$$

$$K_{ij} = 0, \quad \text{for} \quad |i - j| > 1, \tag{3.119d}$$

for $i, j = 1, 2, \ldots, N-1$. In the same way, the entries of the mass matrix are obtained as

$$M_{i,i+1} = \int_{x_i}^{x_{i+1}} \frac{(x_{i+1}-x)N}{\pi-\delta_1-\delta_2} \frac{(x-x_i)N}{\pi-\delta_1-\delta_2} dx = \frac{\pi-\delta_1-\delta_2}{6N}, \tag{3.120a}$$

$$M_{i+1,i} = \int_{x_i}^{x_{i+1}} \frac{(x-x_i)N}{\pi-\delta_1-\delta_2} \frac{(x_{i+1}-x)N}{\pi-\delta_1-\delta_2} dx = \frac{\pi-\delta_1-\delta_2}{6N}, \tag{3.120b}$$

$$\begin{aligned} M_{ii} &= \int_{x_{i-1}}^{x_i} \left(\frac{(x-x_i)N}{\pi-\delta_1-\delta_2} \right)^2 dx + \int_{x_i}^{x_{i+1}} \left(\frac{(x_{i+1}-x)N}{\pi-\delta_1-\delta_2} \right)^2 dx \\ &= \frac{4(\pi-\delta_1-\delta_2)}{6N}, \end{aligned} \tag{3.120c}$$

$$M_{ij} = 0, \quad \text{for} \ \ |i-j| > 1, \tag{3.120d}$$

for $i, j = 1, 2, \ldots, N-1$. Thus, the stiffness and the mass matrices can be written as

$$K = \frac{N}{\pi-\delta_1-\delta_2} \begin{bmatrix} 2 & -1 & & \\ -1 & 2 & \ddots & \\ & \ddots & \ddots & -1 \\ & & -1 & 2 \end{bmatrix}, \tag{3.121}$$

and

$$M = \frac{\pi-\delta_1-\delta_2}{6N} \begin{bmatrix} 4 & 1 & & \\ 1 & 4 & \ddots & \\ & \ddots & \ddots & 1 \\ & & 1 & 4 \end{bmatrix}. \tag{3.122}$$

Since the eigenvalues and eigenfunctions of tridiagonal matrices are known [68], FEM solution of the Laplace EVP on Ω' is obtained as

$$u_h'^{(k)} = \sin\left(\frac{ki(\pi-\delta_1-\delta_2)}{N} \right), \tag{3.123a}$$

$$\lambda_h'^{(k)} = 6 \left(\frac{N}{\pi-\delta_1-\delta_2} \right)^2 \frac{1-\cos\left(\dfrac{k(\pi-\delta_1-\delta_2)}{N} \right)}{2+\cos\left(\dfrac{k(\pi-\delta_1-\delta_2)}{N} \right)}, \tag{3.123b}$$

in analogy with the 1D-case for $k = 1, 2, \ldots, N-1$, and $i = 1, 2, \ldots, N-1$.

3.2.5. Error Estimates with Respect to the Perturbation Parameter δ

The difference between the solutions of second-order elliptic PDEs given with Dirichlet boundary conditions is analyzed in [41] in the case of boundary is perturbed.

A domain Ω and the perturbed domain Ω', which approximates Ω, are considered in this analysis. It is proved that the error between the solutions depends only on the Euclidean distance between the domains Ω and Ω'.

Let Ω be a smooth bounded subset of $\mathbb{R}^d$. Consider the following second order elliptic PDE with the Dirichlet boundary conditions

$$\mathcal{L}u = f \quad \text{in } \Omega, \tag{3.124a}$$

$$u = 0 \quad \text{on } \partial\Omega, \tag{3.124b}$$

where $\mathcal{L}$ is an elliptic second order differential operator on Ω. In order to investigate the effect of boundary perturbations on the solution of (3.124), consider the following perturbed problem

$$\mathcal{L}u' = f \quad \text{in } \Omega', \tag{3.125a}$$

$$u' = 0 \quad \text{on } \partial\Omega'. \tag{3.125b}$$

Definition 3.1: Assume that W_1 *and* W_2 *be bounded subsets of* $\mathbb{R}^d$*. Then, the distance between* W_1 *and* W_2 *is defined as*

$$dist(W_1, W_2) = \sup_{x \in W_1 \cup W_2} \inf_{x' \in W_1 \cap W_2} |x - x'|, \tag{3.126}$$

where $|x - x'|$ *denotes the Euclidean distance between* x *and* x'*.*

The bounds for the error between the solution of (3.124) and (3.125) are given with the following theorem, and the proof of this theorem can be found in [41].

Theorem 3.6: Let $f \in H^0(\mathbb{R}^d)$ *and* u *be the solution of the problem* $\mathcal{L}u = f$ *in* Ω*. Let* Ω' *be an open subset of* S *(*S *is an open neighborhood of* Ω*) and* u' *be the solution of the perturbed problem* $\mathcal{L}u' = f$ *in* Ω'*. Then, there exist constants* C_0 *and* C_1*, independent of* u'*, such that*

i) $\|u - u'\|_{0,w} \leq C_0\delta \|f\|_{0,W}$,

ii) $\|u - u'\|_{1,w} \leq C_1\delta^{1/2} \|f\|_{0,W}$,

for sufficiently small δ*, where* $\delta = dist(\Omega, \Omega')$ *and* $W = \Omega \cup \Omega'$*.*

Based on the study [41], the convergence behavior of the solutions of the Laplace EVP on the perturbed domains to the corresponding exact solutions on the original domains is analytically investigated in this section. Also, the convergence behavior of the analytically known approximate eigenvalues given in (3.123) is obtained. To this end, it is assumed that $\delta_i = \delta$ for $i = 1, 2, 3, 4$. The perturbed problem (3.97) is not defined on Ω/Ω', but the solution of the perturbed problem in this area is assumed to be zero in order to facilitate the calculations. All these results are obtained using Taylor's series expansion about $\delta = 0$. All computations are made by the symbolic math toolbox of MATLAB.

Consider the solutions on the domains $\Omega_1 = [0, \pi]$ and $\Omega_1' = [\delta, \pi - \delta]$. The error between the eigenvalues on the perturbed domain Ω_1' and the original domain Ω_1 is given by

$$|\lambda - \lambda'| = \left| k^2 - \frac{k^2\pi^2}{(\pi - 2\delta)^2} \right|. \tag{3.127}$$

Taylor's series expansion about $\delta = 0$ gives the error

$$|\lambda - \lambda'| = 4k^2 \left| -\frac{\delta}{\pi} - \frac{3\delta^2}{\pi^2} + O(\delta^3) \right| = O(\delta), \tag{3.128}$$

and the estimate

$$E_\lambda(\delta) = \left| -\frac{\delta}{\pi} - \frac{3\delta^2}{\pi^2} \right|, \tag{3.129}$$

to be used in the numerical examples. Besides, the error between the exact eigenvalues of the original problem and the approximate eigenvalues of the perturbed problem are given as

$$|\lambda - \lambda_h'| = \left| k^2 - 6\left(\frac{N}{\pi - 2\delta}\right)^2 \cdot \frac{1 - \cos\left(\dfrac{k(\pi - 2\delta)}{N}\right)}{2 + \cos\left(\dfrac{k(\pi - 2\delta)}{N}\right)} \right|. \tag{3.130}$$

Using Taylor series expansion about $\delta = 0$ yields

$$|\lambda - \lambda_h'| = \left| k^2 - 6\left(\frac{N}{\pi}\right)^2 \frac{1 - \cos\left(\dfrac{k\pi}{N}\right)}{2 + \cos\left(\dfrac{k\pi}{N}\right)} + O(\delta) \right|. \tag{3.131}$$

Note that the second term $6\left(N/\pi\right)^2 (1 - \cos\left(k\pi/N\right))/(2 + \cos\left(k\pi/N\right))$ is the approximate eigenvalue λ_h of the Laplace EVP on the original domain Ω_1, and it converges to the exact eigenvalue $\lambda = k^2$ as h goes to zero. Taylor's series expansion at $h = 0$ $(h = \pi/N)$ gives

$$|\lambda - \lambda_h| = \left| k^2 - k^2 + \frac{h^2k^2}{12} + O(h^4) \right| = O(h^2). \tag{3.132}$$

If it is assumed that $k^2 = 6\,(N/\pi)^2\,(1 - \cos{(k\pi/N)})/(2 + \cos{(k\pi/N)})$ for a sufficiently small mesh parameter h, the error (3.131) implies that

$$|\lambda - \lambda_h'| = O(\delta). \tag{3.133}$$

The errors between the eigenfunctions are obtained by computing the norms

$$\|u - u'\| = \left(\int_0^\delta |u|^2\,dx + \int_\delta^{\pi-\delta} |u - u'|^2\,dx + \int_{\pi-\delta}^{\pi} |u|^2\,dx \right)^{1/2}, \tag{3.134}$$

and

$$\begin{aligned} \|u - u'\|_1 = \Bigg(&\int_0^\delta |u|^2\,dx + \int_\delta^{\pi-\delta} |u - u'|^2\,dx + \int_{\pi-\delta}^{\pi} |u|^2\,dx \\ &+ \int_0^\delta |u_x|^2\,dx + \int_\delta^{\pi-\delta} |u_x - u_x'|^2\,dx + \int_{\pi-\delta}^{\pi} |u_x|^2\,dx \Bigg)^{1/2}. \end{aligned} \tag{3.135}$$

Computing these integrals and Taylor's series expansion about $\delta = 0$ yields

$$\|u - u'\| = \left(O(\delta^2)\right)^{1/2} = O(\delta), \tag{3.136a}$$

$$\|u - u'\|_1 = (O(\delta))^{1/2} = O(\delta^{1/2}), \tag{3.136b}$$

and the estimates

$$\begin{aligned} E(\delta) = ((&\delta(6k\pi^2 - 6\delta\sin(2k\pi) + 2\delta k^3\pi^3 + 6\pi\delta k - 6k\pi^2\cos(2k\pi) \\ &- 3\delta k^2\pi^2\sin(2k\pi) + 6\delta k\pi\cos(2k\pi)))/(12k\pi^2))^{1/2}, \end{aligned} \tag{3.137a}$$

$$E_1(\delta) = (\delta(2k^2 - k^2\sin^2(k\pi) + \sin^2(k\pi)))^{1/2}, \tag{3.137b}$$

to be used the in the numerical examples. The results concerning the eigenfunctions are coherence with the results obtained for the corresponding boundary value (source) problem given in Theorem (3.6).

When the eigenvalues are considered on the domains $\Omega_2 = [0,\pi] \times [0,\pi]$ and $\Omega_2' = [\delta, \pi - \delta] \times [\delta, \pi - \delta]$, the error between the exact eigenvalue on Ω_2 and the analytical eigenvalue on Ω_2' is given as

$$|\lambda - \lambda'| = \left| m^2 + n^2 - \frac{m^2\pi^2}{(\pi - 2\delta)^2} - \frac{n^2\pi^2}{(\pi - 2\delta)^2} \right|. \tag{3.138}$$

Using Taylor series expansion about $\delta = 0$ yields

$$|\lambda - \lambda'| = 4(m^2 + n^2)\left|-\frac{\delta}{\pi} - \frac{3\delta^2}{\pi^2} + O(\delta^3)\right| = O(\delta), \tag{3.139}$$

with estimate

$$E_\lambda(\delta) = \left|-\frac{\delta}{\pi} - \frac{3\delta^2}{\pi^2}\right|. \tag{3.140}$$

Similarly, it is obtained that

$$|\lambda - \lambda'| = \left|\frac{\left(\rho^{(p,q)}\right)^2}{a^2} - \frac{\left(\rho^{(p,q)}\right)^2}{(a-\delta)^2}\right|, \tag{3.141}$$

and

$$|\lambda - \lambda'| = \left(\rho^{(p,q)}\right)^2\left|-\frac{2\delta}{a^3} - \frac{3\delta^2}{a^4} - \frac{4\delta^3}{a^5} + O(\delta^4)\right| = O(\delta), \tag{3.142}$$

with estimate

$$E_\lambda(\delta) = \left|-\frac{2\delta}{a^3} - \frac{3\delta^2}{a^4} - \frac{4\delta^3}{a^5}\right|, \tag{3.143}$$

to be used in the numerical examples for the disc domains Ω_3 and Ω_3'.

As a result, it can be inferred that the eigenvalues on the perturbed domains Ω' converge with order $O(\delta)$ to the exact eigenvalues on the original domains Ω.

3.2.6. Regular Polygon Inscribed in the Unit Disc

Since FEM solution of the Laplace EVP on a disc is actually obtained by discretizing a polygon inscribed in this disc, the Laplace EVP is considered on N-sided regular polygons inscribed in the unit disc. Suppose the N-sided regular polygon is the boundary variation of the unit disc in a such a way that each point on the boundary of the unit disc moves, starting at $t = 0$, along the radial direction with velocity C and arrives at the boundary of the polygon at $t = 1$. Then, the Taylor series expansion at $t = 0$ gives the approximation of the eigenvalues λ_N on the polygon [53] such that

$$\lambda_N = \lambda + \lambda' + \frac{1}{2}\lambda'' + \frac{1}{6}\lambda''' + \cdots, \tag{3.144}$$

where λ is the corresponding simple eigenvalue on the unit disc, and λ' denotes the shape derivative of λ. The first three derivatives λ', λ'', and λ''' are derived in [51, 53]. The first variation λ' is obtained using Hadamard's formula (see [50, 51, 53])

$$\lambda' = -\int_{\partial\Omega} C\,|\nabla u|^2\, d\partial\Omega, \tag{3.145}$$

where C is the velocity. Thus, the simple eigenvalues of the Laplace EVP on N-sided regular polygon can be expressed as a series of power $1/N$ such that [50, 51, 53]

$$\lambda_N = \lambda \left(1 + c_1\frac{1}{N} + c_2\frac{1}{N^2} + c_3\frac{1}{N^3} + \cdots \right), \tag{3.146}$$

where λ_N is the eigenvalues on N-sided regular polygon, and λ is the corresponding eigenvalue on the unit disc. The coefficients c_i can be determined from the Taylor series by expanding each term in powers of $1/N$ such as

$$\begin{aligned} \lambda'(0) &= -2\lambda \left(\frac{N}{2\pi}\cos\left(\frac{\pi}{N}\right)\ln\left(\frac{1+\sin\left(\frac{\pi}{N}\right)}{1-\sin\left(\frac{\pi}{N}\right)}\right) - 1\right) \\ &= \lambda\left(\frac{2\pi^2}{3}\frac{1}{N^2} + \frac{2\pi^6}{315}\frac{1}{N^6} + O\left(\frac{1}{N^8}\right)\right). \end{aligned} \tag{3.147}$$

Thus, the coefficient of the first non-zero term is obtained as $c_2 = 2\pi^2/3$ from the first Taylor term. For the lowest simple eigenvalue on the unit disc, (3.146) takes the form [51]

$$\lambda_N = \lambda\left(1 + \frac{4\zeta(2)}{N^2} + \frac{4\zeta(3)}{N^3} + \frac{28\zeta(4)}{N^4} + ...\right), \tag{3.148}$$

where ζ is the Riemann zeta function. The derivation of (3.146) and (3.148) can be found in [50, 51, 53] with details.

3.2.7. Numerical Results

The numerical results that confirm the convergence behavior of both analytical and FEM solutions on the perturbed domains to the exact solutions on the original domains obtained by the Taylor series expansion are given in this section. Linear elements are used to obtain the numerical results concerning FEM solutions for a fixed number of elements, that is N. The Laplace EVP is considered on four perturbed domains:

- Ω_1': $[\delta, \pi - \delta]$
- Ω_2': $[\delta, \pi - \delta] \times [\delta, \pi - \delta]$
- Ω_3': $x^2 - y^2 = 1 - \delta$
- Regular polygon inscribed in the unit disc

Convergence behaviors are investigated with respect to decreasing perturbation parameter δ for first three domains. These numerical results confirm the convergence results related to the perturbation parameter δ obtained by the Taylor series expansion. For a regular polygon inscribed in the unit disc, it is numerically shown that both simple and multiple eigenvalues of the Laplace EVP on N-sided regular polygon can be expressed as a series of powers of $1/N$. All of the computations and figures are procured using MATLAB.

3.2.7.1. Errors with Respect to δ on Ω_1'

The convergence behaviors of both approximate eigenfunction $u_h'^{(k)}$ and analytical eigenfunction $u'^{(k)}(x) = \sin\left(\dfrac{k\pi}{\pi - 2\delta}(x-\delta)\right) / \cos\left(\dfrac{k\pi}{\pi - 2\delta}\delta\right)$ on the perturbed domain $\Omega_1' = [\delta, \pi - \delta]$ to the corresponding exact eigenfunction $u^{(k)}(x) = \sin(kx)$ on the original domain $\Omega_1 = [0, \pi]$ as the perturbation parameter δ goes to zero are given with the estimates

$$\begin{aligned} E(\delta) = ((\delta(6k\pi^2 - 6\delta\sin(2k\pi) + 2\delta k^3\pi^3 + 6\pi\delta k - 6k\pi^2\cos(2k\pi) \\ - 3\delta k^2\pi^2\sin(2k\pi) + 6\delta k\pi\cos(2k\pi)))/(12k\pi^2))^{1/2}, \end{aligned} \tag{3.149a}$$

$$E_1(\delta) = (\delta(2k^2 - k^2\sin^2(k\pi) + \sin^2(k\pi)))^{1/2}, \tag{3.149b}$$

in Figure 3.25 and Figure 3.26 with respect to L^2- and H^1-norms. It is observed that the analytical eigenfunctions $u'^{(k)}$ and the approximate eigenfunctions $u_h'^{(k)}$ on Ω_1' converge to the exact eigenfunctions $u^{(k)}$ on Ω_1 as the perturbation parameter δ goes to zero, when looking at Figure 3.25 and Figure 3.26. Also, it can be seen that this convergence is of order $O(\delta)$ in L^2-norm, and is of order $O\left(\delta^{1/2}\right)$ in H^1-norm.

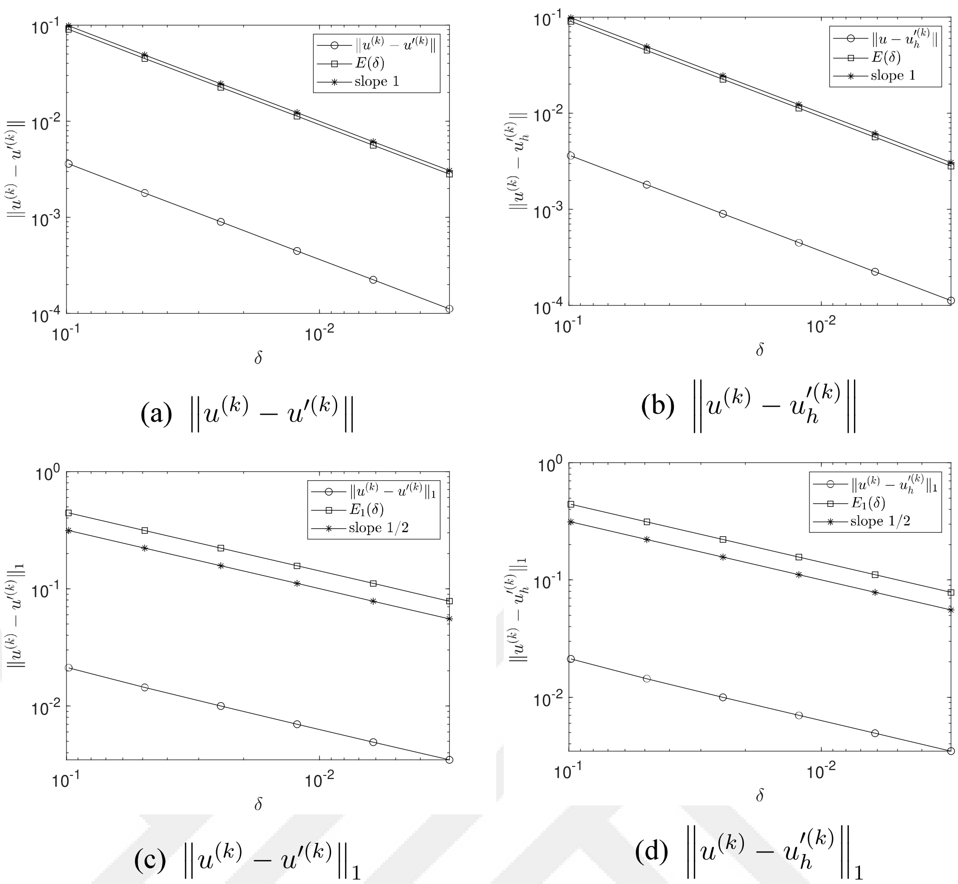

(a) $\left\|u^{(k)} - u'^{(k)}\right\|$

(b) $\left\|u^{(k)} - u_h'^{(k)}\right\|$

(c) $\left\|u^{(k)} - u'^{(k)}\right\|_1$

(d) $\left\|u^{(k)} - u_h'^{(k)}\right\|_1$

Figure 3.25: Log-log scale plot of the errors between the eigenfunctions for Section 3.2.7.1, $k = 1$, $N = 2^{10}$, and $\delta = \pi/2^5, \pi/2^6, \ldots, \pi/2^{10}$.

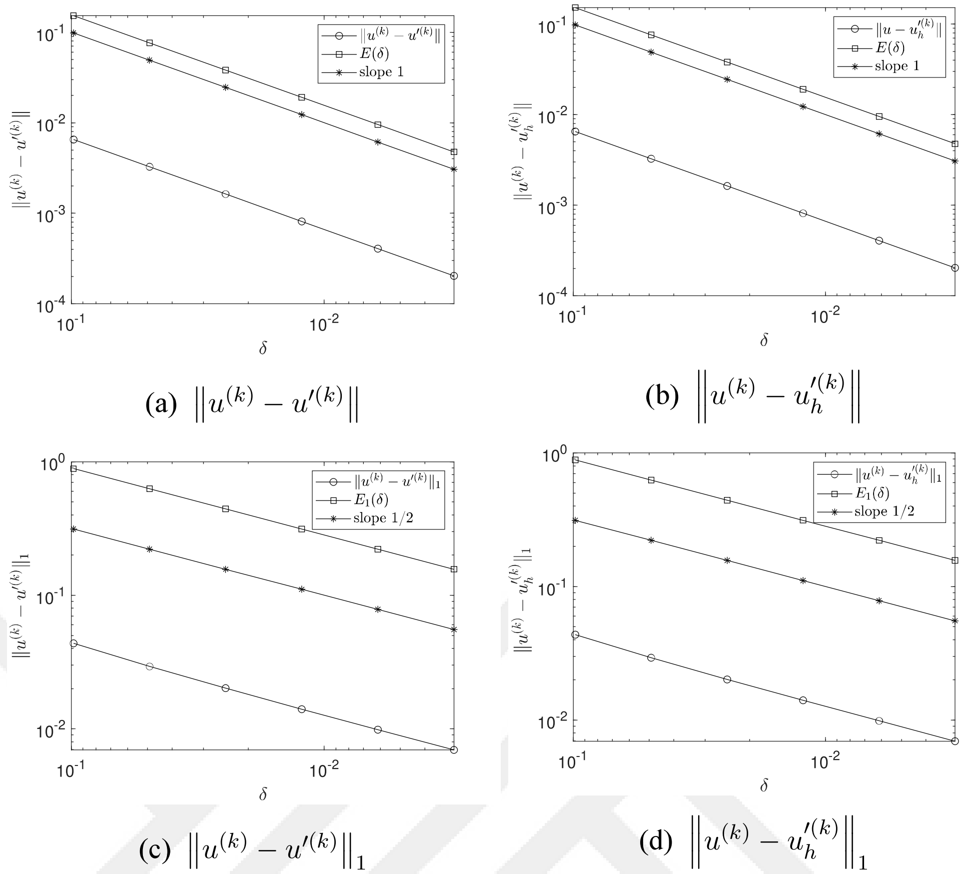

Figure 3.26: Log-log scale plot of the errors between the eigenfunctions for Section 3.2.7.1, $k = 2$, $N = 2^{10}$, and $\delta = \pi/2^5, \pi/2^6, \ldots, \pi/2^{10}$.

The convergence behaviors of analytical eigenvalues $\lambda'^{(k)} = (k\pi/(\pi - 2\delta))^2$ and the approximate eigenvalues $\lambda_h'^{(k)}$ on Ω_1' to the corresponding exact eigenvalue $\lambda^{(k)} = k^2$ on Ω_1 are given with the estimate

$$E_\lambda(\delta) = \left| -\frac{\delta}{\pi} - \frac{3\delta^2}{\pi^2} \right|, \tag{3.150}$$

in Figure 3.27 and Figure 3.28 with respect to decreasing perturbation parameter δ. From Figure 3.27 and Figure 3.28, it is observed that the analytical eigenvalues $\lambda'^{(k)}$ and the approximate eigenvalues $\lambda_h'^{(k)}$ on Ω_1' converge to the corresponding exact eigenvalues $\lambda^{(k)}$ on Ω_1 as the perturbation parameter δ goes to zero. Also, it can be seen that this convergence is of order $O(\delta)$.

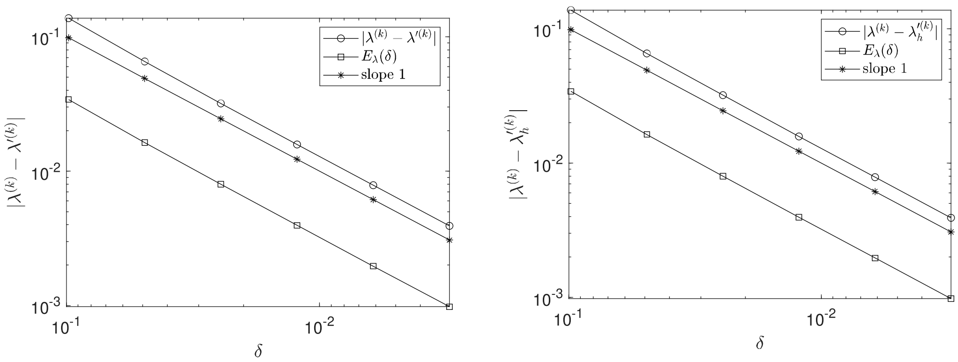

(a) $\left|\lambda^{(k)} - \lambda'^{(k)}\right|$ (b) $\left|\lambda^{(k)} - \lambda_h'^{(k)}\right|$

Figure 3.27: Log-log scale plot of the errors between the eigenvalues for Section 3.2.7.1, $k = 1$, $N = 2^{10}$, and $\delta = \pi/2^5, \pi/2^6, \ldots, \pi/2^{10}$.

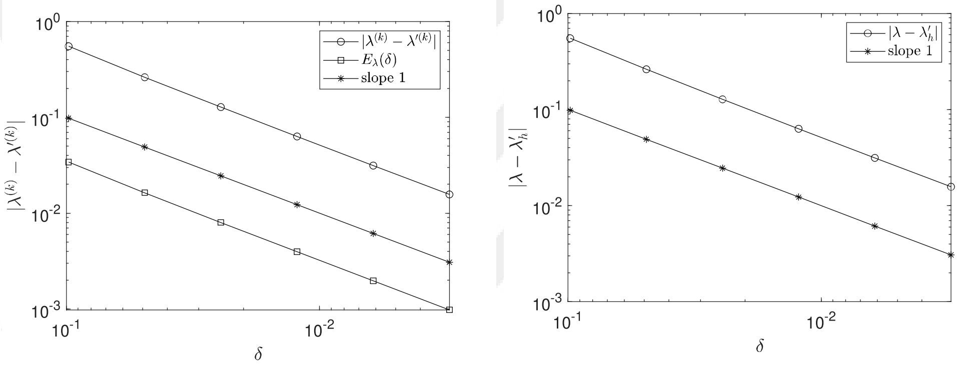

(a) $\left|\lambda^{(k)} - \lambda'^{(k)}\right|$ (b) $\left|\lambda^{(k)} - \lambda_h'^{(k)}\right|$

Figure 3.28: Log-log scale plot of the errors between the eigenvalues for Section 3.2.7.1, $k = 2$, $N = 2^{10}$, and $\delta = \pi/2^5, \pi/2^6, \ldots, \pi/2^{10}$.

3.2.7.2. Errors with Respect to δ on Ω_2'

The convergence behaviors of the analytical eigenvalues

$$\lambda'^{(m,n)} = (m\pi/(\pi - 2\delta))^2 + (n\pi/(\pi - 2\delta))^2, \tag{3.151}$$

and the approximate eigenvalues $\lambda_h'^{(m,n)}$ on the perturbed domain $\Omega_2' = [\delta, \pi - \delta] \times [\delta, \pi - \delta]$ to the corresponding exact eigenvalues $\lambda^{(m,n)} = m^2 + n^2$ on the original domain $\Omega_2 = [0, \pi] \times [0, \pi]$ are given with the estimate

$$E_\lambda(\delta) = \left| -\frac{\delta}{\pi} - \frac{3\delta^2}{\pi^2} \right|, \tag{3.152}$$

in Figure 3.27 and Figure 3.30 with respect to decreasing perturbation parameter δ. It is clearly seen that the analytical eigenvalues $\lambda'^{(m,n)}$ and the approximate eigenvalues $\lambda_h'^{(m,n)}$ on Ω_2' converge to the exact eigenvalues $\lambda^{(m,n)}$ on Ω_2 as the perturbation parameter δ goes to zero. Also, it can be seen that this convergence is of order $O(\delta)$.

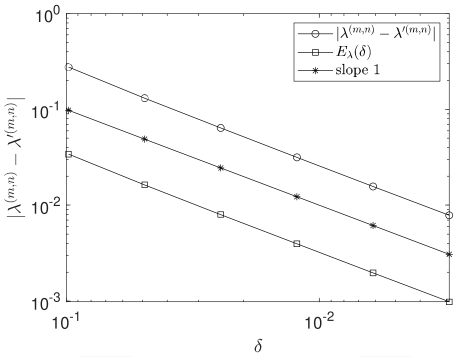

(a) $\left|\lambda^{(m,n)} - \lambda'^{(m,n)}\right|$

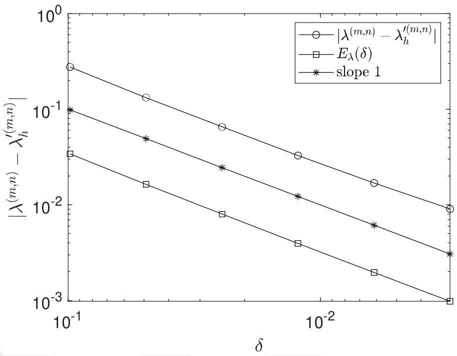

(b) $\left|\lambda^{(m,n)} - \lambda_h'^{(m,n)}\right|$

Figure 3.29: Log-log scale plot of the errors between the eigenvalues for Section 3.2.7.2, $m = n = 1$, $N = 2^6$, and $\delta = \pi/2^5, \pi/2^6, \ldots, \pi/2^{10}$.

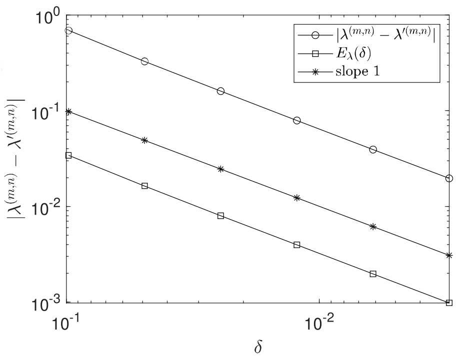

(a) $\left|\lambda^{(m,n)} - \lambda'^{(m,n)}\right|$

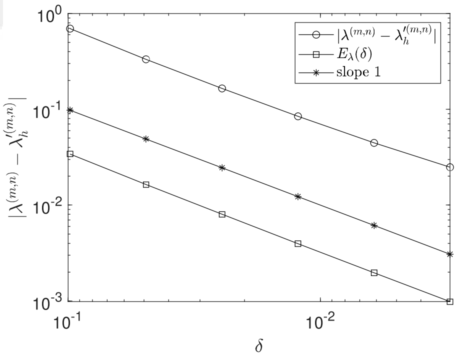

(b) $\left|\lambda^{(m,n)} - \lambda_h'^{(m,n)}\right|$

Figure 3.30: Log-log scale plot of the errors between the eigenvalues for Section 3.2.7.2, $m = 1$, $n = 2$, $N = 2^6$, and $\delta = \pi/2^5, \pi/2^6, \ldots, \pi/2^{10}$.

3.2.7.3. Errors with Respect to δ on Ω_3'

The convergence behaviors of the analytical eigenvalues

$$\lambda'^{(p,q)} = \left(\rho^{(p,q)}/(a-\delta)\right)^2, \tag{3.153}$$

where $\rho^{(p,q)}$ is the qth zero of the Bessel function J_p of order p, and the approximate eigenvalues $\lambda_h'^{(p,q)}$ on the perturbed domain Ω_3', that is the disc with radius $1-\delta$, to the corresponding exact eigenvalue $\lambda^{(p,q)} = \left(\rho^{(p,q)}\right)^2$ on the original domain Ω_3, that is the unit disc, are given in Figure 3.31 and Figure 3.32 with the estimate $E_\lambda(\delta) = |-2\delta - 3\delta^2 - 4\delta^3|$. The results show that the analytical eigenvalues $\lambda'^{(p,q)}$ and approximate eigenvalues $\lambda_h'^{(p,q)}$ on Ω_3' converge to the analytical eigenvalues $\lambda^{(p,q)}$ on Ω_3 in order $O(\delta)$ as in Ω_1' and Ω_2'.

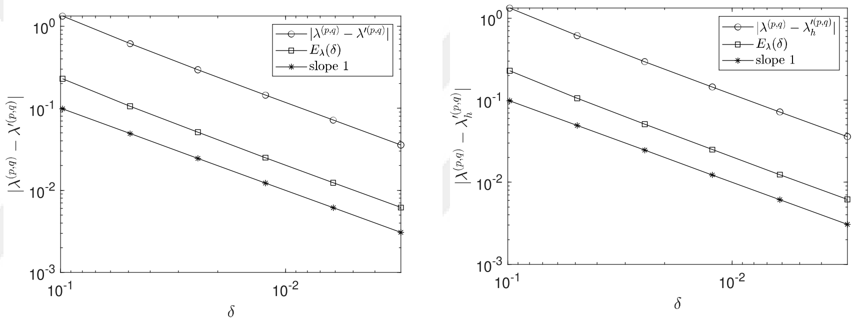

(a) $\left|\lambda^{(p,q)} - \lambda'^{(p,q)}\right|$ (b) $\left|\lambda^{(p,q)} - \lambda_h'^{(p,q)}\right|$

Figure 3.31: Log-log scale plot of the errors between the eigenvalues for Section 3.2.7.3, $p=0$, $q=1$, $h_{max}=0.0125$, and $\delta = \pi/2^5, \pi/2^6, \ldots, \pi/2^{10}$.

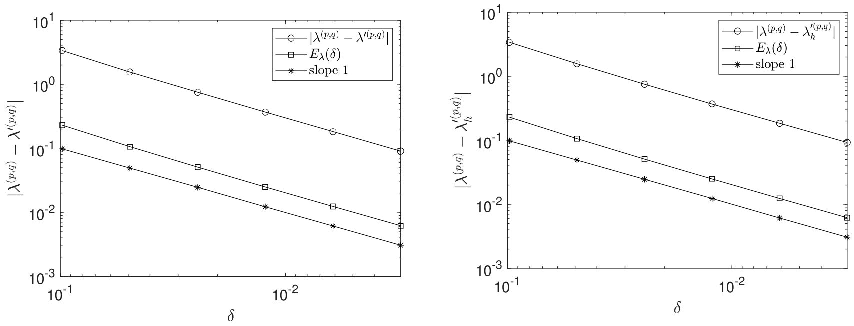

(a) $\left|\lambda^{(p,q)} - \lambda'^{(p,q)}\right|$ (b) $\left|\lambda^{(p,q)} - \lambda_h'^{(p,q)}\right|$

Figure 3.32: Log-log scale plot of the errors between the eigenvalues for Section 3.2.7.3, $p=1$, $q=1$, $h_{max}=0.0125$, and $\delta = \pi/2^5, \pi/2^6, \ldots, \pi/2^{10}$.

3.2.7.4. Regular Polygon Inscribed in the Unit Disc

The approximate eigenvalues λ_N on 128-sided regular polygon corresponding to the first simple eigenvalue of the Laplace EVP on the unit disc are listed in Table 3.8. This table also includes the error between λ_N and the corresponding reference eigenvalue $\lambda_{ref} = 5.78552$, which is given in [50]. According to Table 3.8, λ_N approaches with approximately zero error to the reference eigenvalue $\lambda_{ref} = 5.78552$ when $h_{max} = 0.00625$. For this reason, $h_{max} = 0.00625$ is chosen in the calculations of the numerical examples in this section.

The ratio of the approximate eigenvalues on N-sided regular polygon and the corresponding eigenvalues on the unit disc λ_N/λ is given with the estimate

$$E(\lambda) = 1 + \frac{4\zeta(2)}{N^2} + \frac{4\zeta(3)}{N^3}, \tag{3.154}$$

in Figure 3.33 with respect to increasing number of sides N. From Figure 3.33, it is deduced that the infinite series given in (3.148) represents not only the lowest simple eigenvalue but also the other simple eigenvalues and the multiple eigenvalues as well.

Table 3.8: First simple approximate eigenvalues λ_N and the error between λ_N and λ_{ref} for the Laplace EVP, $N = 128$, and $h_{max} = 0.2, 0.1, \ldots, 0.003125$.

h_{max}	λ_N	$\lvert\lambda_{ref} - \lambda_N\rvert / \lvert\lambda_{ref}\rvert$
0.2	5.826777089710585	0.007131094475619
0.1	5.796671497963499	0.001927484126491
0.05	5.788403281150408	4.983616253003344e-04
0.025	5.786272155113283	1.300064839951145e-04
0.0125	5.785696366930097	3.048419676998874e-05
0.00625	5.785567109135556	8.142593156026770e-06
0.003125	5.785534637721554	2.530061524973944e-06

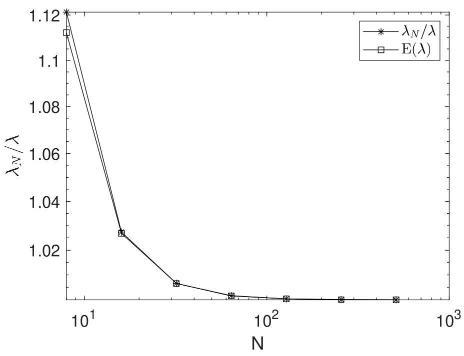

(a) $p = 0,\ q = 1,\ \lambda = \left(\rho^{(0,1)}\right)^2$

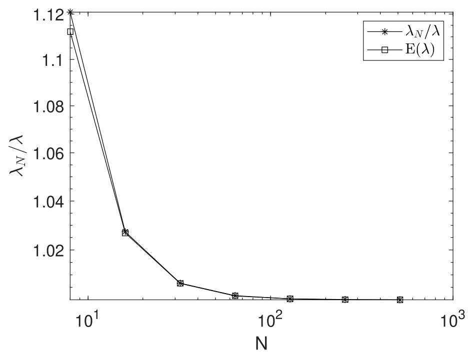

(b) $p = 1,\ q = 1,\ \lambda = \left(\rho^{(1,1)}\right)^2$

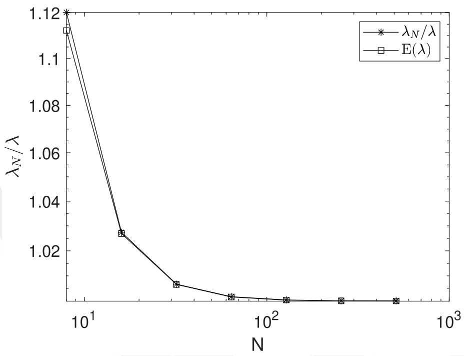

(c) $p = 2,\ q = 1,\ \lambda = \left(\rho^{(2,1)}\right)^2$

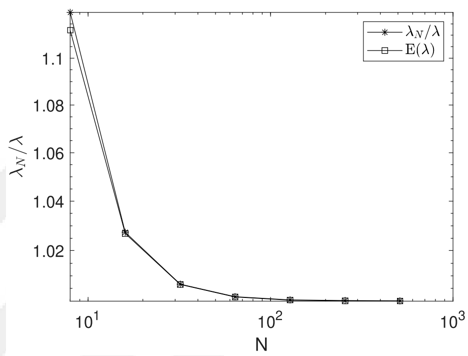

(d) $p = 0,\ q = 2,\ \lambda = \left(\rho^{(0,2)}\right)^2$

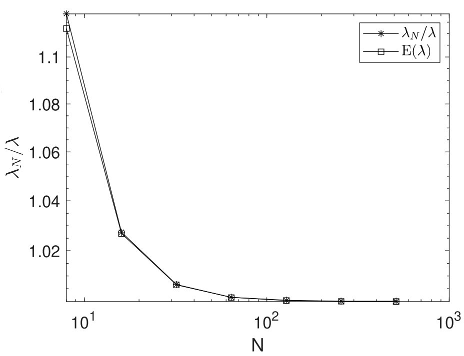

(e) $p = 3,\ q = 1,\ \lambda = \left(\rho^{(3,1)}\right)^2$

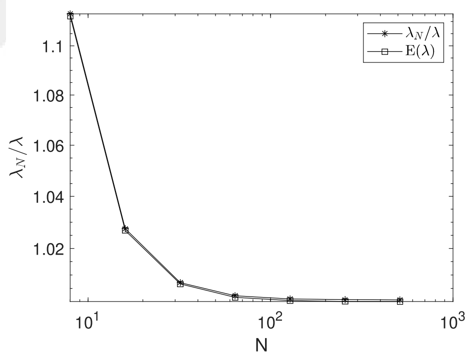

(f) $p = 0,\ q = 5,\ \lambda = \left(\rho^{(0,5)}\right)^2$

Figure 3.33: Log-log scale plot of λ_N/λ and $E(\lambda)$ for the Laplace EVP, $h_{max} = 0.00625$, and $N = 2^3, 2^4, \ldots, 2^9$.

As a conclusion, in this chapter, the Laplace EVP is analyzed on various one and two-dimensional domains. Later on, based on the study [41], the Laplace EVP is considered on the perturbed domain, which is assumed to be inscribed in the original domain and its boundary is approximately close to the boundary of the original domain. Then, the analytical solution of the Laplace EVP is obtained on perturbed one-dimensional, square, and disc domains. The convergence estimates of these solutions to the solutions on the corresponding original (unperturbed) domains are provided according to the perturbation parameter δ using Taylor's series expansions of the errors between the solutions at $\delta = 0$. It is deduced that the analytical eigenvalues on the one and two-dimensional domains converge to the exact eigenvalues on the corresponding original domains in order $O(\delta)$. Besides, the already mentioned behavior is obtained for the approximate eigenvalues of the perturbed problem, which can be obtained analytically using FEM with piecewise linear basis functions on a one-dimensional domain for a fixed mesh. For the eigenfunctions on the one-dimensional domain, it is observed that this behavior is of order $O(\delta)$ and $O(\delta^{1/2})$ with respect to the L^2- and H^1-norms respectively, which is in good agreement with the results obtained for the corresponding boundary value (source) problem in [41]. Moreover, the Laplace EVP is considered on N-sided regular polygon inscribed in the unit disc with an increasing number of sides N. Then, it is numerically shown that both simple and multiple eigenvalues of the Laplace EVP on the polygon can be represented in terms of inverse powers of sides, as given in [51] (see also [50]) for the simple eigenvalues.

4. STEKLOV EIGENVALUE PROBLEM

As mentioned in Chapter 1, the Steklov EVP involving the Laplace operator is of fundamental importance in many applications and is defined as: find eigenvalues $\lambda \in \mathbb{R}$ and eigenfunctions $0 \neq u \in H^1$ such that

$$\Delta u = 0 \quad \text{in } \Omega, \tag{4.1a}$$

$$\frac{\partial u}{\partial n} = \lambda u \quad \text{on } \partial\Omega, \tag{4.1b}$$

where $\partial u/\partial n = n \cdot \nabla u$ is the outward normal derivative and Ω is a domain in $\mathbb{R}^d$, $d = 1, 2, 3$, with boundary $\partial\Omega$. As clearly seen in (4.1b), the eigenvalue parameter of the Steklov EVP appears in the boundary condition, unlike the Laplace EVP. This chapter is devoted to the presentation of the FEM approximation of the Steklov EVP. To start with, the Steklov EVP is considered on the unit disc discretized using linear triangular elements and is analyzed using FEM. Based on the fact that the FEM solution of the Steklov EVP on a disc is actually obtained by discretizing a polygon inscribed in this disc, the eigenvalues of the Steklov EVP is considered on the N-sided regular polygon inscribed in the unit disc. Since the eigenvalues of the Laplace EVP on the N-sided regular polygon can be represented in terms of the inverse powers of N [51] (see also [50]), existence of such series representation for the eigenvalues of the Steklov EVP is numerically investigated.

Exact Solution on the Unit Disc

To investigate the convergence behavior of FEM solution to the exact solution of the Steklov EVP on the unit disc, a procedure that allows to obtain an exact solution is provided in the sequel.

As has already been done for the Laplace EVP, applying the transformations $x = r\cos\theta$ and $y = r\sin\theta$ to (4.1a), and using the chain rule results in

$$\frac{\partial u}{\partial r} = \frac{\partial u}{\partial x}\cos\theta + \frac{\partial u}{\partial y}\sin\theta, \tag{4.2a}$$

$$u_{xx} + u_{yy} = u_{rr} + \frac{1}{r}u_r + \frac{1}{r^2}u_{\theta\theta}. \tag{4.2b}$$

Since the unit outward normal vector is obtained as $n = (\cos\theta, \sin\theta)$, Equation (4.2a) is reduced as $\partial u/\partial r = n \cdot \nabla u$. Thus, the Steklov EVP is written as

$$u_{rr} + \frac{1}{r}u_r + \frac{1}{r^2}u_{\theta\theta} = 0 \quad \text{in } \Omega, \tag{4.3a}$$

$$\frac{\partial u}{\partial r} = \lambda u \quad \text{on } \partial\Omega \tag{4.3b}$$

in the polar coordinates (r, θ). The solution of (4.3) is obtained by separating the variables so that $u(r,\theta) = R(r)\Theta(\theta)$. Substitution of the partial derivatives $u_r = R'\Theta$, $u_{rr} = R''\Theta$, and $u_{\theta\theta} = R\Theta''$ into (4.3a), and multiplying both sides by $r^2/R\Theta$ result in

$$r^2\frac{R''}{R} + r\frac{R'}{R} = -\frac{\Theta''}{\Theta}. \tag{4.4}$$

Assume that both sides of (4.4) are equal to a constant μ. Then, it is obtained that

$$\Theta'' + \mu\Theta = 0, \tag{4.5a}$$

$$r^2R'' + rR' - \mu R = 0. \tag{4.5b}$$

The solution of Equation (4.5a) is given in Chapter 3 as

$$\Theta(\theta) = c_1\cos(k\theta) + c_2\sin(k\theta), \tag{4.6}$$

where $\mu = k^2$ and $k = 0, 1, 2 \ldots$. Besides, Equation (4.5b) is known as Euler equation and its solution is assumed to be in the form $R(r) = r^\eta$. Substitution of the derivatives $R_r = \eta r^{\eta-1}$ and $R_{rr} = \eta(\eta-1)r^{\eta-2}$ into (4.5b) yields

$$(\eta^2 - \mu) \cdot r^\eta = 0. \tag{4.7}$$

Since $\mu = k^2$, it is obtained that $\eta = \pm k$. Thus, the solution of Equation (4.5b) is derived as

$$R(r) = c_3r^k + c_4r^{-k}. \tag{4.8}$$

For the solution on the disc to be finite, c_4 must be equal to zero since $R(r) \to \infty$ as $r \to 0$. Thus, the solution of (4.3) is obtained as

$$u(r,\theta) = r^k\left(c_1\cos(k\theta) + c_2\sin(k\theta)\right). \tag{4.9}$$

Inserting (4.9) into (4.3b) gives

$$\begin{aligned} kr^{k-1}\left(c_1\cos(k\theta)+c_2\sin(k\theta)\right) &= \lambda r^k\left(c_1\cos(k\theta)+c_2\sin(k\theta)\right) \\ \Rightarrow \lambda &= \frac{k}{r}. \end{aligned} \tag{4.10}$$

For the unit disc, the Steklov eigenvalues are obtained as [24]

$$\lambda^{(2k-1)} = \lambda^{(2k)} = k, \ \ \forall k \in \mathbb{N} \tag{4.11}$$

with multiplicity two for $k = 1, 2, \ldots$. The eigenfunctions corresponding to the double eigenvalues are given by

$$u(r,\theta)^{(2k-1)} = r^k \sin(k\theta) \quad \text{and} \quad u(r,\theta)^{(2k)} = r^k \cos(k\theta), \tag{4.12}$$

in polar coordinates (r, θ) for $k = 1, 2, \ldots$. In the case of $k = 0$, the Steklov EVP has the only simple eigenvalue $\lambda^{(0)} = 0$ associated that is with the constant solution $u^{(0)} = c$.

4.1. The Finite Element Method for the Steklov EVP

In some cases, such as on a polygon, it is necessary to obtain approximate solutions using numerical methods when it is difficult or not possible to obtain the exact solution of the Steklov EVP. Therefore, FEM is introduced for the Steklov EVP in this section.

As mentioned before, the basic idea is to obtain the variational formulation of the Steklov EVP, and to seek the approximate solution which is an approximation to the exact solution from the finite-dimensional subspace constructed by piecewise polynomials. Multiplying Equation (4.1a) by a test function $v \in H^1$, and integrating by parts using the boundary condition given in (4.3b) yield

$$\begin{aligned} 0 &= \int_\Omega \Delta u v d\Omega \\ &= -\int_\Omega \nabla u \cdot \nabla v d\Omega + \int_{\partial\Omega} n \cdot \nabla u v d\partial\Omega \\ &= -\int_\Omega \nabla u \cdot \nabla v d\Omega + \lambda \int_{\partial\Omega} u v d\partial\Omega. \end{aligned} \tag{4.13}$$

Thus, the variational formulation of the problem (4.1) is obtained as

$$\int_\Omega \nabla u \cdot \nabla v d\Omega = \lambda \int_{\partial\Omega} u v d\partial\Omega. \tag{4.14}$$

Let $V_h = \text{span}\{\phi_1, \phi_2, \ldots \phi_N\}$ be a finite dimensional subspace of H^1, where ϕ_i are piecewise polynomials for $i = 1, 2, \ldots, N$. The discretization of (4.14) is stated as

$$\int_\Omega \nabla u_h \cdot \nabla v_h d\Omega = \lambda_h \int_{\partial\Omega} u_h v_h d\partial\Omega, \qquad \forall v_h \in V_h. \tag{4.15}$$

According to the Galerkin method, we seek the eigenvalues $\lambda_h \in \mathbb{R}$, and the eigenfunctions $u_h = \sum_{i=1}^{N} \alpha_i \phi_i \in V_h$, where α_i are the unknowns, of the system

$$\int_\Omega \nabla u_h \cdot \nabla \phi_i d\Omega = \lambda_h \int_{\partial\Omega} u_h \phi_i d\partial\Omega. \tag{4.16}$$

Inserting $u_h = \sum_{i=1}^{N} \alpha_i \phi_i$ into (4.16) results in the N linear algebraic equations for the unknowns α_i given as

$$\sum_{i=1}^{N} \alpha_i \int_\Omega \nabla \phi_i \cdot \nabla \phi_j d\Omega = \lambda_h \sum_{i=1}^{N} \alpha_i \int_{\partial\Omega} \phi_i \phi_j d\partial\Omega, \tag{4.17}$$

for $i, j = 1, 2, ..., N$. Equation (4.17) can be represented as the matrix form

$$K\alpha = \lambda R\alpha, \tag{4.18}$$

which is an $N \times N$ linear system for the unknown vector $\alpha = [\alpha_1, \alpha_2, \ldots, \alpha_N]$, where K and R are stiffness and boundary mass matrices respectively. The entries of these matrices are given as

$$K_{ij} = \int_\Omega \nabla \phi_i \cdot \nabla \phi_j d\Omega, \quad R_{ij} = \int_{\partial\Omega} \phi_i \phi_j d\partial\Omega. \tag{4.19}$$

for $i, j = 1, 2, ..., N$. Solution of (4.18) constitutes the FEM approximation of the Steklov EVP.

4.1.1. Assembly of Boundary Mass Matrices

As mentioned in Chapter 3, assembly procedure is required to obtain the entries of the stiffness and boundary mass matrices. Since the stiffness matrix is the same for both Laplace and Steklov EVPs, assembly of only the boundary mass matrix is described in this section.

Assume that $\mathcal{T}$ is a mesh described by the union of disjoint domains $\Omega^e \subset \Omega$, where e denotes the label of the elements in the mesh. Let K^e and R^e denote the local stiffness and local boundary mass matrices, respectively. For each element Ω^e, the entries of these matrices are obtained by computing the integrals

$$K_{ij}^e = \int_{\Omega^e} \nabla\phi_i \cdot \nabla\phi_j d\Omega^e, \tag{4.20a}$$

$$R_{ij}^e = \int_{\partial\Omega^e} \phi_i\phi_j d\partial\Omega^e. \tag{4.20b}$$

The assembly procedure can be defined as the summation of the local matrices over all elements in the mesh, and gives the entries of the global stiffness and boundary mass matrices as

$$K_{ij} = \sum_{e=1}^{N_e} \int_{\Omega^e} \nabla\phi_i \cdot \nabla\phi_j d\Omega^e = \sum_{e=1}^{N_e} K^e, \tag{4.21a}$$

$$R_{ij} = \sum_{e=1}^{N_e} \int_{\partial\Omega^e} \phi_i\phi_j d\partial\Omega^e = \sum_{e=1}^{N_e} R^e, \tag{4.21b}$$

where N_e denotes the number of elements in the mesh. Since the Steklov EVP is considered on a discretized domain using linear triangular elements in this chapter, the assembly procedure is described for a small mesh constructed by two linear triangular elements as an example.

Example 4.1: Consider the domain $\Omega = [0,\pi] \times [0,\pi]$*, and the mesh of this square given in Figure 4.1, with the linear basis functions*

$$\phi_i = 1 - \frac{x}{h} - \frac{y}{h}, \quad \phi_{i+1} = \frac{x}{h}, \quad \phi_{i+2} = \frac{y}{h}, \tag{4.22}$$

where $h = \pi/N$*,* $N = 1$ *for this example.*

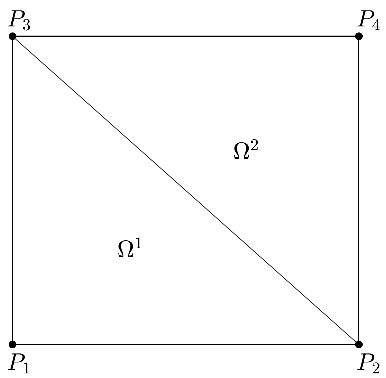

Figure 4.1: A mesh for the square $[0,\pi] \times [0,\pi]$ for $N = 1$.

Note that Ω^e *and* P_n *denote the elements and nodal points of the mesh respectively for* $e = 1, 2$*, and* $n = 1, 2, 3, 4$*.*

For a linear triangular element, the integral in (4.20b) *is computed using the formula [67]*

$$\int_{\partial\Omega^e} \phi_i \phi_j d\partial\Omega^e = \frac{1}{6}\left(1+\delta_{ij}\right) \mathit{length}\left(E\right), \tag{4.23}$$

where length (E) *is the length between the two nodes of an element on the boundary, and* δ_{ij} *is the Kronecker delta function defined as*

$$\delta_{ij} = \begin{cases} 1 & \mathit{if} \quad i = j, \\ 0 & \mathit{if} \quad i \neq j. \end{cases} \tag{4.24}$$

Thus, the local boundary mass matrix for this configuration is obtained as

$$R^e = \frac{h}{6}\begin{bmatrix} 2 & 1 \\ 1 & 2 \end{bmatrix} \tag{4.25}$$

using (4.23)*. It is important to note here that the local stiffness matrix is the same as the one obtained for the Laplace EVP. The entries of the local boundary mass matrix with respect to each element* Ω^e*, are given in Table 4.1 with the corresponding points* P_n*, for* $e = 1, 2$*, and* $n = 1, 2, 3, 4$*.*

Table 4.1: The entries of the local boundary mass matrix R^e with respect to each element Ω^e.

	P_1	P_2
P_1	$\frac{h}{3}$	$\frac{h}{6}$
P_2	$\frac{h}{6}$	$\frac{h}{3}$

(a) R^e on the bottom of $\partial\Omega^1$.

	P_2	P_4
P_2	$\frac{h}{3}$	$\frac{h}{6}$
P_4	$\frac{h}{6}$	$\frac{h}{3}$

(b) R^e on the right of $\partial\Omega^2$.

	P_4	P_3
P_4	$\frac{h}{3}$	$\frac{h}{6}$
P_3	$\frac{h}{6}$	$\frac{h}{3}$

(c) R^e on the top of $\partial\Omega^2$.

	P_3	P_1
P_3	$\frac{h}{3}$	$\frac{h}{6}$
P_1	$\frac{h}{6}$	$\frac{h}{3}$

(d) R^e on the left of $\partial\Omega^1$.

Assembly of the global boundary mass matrix is described in Table 4.2.

Table 4.2: Assembly of global boundary mass matrix R.

	P_1	P_2	P_4	P_3
P_1	$\frac{h}{3}+\frac{h}{3}$	$\frac{h}{6}$	0	$\frac{h}{6}$
P_2	$\frac{h}{6}$	$\frac{h}{3}+\frac{h}{3}$	$\frac{h}{6}$	0
P_4	0	$\frac{h}{6}$	$\frac{h}{3}+\frac{h}{3}$	$\frac{h}{6}$
P_3	$\frac{h}{6}$	0	$\frac{h}{6}$	$\frac{h}{3}+\frac{h}{3}$

Thus, the global boundary mass matrix is obtained as

$$R = \frac{h}{6}\begin{bmatrix} 4 & 1 & 0 & 1 \\ 1 & 4 & 1 & 0 \\ 0 & 1 & 4 & 1 \\ 1 & 0 & 1 & 4 \end{bmatrix}. \tag{4.26}$$

4.1.2. Convergence Analysis

In this section, the Babuška-Osborn spectral theory [9] is introduced in order to obtain the convergence estimates for the eigenvalues and the eigenfunctions of (4.1) approximated with the use of piecewise polynomials.

As mentioned before, the variational form of (4.1) is given as: find eigenvalues $\lambda \in \mathbb{R}$ and eigenfunctions $0 \neq u \in H^1$ such that

$$a(u, v) = \lambda b(u, v) \quad \forall v \in H^1, \tag{4.27}$$

where

$$a(u, v) = \int_\Omega \nabla u \cdot \nabla v d\Omega \quad \text{and} \quad b(u, v) = \int_{\partial\Omega} uvd\partial\Omega. \tag{4.28}$$

The Poincaré inequality yields

$$\begin{aligned} a(u, u) &= \int_\Omega \nabla u \cdot \nabla u d\Omega \\ &\geq C \|\nabla u\|^2 \\ &\geq \|u\|^2, \end{aligned} \tag{4.29}$$

where C is a positive constant. Since

$$\begin{aligned} \|u\|^2 &= \int_\Omega u^2 d\Omega \\ &\leq \int_\Omega \nabla u \cdot \nabla u d\Omega + \int_\Omega u^2 d\Omega \\ &= \|u\|_1^2, \end{aligned} \tag{4.30}$$

$a(u, v)$ does not satisfy the coercivity condition $a(u, u) \geq c \|u\|_1^2$ on H^1. In other words, $a(u, v)$ is not H^1-elliptic. As an example, if $u = c$ (a constant function), then $a(u, u) = 0$. Since $\|u\|_1 > 0$, the coercivity condition is not satisfied. As a consequence, a shift argument is used to rewrite (4.27) as

$$\hat{a}(u, v) = (\lambda + 1)b(u, v) \quad \forall v \in H^1, \tag{4.31}$$

where

$$\begin{aligned}\hat{a}(u,v) &= a(u,v) + b(u,v) \\ &= \int_{\Omega} \nabla u \cdot \nabla v d\Omega + \int_{\partial\Omega} uvd\partial\Omega.\end{aligned} \tag{4.32}$$

The continuity of $\hat{a}(u,v)$ follows from Cauchy-Schwarz inequality

$$\begin{aligned}\hat{a}(u,v) &= \int_{\Omega} \nabla u \cdot \nabla v d\Omega + \int_{\partial\Omega} uvd\partial\Omega \\ &\leq \|\nabla u\| \|\nabla v\| + \|u\|_{L^2(\partial\Omega)} \|v\|_{L^2(\partial\Omega)} \\ &\leq \left(\|\nabla u\|^2 + \|u\|^2_{L^2(\partial\Omega)}\right)^{1/2} \left(\|\nabla v\|^2 + \|v\|^2_{L^2(\partial\Omega)}\right)^{1/2}.\end{aligned} \tag{4.33}$$

From the trace inequality [67] one has

$$\begin{aligned}\|v\|_{L^2(\partial\Omega)} &\leq C \left(\|v\|^2 + \|\nabla v\|^2\right)^{1/2} \\ &\leq C \|u\|_1,\end{aligned} \tag{4.34}$$

where C is a positive constant, and then the continuity of $\hat{a}(u,v)$ follows

$$\hat{a}(u,v) \leq C \|u\|_1. \tag{4.35}$$

The coercivity of $\hat{a}(u,v)$ follows from the generalized Poincaré inequality [65]

$$\left(\int_{\Omega} |\nabla u|^2 d\Omega + \int_{\partial\Omega} u^2 d\partial\Omega\right)^{1/2} \geq C \|u\|_1, \tag{4.36}$$

where is C a positive constant, so that

$$\begin{aligned}\hat{a}(u,u) &= \int_{\Omega} \nabla u \cdot \nabla u d\Omega + \int_{\partial\Omega} u^2 d\partial\Omega \\ &\geq C \|u\|_1^2.\end{aligned} \tag{4.37}$$

The continuity of $b(u,v)$ follows immediately from (4.34). According to the Lax-Milgram lemma, it is observed that (4.31) has a unique solution. It is clearly seen that if $\lambda + 1$ is an eigenvalue of (4.31), then λ is an eigenvalue of (4.27).

Next, define a solution operator

$$T : H^1(\Omega) \to H^1(\Omega) \tag{4.38a}$$

$$f \to Tf := u, \tag{4.38b}$$

such that

$$\hat{a}(Tf,v) = b(f,v) \quad \forall v \in H^1, \tag{4.39}$$

where $u \in H^1$ is the solution of the corresponding source problem given as

$$\hat{a}(u,v) = b(f,v) \quad \forall f, v \in H^1. \tag{4.40}$$

Since $\hat{a}(u,v) = \hat{a}(v,u)$ and $b(u,v) = b(v,u)$, the bilinear forms are symmetric. The positive definiteness of $\hat{a}(u,v)$ follows from

$$\begin{aligned} \hat{a}(u,u) &= \int_{\Omega} \nabla u \cdot \nabla u d\Omega + \int_{\partial\Omega} u^2 d\partial\Omega \\ &= \|\nabla u\|^2 + \|u\|^2_{L^2(\partial\Omega)} > 0. \end{aligned} \tag{4.41}$$

Thus, it is observed that $\hat{a}(u,v)$ is an inner product. Since

$$\hat{a}(Tf,g) = b(f,g) = b(g,f) = \hat{a}(Tg,f) = \hat{a}(f,Tg) \quad \forall f, g \in H^1, \tag{4.42}$$

the solution operator T is self-adjoint with respect to the inner product $\hat{a}(\cdot,\cdot)$.

Now, consider the discrete problem defined as: find eigenvalues $\lambda_h \in \mathbb{R}$ and eigenfunctions $0 \neq u_h \in V_h$ such that

$$a(u_h, v_h) = \lambda_h b(u_h, v_h) \quad \forall v_h \in V_h, \tag{4.43}$$

in the finite dimensional subspace $V_h \subset H^1$. Using the shift argument to rewrite (4.43) results in

$$\hat{a}(u_h, v_h) = (\lambda_h + 1) b(u_h, v_h) \quad \forall v_h \in V_h. \tag{4.44}$$

Then, define a discrete solution operator $T_h : H^1 \to H^1$ is such that

$$\hat{a}(T_h f, v_h) = b(f, v_H) \quad \forall v_h \in V_h. \tag{4.45}$$

and

$$\|T - T_h\|_1 \to 0 \quad \text{as} \quad h \to 0, \tag{4.46}$$

where $V_h \subset H^1$. It is important that T_h is also self-adjoint, since

$$\hat{a}(T_h f, g) = b(f,g) = b(g,f) = \hat{a}(T_h g, f) = \hat{a}(f, T_h g) \quad \forall f, g \in H^1. \tag{4.47}$$

The eigensolution of (4.43) convergence to the eigensolution of (4.31) if and only if the discrete solution operator T_h satisfy (4.46) (see [12]). The following theorems give the convergence estimates for the eigenvalues and eigenfunctions in the symmetric case. The proofs of these theorems can be found in [12].

Theorem 4.1: Let V_h be a finite element space, and $\lambda_h^{(k)}$ be the eigenvalues of (4.43) *converging to the eigenvalues of* (4.27) $\lambda^{(k)}$*. Then, there is a constant C such that the approximate eigenvalues $\lambda_h^{(k)}$ satisfy*

$$\lambda^{(k)} \leq \lambda_h^{(k)} \leq \lambda^{(k)} + C \sup_{\substack{u \in E \\ \|u\|=1}} \inf_{v \in V_h} \|u - v\|_1^2 , \tag{4.48}$$

where E denotes the eigenspace associated with $\lambda^{(k)}$.

Theorem 4.2: Assume that $u^{(k)}$ is an unit eigenfunction associated with the eigenvalue $\lambda^{(k)}$ of multiplicity m, and $w_h^{(1)}, w_h^{(2)}, \ldots, w_h^{(m)}$ are the eigenfunctions associated with m discrete eigenvalues converging to $\lambda^{(k)}$. Then, there exists

$$u_h \in \operatorname{span}\left\{w_h^{(1)}, w_h^{(2)}, \ldots, w_h^{(m)}\right\} , \tag{4.49}$$

such that

$$\|u - u_h\|_1 \leq C \sup_{\substack{u \in E \\ \|u\|=1}} \inf_{v \in V_h} \|u - v\|_1 , \tag{4.50}$$

where E denotes the eigenspace associated with $\lambda^{(k)}$ and C is a constant.

The following lemma is an additional regularity result for the eigenfunctions of (4.1). The proof this lemma can be found in [39] (see also [69]).

Lemma 4.3: There exists $r_\Omega > 1/2$, which is the Sobolev exponent for the Laplace problem with Neumann boundary conditions, such that following result holds:

- *if u is an eigenfunction of* (4.1) *with the associated eigenvalue λ,then there exists a positive constant C such that*

$$\|u\|_{H^{1+r}(\Omega)} \leq C \|u\|_1 \tag{4.51}$$

for all $r \in [1/2, r_\Omega)$ and $u \in H^{1+r}$.

Note that, $r_\Omega > 1$ if Ω is a convex domain and $r_\Omega := \pi/\omega$, with ω being the largest inner angle of Ω, otherwise (see [39] and [69]).

Now, assume that the best approximation result

$$\inf_{v \in V_h} \|u - v\|_1 \leq C h^{\min\{s,r\}} \|u\|_{H^{1+r}(\Omega)} , \tag{4.52}$$

is satisfied for the finite dimensional subspace $V_h \subset H^1$ constructed by piecewise polynomials of degree s. Such results are standard in the case of V_h contains the piecewise polynomials.

From Theorem 4.1, Theorem 4.2, and (4.52), the estimates for the eigenvalues and the eigenfunctions are obtained as

$$|\lambda - \lambda_h| \leq Ch^2, \tag{4.53a}$$

$$\|u - u_h\|_1 \leq Ch, \tag{4.53b}$$

for linear piecewise polynomial, where C is a positive constant. Analogous estimates are also obtained for the virtual element method, using the spectral approximation theory, in [39] (see also [70]). The virtual element method involves the Galerkin discretization of the problem using polygonal or polyhedral elements. For this reason, the virtual element method has the theoretical background of FEM, and the estimates are assured for FEM. Besides, these estimates are analogous with the estimates given in [59] (see also [15]) for FEM analysis of the Steklov EVP in the case the PDE is given as $-\Delta u + u = 0$ in Ω.

4.1.3. Numerical Results

The numerical results obtained by using the linear triangular elements to discretize the unit disc are presented in this section. The convergence behaviors of the approximate solutions to the exact solutions are investigated as h_{max} goes to zero, where h_{max} denotes the maximum of the longest side of the triangles in the mesh. All of the computations and the figures are procured by means of a program written using MATLAB.

4.1.3.1. Linear Elements on the Unit Disc

The first ten approximate eigenvalues $\lambda_h^{(0)}$, $\lambda_h^{(2k-1)}$, $\lambda_h^{(2k)}$ and the corresponding exact eigenvalues $\lambda_h^{(0)} = 0$, $\lambda^{(2k-1)} = \lambda^{(2k-1)} = k$ of the Steklov EVP are given in Table 4.3 with the size S of the solved linear system of equations reduced by imposing the boundary conditions and the rates of convergence for $h_{max} = 0.2, 0.1, 0.05, 0.025$. From Table 4.3, it is observed that the approximate eigenvalues converge to the exact eigenvalues as h_{max} goes to zero.

Table 4.3: First ten approximate and exact eigenvalues of the Steklov EVP for Section 4.1.3.1, $k = 0, 1, \ldots, 5$, and $h_{max} = 0.2, 0.1, 0.05, 0.025$.

$\lambda^{(2k-1)} = k$ $\lambda^{(2k)} = k$	$h_{max} = 0.2$ $S : 105 \times 105$	$h_{max} = 0.1$ $S : 407 \times 407$	$h_{max} = 0.05$ $S : 1457 \times 1457$	$h_{max} = 0.0025$ $S : 6117 \times 6117$
$\lambda^{(0)} = 0$	0.0000	0.0000	0.0000	0.0000
$\lambda^{(1)} = 1$	1.0016	1.0004 (2.0)	1.0001 (1.9)	1.0000 (2.0)
$\lambda^{(2)} = 1$	1.0016	1.0004 (2.0)	1.0001 (1.9)	1.0000 (2.0)
$\lambda^{(3)} = 2$	2.0326	2.0076 (2.1)	2.0020 (1.9)	2.0005 (2.0)
$\lambda^{(4)} = 2$	2.0328	2.0077 (2.1)	2.0020 (1.9)	2.0005 (2.1)
$\lambda^{(5)} = 3$	3.1311	3.0308 (2.1)	3.0081 (1.9)	3.0019 (2.1)
$\lambda^{(6)} = 3$	3.1311	3.0308 (2.1)	3.0081 (1.9)	3.0019 (2.1)
$\lambda^{(7)} = 4$	4.3329	4.0786 (2.1)	4.0206 (1.9)	4.0049 (2.1)
$\lambda^{(8)} = 4$	4.3369	4.0787 (2.1)	4.0206 (1.9)	4.0049 (2.1)
$\lambda^{(9)} = 5$	5.6869	5.1614 (2.1)	5.0423 (1.9)	5.0101 (2.1)

The errors between the exact eigenvalues $\lambda^{(2k-1)} = k$ and approximate eigenvalues $\lambda_h^{(2k-1)}$ of are shown in Figure 4.2. These figures show that the convergence behavior of the approximate eigenvalues $\lambda_h^{(2k-1)}$ is of order $O(h^2)$. Also, the rates of convergence given in Table 4.3 are in well accordance with this behavior.

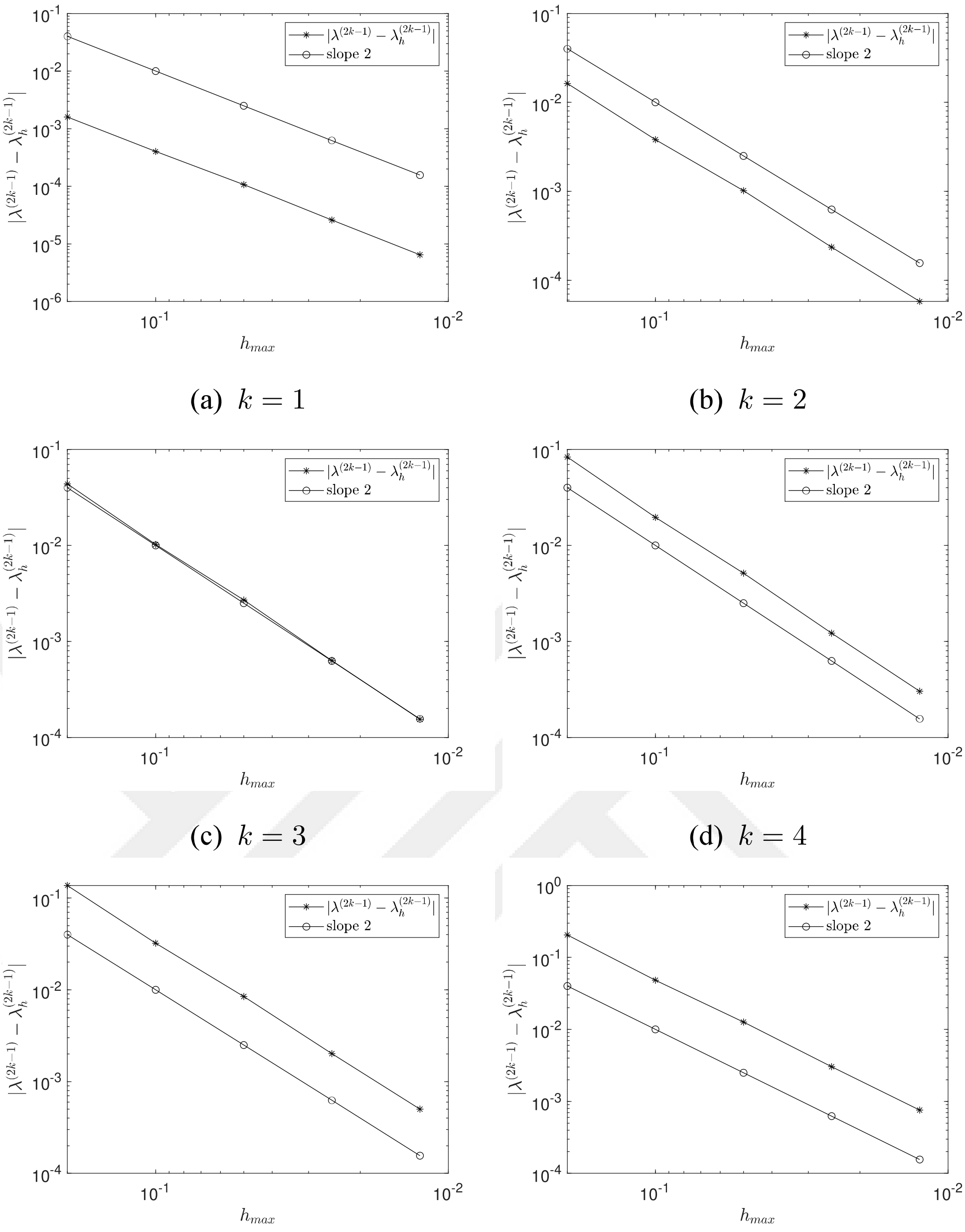

(a) $k = 1$ (b) $k = 2$

(c) $k = 3$ (d) $k = 4$

(e) $k = 5$ (f) $k = 6$

Figure 4.2: Log-log scale plot of $|\lambda^{(2k-1)} - \lambda_h^{(2k-1)}|/|\lambda^{(2k-1)}|$ for Section 4.1.3.1, $k = 1, 2, \ldots, 6$, and $h_{max} = 0.2, 0.1, \ldots, 0.0125$.

It is known that the eigenfunction $u^{(0)}$ is a constant function corresponding to the only simple eigenvalue $\lambda^{(0)} = 0$. To numerically show that the approximate eigenfunction $u_h^{(0)}$ is also a constant function, plots of the eigenfunctions $u^{(0)}$ and $u_h^{(0)}$ normalized with respect to infinity norm are given in Figure 4.3.

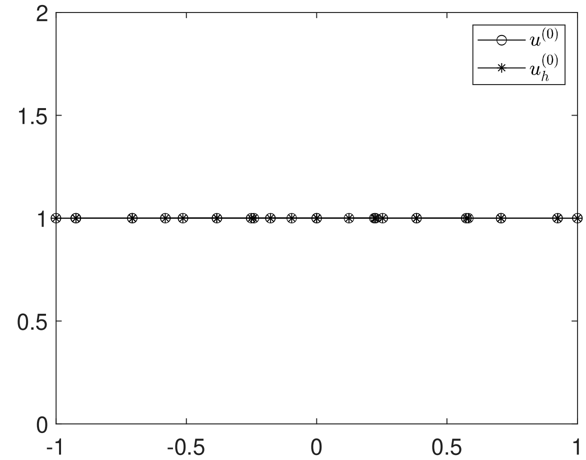

Figure 4.3: Plot of $u^{(0)}$ and $u_h^{(0)}$ corresponding to $\lambda = 0$ for Section 4.1.3.1 and $h_{max} = 0.4$.

If the approximate eigenfunctions corresponding to the double eigenvalues of the Steklov EVP are considered, it can be observed that the linear combinations of the approximate eigenfunctions associated with the double eigenvalues are reasonable approximations to the corresponding exact eigenfunctions as given in (3.96). To illustrate this behavior on the unit disc, the contour plots of the approximate eigenfunctions $u_h^{(2k-1)}$, $u_h^{(2k)}$, and the corresponding exact eigenfunctions $u^{(2k-1)} = r^k \sin(k\theta)$, $u^{(2k)} = r^k \cos(k\theta)$ are given in Figure 4.4 and Figure 4.5 together with the linear combinations of the approximate eigenfunctions $\beta_{(2k-1)} u_h^{(2k-1)} + \beta_{(2k)} u_h^{(2k)}$ where $k = 1, 2$ and $\beta_{(2k-1)}$, $\beta_{(2k)}$ are constants obtained similarly from (3.93).

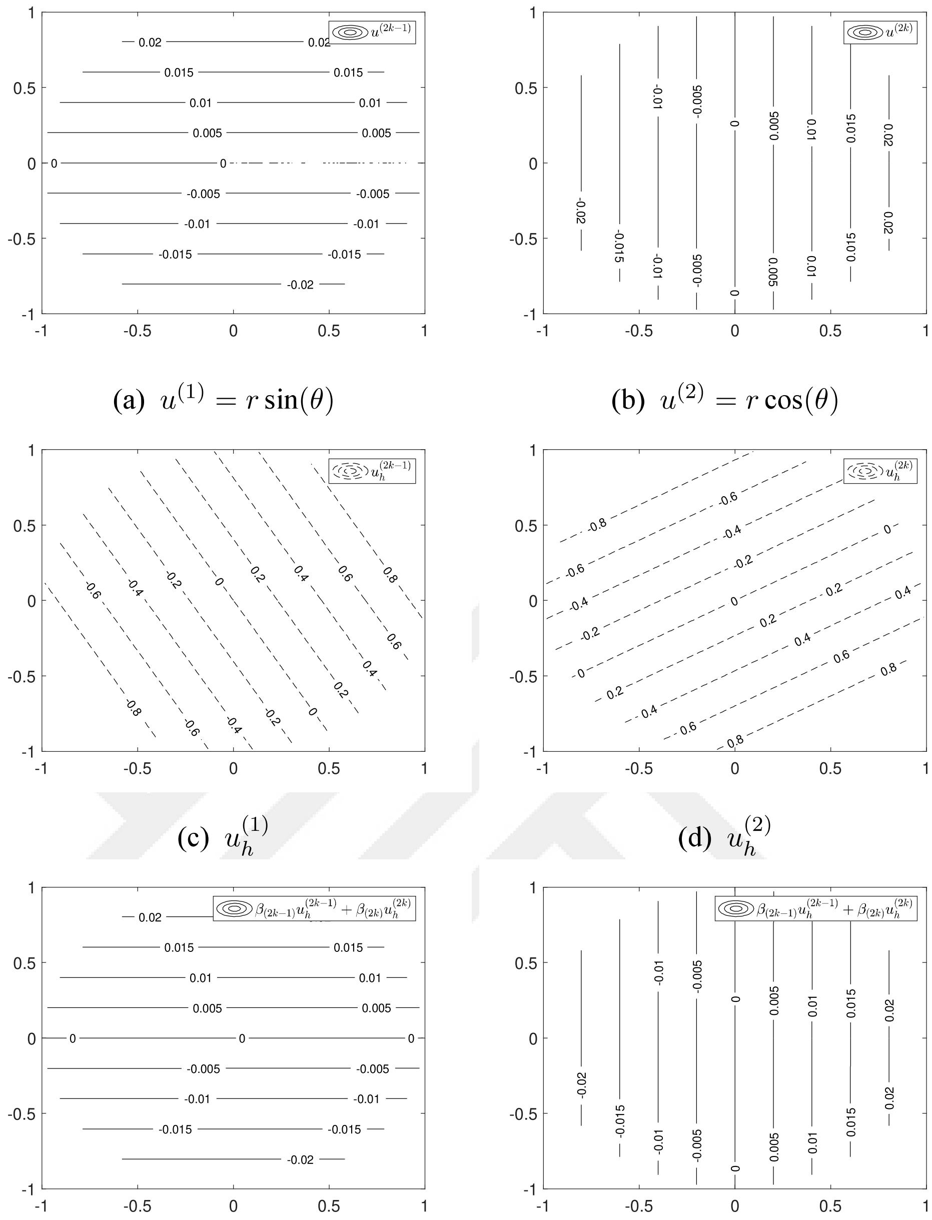

(a) $u^{(1)} = r\sin(\theta)$

(b) $u^{(2)} = r\cos(\theta)$

(c) $u_h^{(1)}$

(d) $u_h^{(2)}$

(e) $0.5123u_h^{(1)} - 0.8703u_h^{(2)}$

(f) $0.8590u_h^{(1)} + 0.4933u_h^{(2)}$

Figure 4.4: Contour plots of approximate and exact eigenfunctions corresponding to the multiple eigenvalues for Section 4.1.3.1, $k = 1$ and $h_{max} = 0.025$.

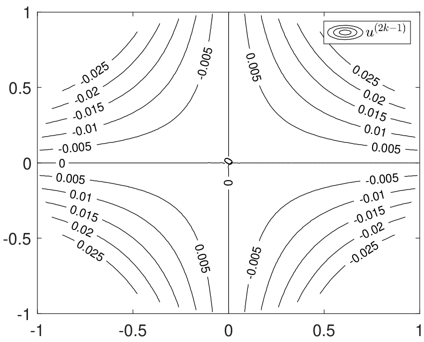

(a) $u^{(3)} = r^2 \sin(\theta)$

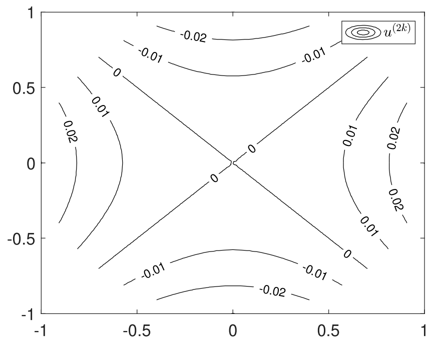

(b) $u^{(4)} = r^2 \cos(\theta)$

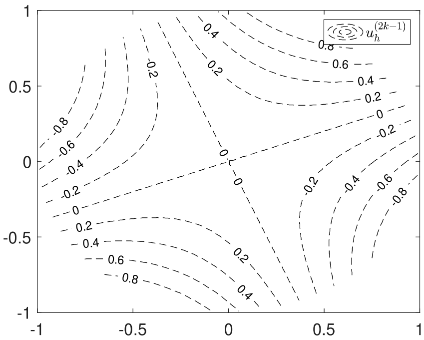

(c) $u_h^{(3)}$

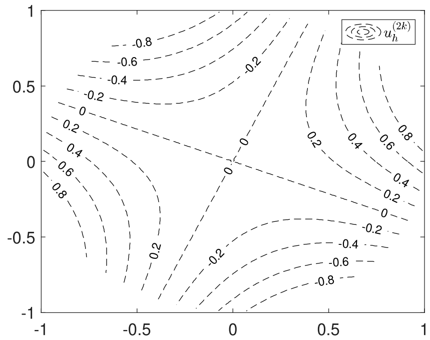

(d) $u_h^{(4)}$

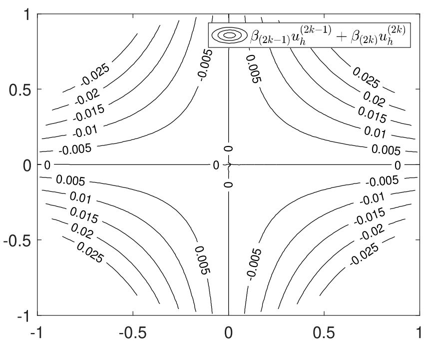

(e) $0.7229u_h^{(3)} + 0.6916u_h^{(4)}$

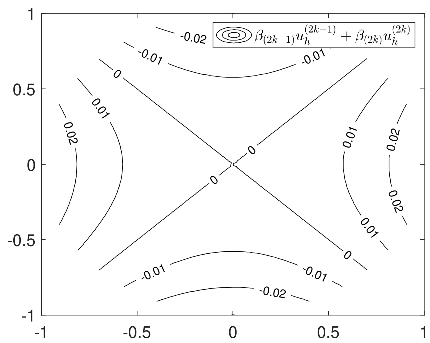

(f) $-0.6896u_h^{(3)} + 0.7235u_h^{(4)}$

Figure 4.5: Contour plots of approximate and exact eigenfunctions corresponding to the multiple eigenvalues for Section 4.1.3.1, $k = 1$ and $h_{max} = 0.025$.

4.2. Regular Polygon Inscribed in the Unit Disc

In this section, the Steklov EVP is considered on N-sided regular polygons, which are assumed to be a boundary variation of the unit disc in such a way that each point on the boundary of the unit disc moves, starting at $t = 0$, along the radial direction with velocity C and arrives at the boundary of the polygon at $t = 1$. From the studies [50, 51], it is theoretically known that the simple eigenvalues of the Laplace EVP on N-sided regular polygon can be represented in terms of inverse powers of sides N such that

$$\lambda_N = \lambda \left(1 + c_1 \frac{1}{N} + c_2 \frac{1}{N^2} + c_3 \frac{1}{N^3} + \cdots \right), \tag{4.54}$$

where λ_N is the eigenvalue on the N-sided regular polygon, and λ is the corresponding eigenvalue on the unit disc. As mentioned in Chapter 3, the series given in (4.54) is obtained by using Hadamard's shape derivative formula (3.145) for the lowest simple eigenvalue of the Laplace EVP. Based on this study, the relation between the eigenvalues of the Steklov EVP on the unit disc and the eigenvalues on N-sided regular polygon inscribed in the unit disc is investigated in this section. This investigation aims to numerically show that the eigenvalues of the Steklov EVP on the regular polygon can be represented in terms of inverse powers of sides as in the Laplace EVP. In this investigation, the eigenvalues of the Steklov EVP on N-sided regular polygon are denoted as λ_N and are computed by using FEM on the discretized regular polygons by using linear triangular elements. Then, the plots of λ_N/λ procured by means of a program written using MATLAB are given in Figure 4.6 and Figure 4.7 for increasing number of sides N. From Figure 4.6, it is observed that the nonzero eigenvalues of the Steklov EVP on N-sided regular polygon can be represented as infinite series in terms of the inverse powers of N as given in (4.54).

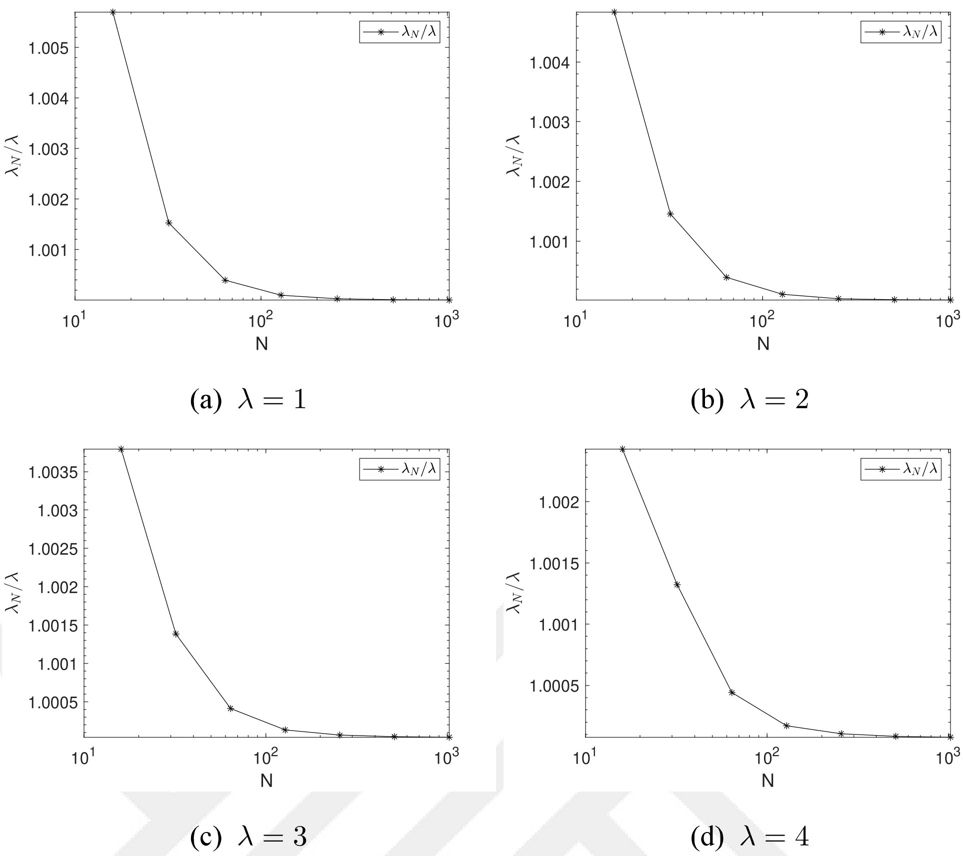

(a) $\lambda = 1$ (b) $\lambda = 2$

(c) $\lambda = 3$ (d) $\lambda = 4$

Figure 4.6: Log-log scale plot of λ_N/λ for the Steklov EVP, $h_{max} = 0.00625$, and $N = 2^4, 2^5, .., 2^{10}$.

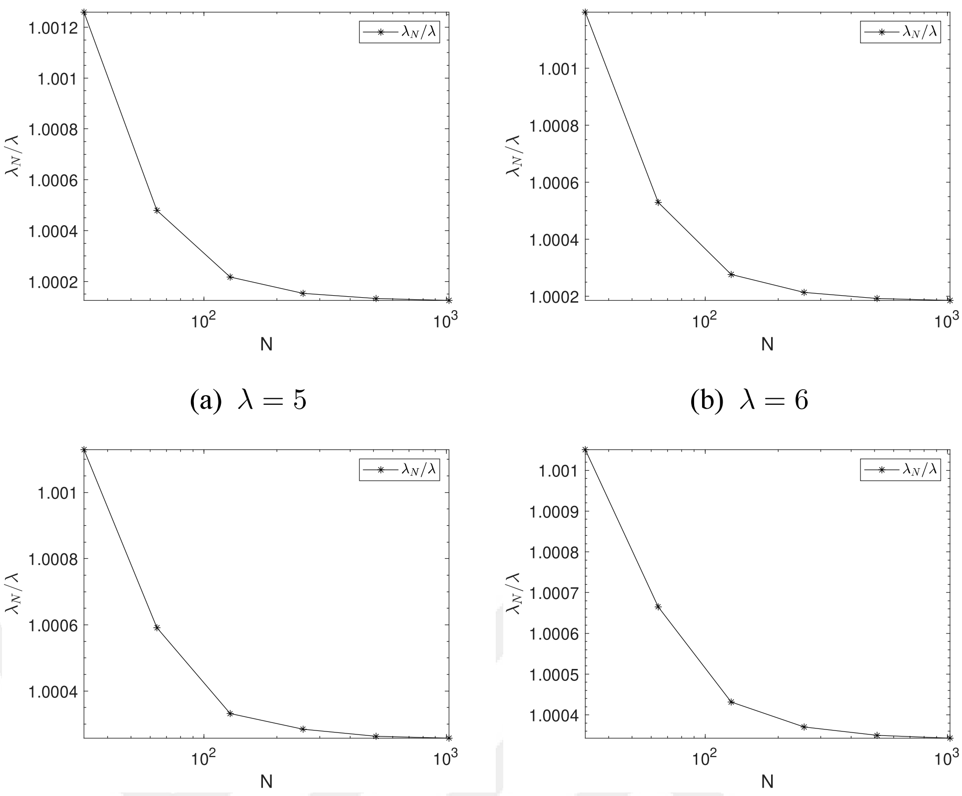

(a) $\lambda = 5$ (b) $\lambda = 6$

(c) $\lambda = 7$ (d) $\lambda = 8$

Figure 4.7: Log-log scale plot of λ_N/λ for the Steklov EVP, $h_{max} = 0.00625$, and $N = 2^5, 2^6, .., 2^{10}$.

As a conclusion, in this chapter, the Steklov EVP is considered on the unit disc. FEM is applied to this problem using linear triangular elements to discretize the unit disc. It is observed that the approximate eigenvalues of the Steklov EVP converge to the corresponding exact eigenvalues as the number of elements is increasing, and this convergence behavior is observed to be of order $O(h^2)$. Besides, it is deduced that the linear combinations of the approximate eigenfunctions associated with the double eigenvalues are reasonable approximations to the exact eigenfunctions. Also, it is numerically shown that the eigenvalues of the Steklov EVP on the regular polygon inscribed in the unit disc can be represented as a series in terms of inverse powers of sides of the polygon which are not available in the open literature to the best of author's knowledge.

It is known that analogous series is obtained using Hadamard's shape derivative formula for the Laplace EVP. The shape derivative formulas derived in [56] for the both simple and multiple eigenvalues of the EVP with Wentzell boundary conditions

$$-\Delta u = 0 \quad \text{in } \Omega, \tag{4.55a}$$

$$-\beta \Delta_S u + \frac{\partial u}{\partial n} = \lambda u \quad \text{on } \partial\Omega, \tag{4.55b}$$

where Δ_S is the Laplace operator on $\partial\Omega$, β is a given real number, and $\partial u/\partial n$ is the outward normal derivative. Note that, (4.55) becomes the Steklov EVP in the case of $\beta = 0$. For this case, the shape derivative formula (see Appendix E in [56]) is given as $M \times M$ matrix D with the entries

$$D_{m,n} = \int_S C\left(\nabla u_m \nabla u_n - 2\lambda^2 u_m u_n - \lambda\kappa u_m u_n\right) dS, \tag{4.56}$$

where κ is the mean curvature, C is the velocity, $m, n = 1, 2, \ldots, M$, and u_m are the orthonormal eigenfunctions which correspond to the eigenvalues of the Steklov EVP with multiplicity M. The eigenvalues of D give the shape derivatives of the multiple eigenvalues of the Steklov EVP denoted by λ'.

It is known that, the Taylor series expansion at $t = 0$ gives the approximation of the eigenvalues λ_N on the polygon [53] such that

$$\lambda_N = \lambda + \lambda' + \frac{1}{2}\lambda'' + \frac{1}{6}\lambda''' + \cdots, \tag{4.57}$$

where λ is the corresponding eigenvalue on the unit disc. As a future work, the other derivatives λ'' and λ''' can be obtained by taking the derivative of (4.56) with respect to the time parameter t. Then, the series given in (4.54) can be obtained with coefficients by substituting the Taylor series expansion of the derivatives λ', λ'', and λ''' in terms of powers of $1/N$ into (4.57).

5. CONCLUSION

In this thesis, numerical approximations of the Laplace and Steklov EVPs posed on one- and two-dimensional domains obtained using FEM are presented. In the one-dimensional case, the FEM solution of the Laplace EVP is obtained by means of the analytically known eigensolutions of the resulting tridiagonal matrices, and its convergence behavior to the exact eigensolution is presented with numerical results obtained on an interval discretized by linear and quadratic elements. As for the two-dimensional cases, the Laplace EVP is considered on square and disc domains discretized by linear triangular elements. The convergence behavior of the FEM solution is obtained on both uniform and non-uniform meshes for the square domain and the non-uniform meshes for the disc domain.

It is theoretically known that the convergence behaviors with respect to the mesh parameter h are of order $O(h^2)$ and $O(h^4)$ for the eigenvalues obtained on discretized domains using linear and quadratic elements, respectively. For the approximate eigenfunctions obtained using linear elements, the convergence is of order $O(h)$ and $O(h^2)$ in H^1-and L^2-norms, respectively. On the other hand, the convergence behavior of the eigenfunctions considering the quadratic elements is of order $O(h^2)$ and $O(h^3)$ in H^1-and L^2-norms, respectively. In all cases considered in this study, it is observed that the convergence results obtained with numerical experiments are in good agreement with the already known theoretical results for the eigenvalues and the eigenfunctions corresponding to the simple eigenvalues. Besides, linearly independent eigenfunctions of the Laplace EVP corresponding to the multiple eigenvalues are considered separately in the two-dimensional cases, and it is deduced that their linear combinations constitute reasonable approximations to the corresponding exact eigenfunctions associated with the multiple eigenvalues. Moreover, the obtained numerical results show that the linear combinations satisfy the convergence behavior for the eigenfunctions ($O(h)$ and $O(h^2)$) on the uniform mesh of the square constructed using linear triangular elements. On the other hand, the convergence behavior of the eigensolutions to the exact solutions of the Steklov EVP is provided using the spectral theory for the symmetric case presented in [12]. It is observed that the convergence behavior of the approximate eigenvalues and eigenfunctions are of order $O(h^2)$ and order $O(h)$ (with respect to H^1-norm), respectively. The convergence results obtained that concerns the approximate eigenvalues for this case are confirmed numerically on non-uniform discretizations of the unit disc constructed by linear triangular elements. As in the Laplace EVP, it is shown that the linear combinations of the approximate eigenfunctions of the Steklov EVP constitute reasonable approximations to the corresponding exact eigenfunctions associated with the multiple eigenvalues.

Since the boundary perturbations can be the cause of various errors in finite element methods, the influences of the boundary perturbations on the eigensolutions of the Laplace and Steklov EVPs are investigated in this thesis. First, it is assumed that the perturbed domain is inscribed into the original domain, and it approximates the boundary of the original domain by means of a perturbation parameter δ. Then, the analytical solutions of the Laplace EVP are obtained in terms of this perturbation parameter on the perturbed one-dimensional domain, rectangle, and disc domain. In addition, the FEM solution of the Laplace EVP on the one-dimensional perturbed domain is analytically derived by means of known eigensolutions of the resulting tridiagonal matrices. The convergence of the analytically obtained perturbed solutions to the original solutions is explored by Taylor's series expansion of the errors between the two solutions at $\delta = 0$. It is observed that the perturbed eigenvalues converge to the corresponding original eigenvalues as δ goes to zero, and this convergence behavior is of order $O(\delta)$ in both one- and two-dimensional cases. An analogous result is shown to hold numerically for the approximate eigenvalues. Further, it is shown that the convergence behavior of the perturbed eigenfunctions in the one-dimensional case is of order $O(\delta)$ and $O(\delta^{1/2})$ in L^2- and H^1-norms, respectively. These convergence results are in coherence with the numerical experiments conducted in this study, and also with the results obtained for the corresponding boundary value (source) problem in [41]. Numerical examples are provided to show that analogous behaviors are found by the approximate eigenfunctions on the one-dimensional domain.

Finally, the Laplace and Steklov EVPs are considered on N-sided regular polygons assumed to be inscribed in the unit disc to address the evolution of the eigensolutions on domains induced by the motions of the boundaries. It is known that the simple eigenvalues of the Laplace EVP on the polygon can be represented as a series in terms of the inverse powers of the number of sides such that

$$\lambda_N = \lambda \left(1 + c_1 \frac{1}{N} + c_2 \frac{1}{N^2} + c_3 \frac{1}{N^3} + \cdots \right), \tag{5.1}$$

where λ_N is the eigenvalue on the polygon, and λ is the corresponding eigenvalue on the unit disc. For the lowest simple eigenvalue, this series is obtained as

$$\lambda_N = \lambda \left(1 + \frac{4\zeta(2)}{N^2} + \frac{4\zeta(3)}{N^3} + \frac{28\zeta(4)}{N^4} + \cdots \right), \tag{5.2}$$

using Hadamard's formula (see [50, 51]), where ζ is the Riemann zeta function. In this thesis, it is numerically shown that analogous results hold for the multiple eigenvalues obtained using FEM on the polygon discretized by linear triangular elements. Furthermore, a similar investigation is conducted for the multiple eigenvalues of the Steklov EVP on the polygon, and the analogous series representation with different coefficients is numerically shown to hold for the Steklov eigenvalue problem. As a future study, the series given in (5.1) can be derived with coefficients using the shape derivative formula for the multiple eigenvalues of the Steklov EVP.

REFERENCES

[1] Strang G., Fix G., (2018), "An Analysis of the Finite Element Method", 2nd Edition, Wellesley-Cambridge Press.

[2] Sun J., Zhou A., (2016), "Finite Element Methods for Eigenvalue Problems", 1st Edition, Chapman and Hall/CRC.

[3] Bramble J. H., Osborn J. E., (1973), "Rate of Convergence Estimates for Nonselfadjoint Eigenvalue Approximations", Mathematics of Computation 27(123), 525–549.

[4] Fix G. J., (1973), "Eigenvalue approximation by the finite element method", Advances in Mathematics 10(2), 300–316.

[5] Osborn J. E., (1975), "Spectral approximation for compact operators", Mathematics of Computation 29(131), 712–725.

[6] Kolata W. G., (1978), "Approximation in variationally posed eigenvalue problems", Numer. Math. 29(2), 159–171.

[7] Canuto C., (1978), "Eigenvalue approximations by mixed methods", ESAIM: Mathematical Modelling and Numerical Analysis - Modélisation Mathématique et Analyse Numérique 12(1), 27–50.

[8] Babuška I., Osborn J. E., (1989), "Finite element-Galerkin approximation of the eigenvalues and eigenvectors of selfadjoint problems", Mathematics of Computation 52(186), 275–297.

[9] Babuška I., Osborn J., (1991), Eigenvalue problems, in "Finite Element Methods (Part 1)", Vol. 2 of Handbook of Numerical Analysis, Elsevier, pp. 641 – 787.

[10] Larson M. G., (2000), "A posteriori and priori error analysis for finite element approximations of self-adjoint elliptic eigenvalue problems", SIAM Journal on Numerical Analysis 38(2), 608–625.

[11] Knyazev A. V., Osborn J. E., (2006), "New a priori FEM error estimates for eigenvalues", SIAM J. Numerical Analysis 43(6), 2647–2667.

[12] Boffi D., (2010), "Finite element approximation of eigenvalue problems", Acta Numerica 19, 1–120.

[13] Grebenkov D., Nguyen B., (2013), "Geometrical Structure of Laplacian Eigenfunctions", SIAM Review 55(4), 601–667.

[14] Rayleigh J. W. S., (1945), "The Theory of Sound", Vol. 1 and 2, 2nd Edition, Dover Publications.

[15] Armentano M., Duran R., (2004), "Asymptotic lower bounds for eigenvalues by nonconforming finite element methods", ETNA. Electronic Transactions on Numerical Analysis [electronic only] 17, 93–101.

[16] FuSheng L., Qun L., HeHu X., (2012), "Computing the lower and upper bounds of Laplace eigenvalue problem: by combining conforming and nonconforming finite element methods", Science China Mathematics 55(5), 1069–1082.

[17] Antonietti P. F., Buffa A., Perugia I., (2006), "Discontinuous Galerkin approximation of the Laplace eigenproblem", Computer Methods in Applied Mechanics and Engineering 195(25), 3483–3503.

[18] Zhai Q., Xie H., Zhang R., Zhang Z., (2019), "Acceleration of weak Galerkin Methods for the Laplacian eigenvalue problem", Journal of Scientific Computing 79, 914–934.

[19] Liu X., Oishi S., (2013), "Verified Eigenvalue Evaluation for the Laplacian over Polygonal Domains of Arbitrary Shape", SIAM Journal on Numerical Analysis 51(3), 1634–1654.

[20] Xiao W., Gong B., Sun J., Zhang Z., (2020), "A new finite element approach for the Dirichlet eigenvalue problem", Applied Mathematics Letters 105, 106295.

[21] Canavati J., Minzoni A. A., (1979), "A discontinuous Steklov problem with an application to water waves", Journal of Mathematical Analysis and Applications 69(2), 540–558.

[22] Bermúdez A., Rodríguez R., Santamarina D., (2003), "Finite element computation of sloshing modes in containers with elastic baffle plates", International Journal for Numerical Methods in Engineering 56(3), 447 – 467.

[23] Kozlov V., Kuznetsov N., Motygin O., (2004), "On the two-dimensional sloshing problem", Proceedings of The Royal Society A: Mathematical, Physical and Engineering Sciences 460(2049), 2587–2603.

[24] Girouard A., Polterovich I., (2017), "Spectral geometry of the Steklov problem (Survey article)", Journal of Spectral Theory 7(2), 321–359.

[25] Riva M. D., Provenzano L., (2018), "On vibrating thin membranes with mass concentrated near the boundary: An asymptotic analysis", SIAM Journal on Mathematical Analysis 50(3), 2928–2967.

[26] Armentano M. G., Lombardi A. L., (2020), "The Steklov eigenvalue problem in a cuspidal domain", Numerische Mathematik 144(2), 237–270.

[27] Türk Ö., (2021), "A DRBEM approximation of the Steklov eigenvalue problem", Engineering Analysis with Boundary Elements 122, 232–241.

[28] Bramble J., Osborn J., (1972), Approximation of Steklov eigenvalues of non-selfadjoint second order elliptic operators, in A. Aziz, ed., "The Mathematical Foundations of the Finite Element Method with Applications to Partial Differential Equations", Academic Press, pp. 387–408.

[29] Andreev A. B., Todorov T. D., (2004), "Isoparametric finite-element approximation of a Steklov eigenvalue problem", IMA Journal of Numerical Analysis 24(2), 309–322.

[30] Yang Y., Li Q., Li S., (2009), “Nonconforming finite element approximations of the Steklov eigenvalue problem”, Applied Numerical Mathematics 59(10), 2388–2401.

[31] Bi H., Yang Y., (2011), “A two-grid method of the non-conforming Crouzeix-Raviart element for the Steklov eigenvalue problem”, Applied Mathematics and Computation 217(23), 9669–9678.

[32] Li Q., Lin Q., Xie H., (2013), “Nonconforming finite element approximations of the Steklov eigenvalue problem and its lower bound approximations”, Applications of Mathematics 58(3), 129–151.

[33] Han X., Li Y., Xie H., (2015), “A multilevel correction method for Steklov eigenvalue problem by nonconforming finite element methods”, Numerical Mathematics: Theory, Methods and Applications 8(3), 383–405.

[34] Bi H., Ren S., Yang Y., (2011), “Conforming finite element approximations for a fourth-order Steklov eigenvalue problem”, Mathematical Problems in Engineering.

[35] Weng Z., Zhai S., Feng X., (2015), “An improved two-grid finite element method for the Steklov eigenvalue problem”, Applied Mathematical Modelling 39(10), 2962–2972.

[36] Kuttler J. R., (1974), “Direct Methods for Computing Eigenvalues of the Finite-Difference Laplacian”, SIAM Journal on Numerical Analysis 11(4), 732–740.

[37] Steinbach O., Unger G., (2009), “A boundary element method for the Dirichlet eigenvalue problem of the Laplace operator”, Numerische Mathematik 113(2), 281–298.

[38] Meng J., Zhang Y., Mei L., (2020), “A virtual element method for the Laplacian eigenvalue problem in mixed form”, Applied Numerical Mathematics 156, 1–13.

[39] Mora D., Rivera G., Rodriguez R., (2015), “A virtual element method for the Steklov eigenvalue problem”, Mathematical Models and Methods in Applied Sciences 25(8), 1–25.

[40] Strang G., Berger A. E., (1971), “The change in solution due to change in domain”, Proceedings of Symposia in Pure Mathematics 23(1), 199 – 205.

[41] Blair J. J., (1973), “Bounds for the change in the solutions of second order elliptic PDEs when the boundary is perturbed”, SIAM Journal on Applied Mathematics 24(3), 277–285.

[42] Dauge M., Helffer B., (1993*a*), “Eigenvalues variation. I.: Neumann Problem for Sturm-Liouville operators”, Journal of Differential Equations 104(2), 243–262.

[43] Dauge M., Helffer B., (1993*b*), “Eigenvalues variation. II.: Multidimensional problems”, Journal of Differential Equations 104(2), 263–297.

[44] Hadamard J., (1908), “Mémoire sur le problème d’analyse relatif à l’équilibre des plaques élastiques encastrées”, 1st Edition, Paris: Imprimerie nationale de France.

[45] Vanmaele M., Zenísek A., (1993), “External finite element approximations of eigenvalue problems”, ESAIM: M2AN 27(5), 565–589.

[46] Vanmaele M., Zenísek A., (1994), “External finite-element approximations of eigenfunctions in the case of multiple eigenvalues”, Journal of Computational and Applied Mathematics 50(1), 51 – 66.

[47] Vanmaele M., Ženíšek A., (1995), “The combined effect of numerical integration and approximation of the boundary in the finite element method for eigenvalue problems”, Numerische Mathematik 71(2), 253–273.

[48] Kozlov V., (2006), “On the Hadamard formula for nonsmooth domains”, Journal of Differential Equations 230(2), 532–555.

[49] Kozlov V., Nazarov S., (2012), “On the Hadamard formula for second order systems in non-smooth domains”, Communications in Partial Differential Equations 37(5), 901–933.

[50] Grinfeld P., Strang G., (2004), “The Laplacian eigenvalues of a polygon”, Computers and Mathematics with Applications 48(7), 1121 – 1133.

[51] Grinfeld P., Strang G., (2012), “Laplace eigenvalues on regular polygons: A series in 1/N”, Journal of Mathematical Analysis and Applications 385(1), 135 – 149.

[52] Fiore A., Grinfeld P., (2010), “The calculus of moving surfaces and Laplace eigenvalues on an ellipse with low eccentricity”, Numerical Functional Analysis and Optimization 31(6), 679–690.

[53] Grinfeld P., (2010), “Hadamard’s formula inside and out”, Journal of Optimization Theory and Applications 146(3), 654–690.

[54] Grinfeld P., (2013), “Introduction to Tensor Analysis and the Calculus of Moving Surfaces”, 1st Edition, Springer New York.

[55] Bandle C., Wagner A., (2015), “Second domain variation for problems with Robin boundary conditions”, Journal of Optimization Theory and Applications 167(2), 430–463.

[56] Dambrine M., Kateb D., Lamboley J., (2016), “An extremal eigenvalue problem for the Wentzell-Laplace operator”, Annales de l’Institut Henri Poincare (C) Non Linear Analysis 33(2), 409 – 450.

[57] Akhmetgaliyev E., Kao C.-Y., Osting B., (2017), “Computational methods for extremal Steklov problems”, SIAM Journal on Control and Optimization 55(2), 1226–1240.

[58] Alhejaili W., Kao C.-Y., (2019), “Numerical studies of the Steklov eigenvalue problem via conformal mappings”, Applied Mathematics and Computation 347, 785–802.

[59] Armentano M. G., Padra C., (2008), “A posteriori error estimates for the Steklov eigenvalue problem”, Applied Numerical Mathematics 58(5), 593–601.

[60] Armentano M., (2004), “The effect of reduced integration in the Steklov eigenvalue problem”, ESAIM: Mathematical Modelling and Numerical Analysis 38(1), 27–36.

[61] Kreyszig E., (1989), “Introductory Functional Analysis with Applications”, Wiley Classics Library, 1st Edition, Wiley.

[62] Brenner S., Scott R., (2008), “The Mathematical Theory of Finite Element Methods”, Texts in Applied Mathematics, 3rd Edition, Springer New York.

[63] Gockenbach M. S., (2006), “Understanding And Implementing the Finite Element Method”, 1st Edition, Society for Industrial and Applied Mathematics, USA.

[64] Lui S., (2011), “Numerical Analysis of Partial Differential Equations”, Pure and Applied Mathematics: A Wiley Series of Texts, Monographs and Tracts, 1st Edition, Wiley.

[65] Knabner P., Angermann L., (2003), “Numerical Methods for Elliptic and Parabolic Partial Differential Equations”, Vol. 44, 1st Edition, Springer New York.

[66] Surana K., Reddy J., (2016), “The Finite Element Method for Boundary Value Problems: Mathematics and Computations”, 1st Edition, Chapman and Hall/CRC.

[67] Larson M., Bengzon F., (2013), “The Finite Element Method: Theory, Implementation, and Applications”, Vol. 10, 1st Edition, Springer-Verlag Berlin Heidelberg.

[68] Noschese S., Pasquini L., Reichel L., (2013), “Tridiagonal Toeplitz matrices: properties and novel applications”, Numerical Linear Algebra with Applications 20(2), 302–326.

[69] Grisvard P., (2011), “Elliptic Problems in Nonsmooth Domains”, Classics in Applied Mathematics, 1st Edition, Society for Industrial and Applied Mathematics.

[70] Mora D., Rivera G., Rodríguez R., (2017), “A posteriori error estimates for a virtual element method for the Steklov eigenvalue problem”, Computers & Mathematics with Applications 74(9), 2172–2190.